Fall 2016

Emergent Wetland Plant Biophysical Characteristics Associated with Wave Attenuation and Sediment Retention

Chad D. Stellern
stellec@wwu.edu

Emergent Wetland Plant Biophysical Characteristics Associated with Wave Attenuation and Sediment Retention

By

Chad D. Stellern

Accepted in Partial Completion

of the Requirements for the Degree

Master of Science

Kathleen L. Kitto, Dean of the Graduate School

ADVISORY COMMITTEE

Chair, Dr. Scott R. Linneman

Dr. Eric E. Grossman

Dr. David Wallin

Dr. Brady Foreman

MASTER'S THESIS

In presenting this thesis in partial fulfillment of the requirements for a master's degree at Western Washington University, I grant Western Washington University the non-exclusive royalty-free right to archive, reproduce, distribute, and display the thesis in any and all forms, including electronic format, via any digital library mechanisms maintained by WWU.

I represent and warrant this is my original work, and does not infringe or violate any rights of others. I warrant that I have obtained written permissions from the owner oy any third party copyrighted material included in these files.

I acknowledge that I retain ownership rights to the copyright of this work, including but not limited to the right to use all or part of this work in future works, such as articles or books.

Library users are granted permission for individual, research and non-commercial reproduction of this work for educational purposes only. Any further digital posting of this document requires specific permission from the author.

Any copying or publication of this thesis for commercial purposes, or for financial gain, is not allowed without my written permission.

Chad Stellern

October 26, 2016

Emergent Wetland Plant Biophysical Characteristics Associated with Wave-Attenuation and Sediment Retention

A Thesis

Presented to

The Faculty of

Western Washington University

Accepted in Partial Fulfillment

of the Requirements for the Degree

Master of Science

By

Chad D. Stellern

December, 2016

Abstract:

Coastal lowlands serve society with important natural and agricultural resources yet, are vulnerable to coastal hazards such as inundation from rising-sea level and storm-surge impacts. Estuarine wetlands have proven a long term and cost effective buffer against such hazards because, wetlands serve as a barrier against erosive wave energy and enable sediment retention by producing hydraulic friction and a positive feedback loop (Shepard et al., 2011; Kirwan et al., 2010; Koch et al., 2009). However, human modifications to coastal hydrology and sediment transport have resulted in extensive losses of wetland land cover and protection (Fresh et al., 2011; Simenstad et al., 2011; Collins and Sheikh, 2005; Jones et al., 2001). Historically, the Puget Sound is estimated to have contained nearly 270 km^2 of tidal wetlands in the late nineteenth century (Thom and Hallum, 1990) and suffered nearly a 56% wetland loss within the 16 major deltas from agriculture and urban growth (Fresh et al., 2011). Our study area, the Stillaguamish Delta, historically maintained 65km^2 of wetlands but currently holds only 36km^2, a 55% loss (Simenstad et al., 2011), and has witnessed up to a kilometer of marsh edge (shoreline) retreat since 1964 (Grossman and Curran (in review)).

The purpose of this study was to:

1) Quantify canopy structures and physical characteristics of vegetation (elasticity, biomass, height, stem density, stem diameter) that effect wave attenuation using Side-On Photo image analysis and in-situ measurements.
2) Delineate wetland assemblages using remote sensing efforts using Compact Aerial Spectral Imager (CASI) hyperspectral imagery and LiDAR.
3) Estimate wetland biomass and extrapolate variability across the delta.
4) Produce a winter sediment budget for the vulnerable northern region of the study area.
5) Evaluate ecologic, hydrologic and climatic influences on sediment dynamics using turbidity data.

We found:

1) Our Side-On Photo methods to accurately predict plant height and biomass; however, our stem density and diameter analysis was not conclusive. BOMA and BOFL maintained rigidity and biomass through most of the winter (November through March); however, tended to break more frequently in later months. Our data indicated vegetation has the highest rigidity and biomass within the first 0.5 m of the canopy from the marsh ground surface and therefore has greatest potential for flow attenuation.
2) Supervised classifications (Maximum-Likelihood and Decision Tree Classifiers) of CASI (Compact Aerial Spectral Imager) hyperspectral imagery to successfully delineate the spatial extent of vegetation assemblages with an overall accuracy of 76.9%.
3) Biomass to be highest within the first 30 m of the winter marsh edge where plant material would have the largest impact on flow attenuation, sediment retention and coastline stabilization during the early monsoon season.
4) The highest winter sediment deposition occurred in the High to Mid-Marsh boundary, up to 300 m inland of the marsh edge. Overall deposition within the wetland is estimated to be 2.6% of the sediment yield from the primary sediment source, the Stillaguamish River. Sediment coating vegetation may contribute up to 0.5% of the marsh sediment budget. Sediment deposition and vegetation coating is likely abnormally high owing to an increased sediment supply from the recent Oso (SR 530) Landslide.
5) Turbidity of a tidal channel is closely related to turbidity and discharge responses from the Stillaguamish River, the assumed primary sediment source. The northern marsh turbidity indicated a delayed (~2 days) sediment response to the river and uniform delivery. Turbidity within the northern marsh showed relationships to regional winds that generate waves. We conclude that

during the study (winter of 2014-15) hydraulic energy was likely high enough to erode the marsh edge, suspend sediment from associated tidal flat, and transport material landward.

Overall, these results inform efforts to restore marshland and associated sediment supply, as well as, the overall understanding of vulnerability and adaptability of coastal marshlands to climate change and sea-level rise. This information is valuable for coastal managers and decision makers that are interested in ecologically sustainable alternatives to coastline armoring. These ecosystems maintain natural resources while providing protection against increasing coastal hazards from SLR.

This thesis is formatted into two chapters addressing vegetation characteristics / distribution and sediment dynamics separately.

Acknowledgements

I am very grateful to all those that have helped, guided, funded, and otherwise supported this project.

First, I would like to acknowledge my funders, United States Geologic Survey (USGS), Western Washington University (WWU) Enhancement of Graduate Research Grant and, WWU Geology Department's Advance for Research.

To my Thesis Committee, Dr. Eric Grossman, Dr. Scott Linneman, Dr. David Wallin and Dr. Brady Foreman, thank you for tolerating all the short deadlines and providing timely, salient and even critical feedback.

At the beginning of this project, as a geologist, I lacked the fundamental knowledge of plant taxonomy and ecology of the nearshore. Roger Fuller deserves special kudos for introducing me to the plants and ecologic processes within Port Susan Bay. Roger Fuller allowed access to several datasets that helped solidify key analyses of this project. Thank you.

Field Assistants: Katy Hancock, Grace Sutherland, Kristina Gustovich, Katherine Beeler and, Kether Scharff-Gray. You answered the call to traipse through the estuary during the wet and the cold and the dark winter months; I cannot be more grateful. Special thank you to Katy Hancock, who spent the most time with me in the field.

Table of Contents

List of Tables

Chapter 1

Chapter 2

Appendix 1: RTKGPS Analysis

Appendix 2: Cover Classes and Spectral Signatures

Appendix 3: Decision Tree Classification (DTC)

Appendix 4: Biomass Model Derivation

Appendix 5: Exploratory Analysis of Side-on Photography Data

No Tables

Appendix 6: Exploratory Analysis of Elasticity Data

Appendix 7: Eelgrass analysis

List of Figures

Chapter 1:

Chapter 2:

Appendix 5: Exploratory Analysis of Side-On Photography Data

Appendix 6: Exploratory Analysis of Elasticity Data

Appendix 7: Eel Grass Analysis

Chapter 1

Title: Characterization of estuarine wetland biophysical characteristics and distribution in a Pacific Northwest Delta, Port Susan Bay

Keywords:

tidal marsh, sedimentation, vegetation, flow attenuation, Puget Sound, hydrodynamics

Abstract:

Emergent wetland vegetation has been shown to mitigate coastal inundation and erosion hazards by reducing wave energy through friction (Shepard et al., 2011), although its use in coastal protection planning is limited because predictive models require improved vegetation data. Port Susan Bay (PSB), the delta for the Stillaguamish River of Western Washington State, a vulnerable estuary that has experienced up to 1 kilometer of marsh retreat since the mid-1960s. Marsh retreat is thought to be caused by a historic river avulsion trending to the south west. We isolated biophysical characteristics (biomass, stem density, elasticity, etc.) of plants using horizontal digital photographs (Side-On Photos (SOPs)) and direct field measurements/observations from fall to early spring (August 2014 through April 2015). Our SOP data was successful in predicting height and biomass; however, stem density and diameter showed a very weak relationship (Kendall's tau p-values =0.04). Vegetation elasticity was measured in-situ with a handheld digital hanging scale with respect to measurement height and bending angle. Plant elasticity showed a strong correlation to stem diameter in two dominant bulrush species, *Bulboschoenus maritimus* (BOMA) *Bulboschoenus fluviatilis (*BOFL). BOMA and BOFL maintain material strength and biomass through the majority of the winter (November through March); however, tended to break more frequently in the later months. Our data showed a strong logarithmic relationship with potential wave attenuation (bending strength) that was insensitive to seasonality but may be influenced by daily temperature. Elasticity and SOP vertical assessments indicate that the first 0.5 m of marsh

canopy had the greatest potential for flow attenuation. We employed supervised classifications (Maximum-Likelihood and Decision Tree Classifiers) of CASI (Compact Aerial Spectral Imager) hyperspectral imagery to map the spatial extent of vegetation assemblages with an overall accuracy of 76.9%. Decision Tree Classification a series of conditional statements that is based on the empirical elevation and Normalized Difference Vegetation Index data of 345 ground truth areas. Vegetation biomass was extrapolated broadly across the PSB estuary using remote sensing efforts. This analysis showed elevated biomass within the first 300 m of the marsh edge that had a greater potential to attenuate flow than directly inland. The information provided here will allow future workers to incorporate wetland characteristic information into coastal hazard and residency models; as well as, provides a robust method to quantify and distribute salient wetland variables.

1 Introduction and Background:

Coastal lowlands serve society with important natural and agricultural resources, yet are vulnerable to coastal hazards such as inundation from rising-sea level and storm-surge impacts. Human modifications to coastal hydrology and sediment transport have resulted in extensive losses of wetland land cover and protection (Simenstad et al., 2011; Fresh et al., 2011; Collins and Sheikh, 2005; Jones et al., 2001). Estuarine wetlands serve as a long term and cost effective buffer against such hazards (Shepard et al., 2011; Koch et al., 2009). However, wetland restoration is not consistently considered in coastal protection strategies because additional research is required to quantify their services across a variety of regions. Coastal wetlands' response patterns to climate change are challenging to validate because they are dependent on terrestrial, marine, and climatic forcings (Kirwan et at., 2010). Coastal resilience planners require a more robust understanding and efficient methods to characterize wetland influences on wave attenuations (Shepard et al. 2011).

Wetlands function as a barrier against erosive wave energy and enable sediment retention through a positive feedback loop (Koch et al., 2009; Kirwan et al., 2010). Friction imparted by vegetation can produce attenuation rates up to two magnitudes higher than a smooth non-vegetated tidal flat (Yang et al., 2011). Wave-vegetation interactions enable wave attenuation and sediment deposition necessary for plant growth that, in turn, reduces wave energy. The rate of wave attenuation along the wave flow path is a function of wetland biophysical characteristics: canopy height, stem diameter, stem density and elasticity (flexibility) (Mendez and Losada, 2004). Wave energy is lost through the direct interaction with plants through friction; thereby, surface area of plant material influences water velocity and wave attenuation (Chen and Zhao, 2012). Wave attenuation is also sensitive to plant flexibility; a rigid stem provides more resistance and friction than pliable stem (Anderson and Smith, 2014; Augustin et al., 2009; Mullarney and Henderson).

Here we refine methods to efficiently quantify vegetation composition and structural characteristics that influence water flow and sedimentation. We isolated species-specific biophysical metrics such as height, stem diameter, stem density and elasticity using a combination of field and image analysis methods based on the work of Moller (2006) and Zehm et al. (2003). These biophysical characteristics were then extrapolated using remote sensing methods after Hladik et al. (2013) by implementing Maximum Likelihood (MLC) and Decision Tree (DTC) classifications (DTC) to hyperspectral Compact Aerial Spectral Imager (CASI) and LiDAR datasets.

1.1 Site description

Port Susan Bay (PSB) is a temperate and protected estuary located within the Salish Sea of Washington State (Figure 1); PSB serves as outlet and delta for the Stillaguamish River. Marshlands occupy the intertidal zone of the deltaic shelf (Figure 1).

The Stillaguamish River watershed covers approximately 1,813 km^2 from the flat Puget Lowlands, dominated by unconsolidated glacio-fluvial deposits and soils, into the high-relief, bedrock dominated, North Cascades (Tabor et al., 2002). The Stillaguamish River is supplied largely by rainfall and snowmelt and, the river maintains a mean annual discharge of approximately 85 m^3/s (3000ft^3/s) (Grossman and Curran (in review)). Prior to a lahar from Glacier Peak dated at 5kya, the Sauk River likely flowed into the north fork of the Stillaguamish (Tabor et al., 2002). The Stillaguamish River recently came under national spotlight because of the tragic 2014 Oso Landslide. A recent study estimates that the catastrophic landslide increased the river's sediment load 50% during the first two years following the slide (Grossman and Curran (in review). During the winter monsoon season, the dominant wind direction is from the south-southwest, the same direction as the bay exposure, and has a fetch of 35-50 km (Grossman and Curran (in review)) (Figure 1). Tidal range is generally mesomareal for PSB with a tidal range from 2.44 m and -0.27 m of MLLW.

PSB offers an opportunity to examine the effects of vegetation on wave attenuation in concert with other ongoing scientific efforts. Efforts by the U. S. Geological Survey (USGS), The Nature Conservancy and partners are measuring and monitoring hydrodynamics, sediment transport, and marsh response and, ambient conditions to guide adaptive actions to climate change. The Nature Conservancy recently purchased abandoned farmland for the purpose of wetland restoration (Fuller, 2015) (Figure 1).

Vegetation distribution is largely controlled by gradients along limiting factors such as: elevation (inundation, salinity), sedimentation, hydraulic energy, and nutrient cycling (Hutchinson, 1988 and Seliskar and Gallagher, 1983). Marshland biomass is also sensitive to temporal change; within the PNW, winter dieback of above-ground plant biomass is concurrent with the stormy winter months when the annual wave energy is highest (Finlayson, 2006).

PSB has three general marsh assemblages:

1) High-Marsh is found above the MHW (>2.5 m NAVD88) and is inundated during unusually high tides (Fuller, 2015). It characteristically has the largest species richness dominated by graminoid (grass) species (*Agostis stolonifera* and *Distychlis spirata*), rush (*Juncus balticus*), sedges (*Carex lyngbyei*) and Pacific Silverweed (*Potentilla pacifica*) (Fuller, 2015).
2) Mid-Marsh occurs below MHW, between 2.5 and 2.0 m elevation and is dominated by dense (mean ~117 ± 30 stems/m^2) bulrush species (Fuller, 2015). The Mid-Marsh is largely the focus of this study because it serves as the winter marsh edge and is assumed to be the key agent in wetland wave attenuation.
    a. BOMA (*Bulboschoenus maritimus*) – Hip to waist height (mean ~ 0.75 m), semi-rigid stems, ~3 bladed leaves up to 2ft in length.
    b. BOFL (*Bulboschoenus fluviatilis*) – Chest to head height (mean ~1.5 m), semi-rigid stems, ~3 bladed leaves up to 2.5ft in length.
    c. SCAM (*Schoenoplectis americanus*) – Knee to hip height (mean ~0.5 m), semi-flexible stems, no significant leaves.

    The majority of the Mid-Marsh is co-dominated (50/50) by BOMA and SCAM; however, BOFL covers a narrow but continuous band in the higher reaches of the Mid-Marsh and only in the northern parts of the study area (between the restoration site and South Pass) (Fuller, 2015). Note: previous to Fuller (2015), BOFL was considered the tall morph clone of BOMA and potentially misclassified. BOMA and BOFL remain present throughout the fall and winter as semi-rigid stems and therefore are more likely to interact with waves; whereas, SCAM tends to deteriorate and lay flat by December.
3) The Low-Marsh is dominated by SCAM (low species richness) which generally occurs between 1.3 and 2 m elevation (Fuller, 2015). The density of stems within the Low-Marsh varies widely (78 ± 156 stems/m^2) and can be particularly patchy in the northern portions of the study area (Fuller, 2015)

(Figure 2). Although SCAM deteriorates relatively early (mid-October – December), it may contribute to bed roughness and wave attenuation.

PSB has experienced up to a kilometer of marsh retreat since 1964 and a historic 55% of marshland loss to agriculture (Simenstad et al., 2011; Collins and Sheikh, 2005; Thom and Hallum, (1990); Grossman and Curran (in review)) (Figure 1). Marsh retreat in the northern region is associated with lower sediment delivery rates from a rerouted Stillaguamish River; the main fork currently flows south instead of a historic WNW orientation (Figure 1). Sea level rise, increased wave-energy and other climatic forces are also probable factors in the marsh retreat.

2 Methods:

For this study, we quantified marsh plant biophysical metrics by combining image analysis, physical elasticity measurements, and remote sensing to assess potential vegetation influence on wave attenuation. Data were collected from September 2014 through April 2015 with a focus on the northern marsh that has experienced historical loss of marsh.

2.1 Side-On Photos (SOPs)

To characterize vegetation metrics including plant height, stem density, stem diameter and biomass, that influence water flow and sediment attenuation, we conducted side-on photography (SOP) following methods developed by Zehm et al. (2003) and Moller (2006). This consisted of photographing a thin strip of vegetation (Figure 3) and processing the images using ENVI and VESTA software. This method has been proven as an efficient tool for analyzing vertical vegetation structures and other seasonally – dependent biophysical characteristics (height, stem density, biomass, and stem diameter) (Leiman at al., 2015; Rogers et al., 2015; Tackenberg, 2006).

For this study, we sampled 20 SOP sites with a focus on the mid and Low-Marsh bulrush assemblages. We selected sites to capture the diverse range of assemblages that follow Fuller's (2015) transects for comparison; transects and sites run perpendicular to the marsh edge to document variation in assemblages with respect to elevation gradients. We focused largely on the northern and central delta that were more accessible. The majority of data were collected in the late summer 2014 (August 9th through September 12th) with repeat sampling in January and April to assess seasonal changes in plant characteristics.

At each SOP site, we carefully sectioned off a 0.2 m by 1.3 m strip of emergent vegetation using a red backdrop and ground cloth (Figure 3). A total of 5 pictures were taken at a distance of 2 m from the backdrop and 0.7 m above the ground surface using a 10-megapixel Canon digital camera (Figure 3). Vegetation was then cut at the ground surface, carefully bagged and brought back to the lab.

In the lab, plants were dried on large tarps for a period of one week and stems were separated by species and size (>25 cm). Stems greater than 25 cm were measured for height and diameter and weighed using a digital hanging scale (American Weigh Scales; Model SR-20) with an accuracy to 1g. Stem diameter was measured at 25 cm above the cut surface. Fragments (stems <25 cm in length) were not measured for height or diameter but, they were included in overall biomass. Overall biomass was calculated as the sum of all sampled plant material.

Image processing procedures involved a supervised Maximum Likelihood Classification scheme in ENVI where ground truth areas were digitized for information classes (i.e. vegetation, sediment coated vegetation, shadow, backboard). These information classes were then combined into vegetated and non-vegetated classes. In some cases, there was significant mud splatter on the backboard that was misclassified as vegetation. These misclassified pixels were corrected using the Aggregation Tool in ENVI,

eliminating any vegetated pixels that had less than 40 contiguous pixels. Last, remaining misclassified pixels were identified and removed using the 'block out' tool SideLook Software.

Once classified, images were processed using the SideLook Software developed to measure pertinent vegetation attributes. Generally, we compared lab measurements of average plant height, stem density, stem diameter, and biomass to SideLook metrics: Mean-Max Vegetated Pixels (overall image average of maximum height of vegetated pixels per 1 cm column); Row-Hole Count (the number of contiguous nonvegetated spaces for a specific 1 cm wide row); Average Row-Hole Size (the average length of space between vegetated pixels for a specified row), and Total Vegetated Pixel Count (total number of vegetated pixels), respectively. SideLook metrics were calculated using 1 cm wide rows and columns. We used data from the 25 cm (25 cm to 26 cm in vertical height) row for our stem density and stem diameter comparisons. A detailed account of our image processing and exploratory analysis is in Appendix 5.

2.2 Elasticity

We measured elasticity for key bulrush species (BOMA and BOFL) to empirically define potential wave attenuation traits with respect to plant species. Measurements were taken using a digital scale to determine the amount of force required to bend stems to three angles (15, 30 and 45 degrees) at three heights (full height, half height, 25 cm) for a total of 9 measurements per plant (Figure 4). We collected biweekly data for October and November 2014 then monthly through March 2015. Measured stems were vertical; by November SCAM was no longer vertical and was excluded from data collection and analysis. We also collected height and diameter measurements following Freeman et al. (2000) found that bending strength for spartina could be predicted as a function of plant height and diameter. Appendix 6 further describes the methods and results of our vegetation elasticity analysis, including exploratory analysis.

2.3 Remote Sensing

We used hyperspectral (CASI) and LiDAR derived elevation models to remotely classify wetland assemblages, to extrapolate the field-measured, species-specific, vegetation metrics (stem density, height, biomass, etc.). We paired supervised classification methods, Maximum Likelihood (MLC) and Decision Tree (DTC) classifications, following the work of Hladik et al. (2013) to isolate unique marsh assemblages. We developed a linear regression model, based on our SOP sample sites, and employed it to estimate biomass characteristics across our study area.

Normalized difference indices have a long history in remote sensing; most notable is the Normalized Difference Vegetation Index (NDVI) that has proven a successful indicator biomass (Delegido et al, 2013) (Eqn. 1). NDVI compares the high absorption of solar radiation in the red spectrum (~675 nm) and high reflectance in the near-infrared spectrum (~800 nm) (Delegido et al. 2013). The Red-Edge Normalized Difference Index (RE-NDI) is the normalized index between the red spectrum and the transition between red and NIR spectrums (~715 nm). Delegido et al. (2013), compared vegetation indices and found that RE-NDI to have the strongest correlation with LAI and is not prone to the saturation effects of NDVI. Our DTC and biomass model are based on normalized difference vegetation indices (NDVI and RE-NDI) and elevation.

Compact Airborne Spectrographic Imager (CASI) hyperspectral imagery and LiDAR were collected by the US Army Corps of Engineers' Joint Airborne LiDAR Bathymetry Technical Center of Expertise (JALBTCX) as part of the USGS's Coastal Habitat in Puget Sound (CHIPS) project. These data were collected over a 2 hour period centered on 1500 hours of September 10th 2014 from an elevation of 2000 m during low tide. The CASI imagery contains 48 spectral bands that are evenly spaced (14.0625nm bandwidths) to provide continuous spectral coverage from 375nm to 1050nm at 1 m pixel resolution.

Accurate elevation data within densely vegetated wetland environments is often difficult to acquire and validate (Hladik et al., 2013). Often LiDAR cannot penetrate the dense canopies of marshlands and residual errors remain despite the LiDAR Bare-Earth correction methods attempted by the vendor. Here, the DEM values are considered the sum of partial vegetation height and elevation. Using RTKGPS data, we estimated the LiDAR bare earth DEM to be over predicted by 0.40 m +/- 0.27 m in the High-Marsh, 0.49 m +/- 0.17 in BOFL dominated Mid-Marsh, 0.43 m +/- 0.26 in the BOMA dominated Mid-Marsh, and 0.38 m +/- 0.24 in the Low-Marsh (Appendix 1).

2.3.1 Maximum Likelihood Classification (MLC)

Maximum Likelihood Classification (MLC) is a supervised classification method that classifies pixels based on the similarity of the pixel's spectral signature to the spectral signature of the assigned cover type. For example, if a pixel has a spectral signature that is comparable to the High-Marsh then it will be classified as such. Following the work of Hladik et al., 2013), we clipped the CASI imagery to the marsh extent and applied MLC within ENVI software. The study area was digitized using a real color display of the CASI imagery that isolated the vegetation extent from major water filled channels.

As a supervised classification algorithm, MLC requires ground truth points assign a cover class to each pixel based on their respective spectral signature. Total, we used 345 ground truth points for our classification and statistical validation that were assigned randomly into training (50%) and testing (50%) areas. Ground truth points were defined in two ways: (1) using ground truth GPS data from this study (157 points) and Fuller's (2015) (104 points) vegetation survey data and (2) by digitizing large homogeneous regions of land-cover (eelgrass, blackberries, beachwood, etc) based image interpretation of a real color display of the CASI dataset. The GPS ground truth points were used for all marsh types, while the digitized areas were for non-marsh cover-types and those outside the wave dissipation area.

We collected GPS ground truth points from the summer of 2014 through spring of 2015. Ground truth points for our study were taken in large (25 m^2) homogeneous patches of cover-type (bare sediment, vegetation assemblage, etc) and include our SOP sites. Fuller's (2015) data contained categorical plant height, density and present cover information. Fuller's (2015) vegetation surveys also contained detailed dominant, codominant and present species information. We assigned a cover-type (high, mid, Low-Marsh) to Fuller's (2015) these data based on their dominant and co dominant species information.

Wetland vegetation assemblages and species have historically been difficult to separate through remote sensing efforts because their spectral signatures are very similar leading to misclassification (Hladik et al., 2013). Our plant assemblages exhibited similar patterns (Figure 5). Following Hladik et al. (2013), we processed the MLC results using a Decision Tree Classification (DTC).

2.3.2 Decision Tree Classification (DTC)

We applied a Decision Tree Classification (DTC) to incorporate elevation and Normalized Difference Vegetation Index (NDVI) variables to our MLC results in order to improve accuracy of our classification. In essence, our DTC reclassifies suspect pixels based on a sequence of conditional if-then statements developed utilizing spectral and elevation characteristics of vegetation assemblages (Figure 6). The primary species of interest (SCAM, BOMA and BOFL) generally occupy separate elevation zones and can further be separated using the NDVI (Eqn. 1). We calculated the elevation and NDVI statistics for the vegetation assemblages from the training ground truth points (Table 1). Fuller (2015) found similar elevation for vegetation assemblages (Table 1). We used these empirical data to deduce separation values and create the condition statements of the DTC.

Decision trees were created to isolate pixels that were within one standard deviation of both the mean elevation and NDVI values (Figure 6; Appendix 3). Decision trees were developed where elevation was

accounted for before NDVI. This is because assemblage-specific elevation ranges are more statistically distinct than the NDVI ranges (Table 1). For a pixel to be reclassified by the DTC, it would need to fail at least two conditional statements and be outside 1 standard deviation in both NDVI and elevation. All bulrush species were determined to have a NDVI value greater than 0.06; less than 0.06 is assumed to be sediment (Table 1).

Elevation ranges for vegetation species vary across our study area (Fuller, 2015). For example, vegetation species tended to occupy higher elevation ranges in the southern study area by the mouth of the Stillaguamish River where there is an assumed higher sediment supply/retention. Also, the Mid-Marsh bulrush species (BOMA and BOFL) occupied lower elevation ranges in the restoration area because of subsidence (Fuller, 2015). To improve our DTC analysis, we defined 3 geographic zones with unique assemblage elevation characteristics: 1) Northern Zone located north of the main branch of the Stillaguamish River; 2) South Zone – located south of the main branch; 3) Restoration Area – recovered marshland from the 2012 Nature Conservancy estuary restoration. Geographic zones were addressed separately using individual decision trees (Appendix 3). Appendix 3 details cover class decision trees and statistics for all marsh types, as well as a detailed rational for our decision tree development.

2.3.3 Biomass Analysis

We used the 20+ SOP sites to predict biomass as a function of elevation and vegetation spectral indices (Eqn. 3) (Figure 7). We compared 13 published vegetation indices to our biomass data to extrapolate biomass across the delta (Appendix 4). We compared our biomass values with the Fuller (2015) data for validation. In 2014, Fuller (2015) collected categorical plant data, including stem density of bulrush species, percent cover (% of marsh floor visible from a bird's eye viewpoint) and plant height.

3 Results:

3.1 Side-on Photos (SOPs)

3.1.1 Plant Biophysical Characteristics

We compared lab-measured plant data (height, biomass, stem density and, stem diameter) to their respective image derived data (Mean-Max Vegetated Pixel Height, Vegetated Pixel Count, Row-Hole Count, etc.). We found that plant height and biomass data were correlated to SOP data (Figure 8). Stem density and stem count data did not show a strong relationship with SOP data (Figure 8). Lab-measured stem density did not show a correlation with measured biomass for any marsh species (Figure 9).

Mean-Max Vegetated Pixel Height, the average maximum height of vegetated pixels at 1 cm columns within an SOP image, showed a strong relationship with measured height (Kendall's p-value = 1.76×10^{-5}) (Figure 8a and 10). Measured biomass showed a strong relationship with total vegetated pixels of SOP images (Kendall's p-value = 5.25×10^{-5}) (Figure 8b). Row-Hole Count, taken at 25 cm above marsh floor, showed a weak relationship with measured stem count (Kendall's p-value = 0.04) (Figure 8c). We tested Row-Hole Count at row heights 50 cm and 75 cm did not show a correlation using Kendall's tau with lab-measured stem height (Appendix 5). Measured stem diameter showed a weak correlation with the ration Vegetated Pixel Count over Row-Hole Count (Kendall's Tau p-value = 0.04) (Figure 8d).

We assessed vertical biomass patterns through the number of vegetated pixels per row (1 cm tall) (Figure 11). BOFL showed decreasing vegetated pixels from 0 to 50 cm then relatively stable biomass values up to 150 cm (Figure 11a). BOMA exhibits a similar pattern, though more nuanced, with a steady decline in plant material from 0 to 25 cm and slighter decline in plant material above 25 cm (Figure 11b). SCAM showed a relatively consistent decline in biomaterial as approaching maximum canopy height (Figure 11c). High-Marsh species showed a wide variety of vertical plant structures owing to assemblage heterogeneity (Figure 11d).

3.1.2 Seasonal Changes

Biomass appeared to be stable though January then declines rapidly within BOMA and BOFL dominated Mid-Marsh (Figure 12a). SCAM biomass data tended to decline steady though November and is non-existent by early December; this matched field observations (Figure 12a). SOP data showed a slightly different story, where the total number of vegetated pixels tended to decline steady from September to march for BOFL and BOMA (Figure 12b).

We used the SOP analysis to examine seasonal changes with vertical biomass structures (Figure 13). BOFL showed the loss of plant material above 50 cm in the canopy but not a loss in height (Figure 13a). BOMA showed a loss in canopy height and biomass as the winter progressed (Figure 13b).

3.2 Elasticity:

In both BOMA and BOFL dominated regions, stem diameter did not appear to have any apparent relationship to seasonality through the fall and winter (Figure 14c-d). We observed increases in stem breakage with seasonality in both species(Figure 14e-f). Stems also are susceptible to brittle breaking during temperatures below freezing. For example, during a November sampling day where temperatures were below freezing with floating ice present in the marsh, we observed an anomalously high percentage of broken stems (Figure 14e-f).

BOMA and BOFL both showed strong relationships with diameter and bending force (Figure 14). Force measurements taken low in the canopy (half height, 25 cm) and at higher angles (30, 45 degree) tended to have a stronger correlation with diameter (Appendix 6). In general, BOFL plants tended be more resistant to deformation and have a larger diameter (Figure 14a-b and Figure 15 a-b).

In both species, there tended to be a weak and inconsistent relationship of bending force with total plant height (Figure 15c-d; Appendix 6). This relationship tended to be stronger with BOFL than BOMA

and to have a stronger relationship at lower measurement heights (half height, 25 cm) and higher angles (Appendix 6). The relationship between force and height, if present, tended to be positive; however, in some cases the relationship tended to have parabolic relationship (Figure 15c).

There were strong logarithmic relationships between bending force and measurement height in both species (Figure 15e-f). Our regression analysis showed slight and inconsistent variations between regressions with respect to month; elasticity data did not exhibit a relationship to seasonality though stems became brittle (Figure 15; Table 2).

3.3 Remote Sensing Analysis

Through our remote sensing analysis, we mapped the major marsh assemblages and land cover within the delta with an overall accuracy of ~77%. The DTC classification increased the overall accuracy by 10% from our MLC results. Our DTC focused on bare sediment, Low-Marsh (SCAM), BOMA/SCAM codominant Mid-Marsh, BOFL dominant Mid-Marsh; each of which saw an increase in producer's accuracy: 7%, 13%,6%, and 22% respectfully (Figures 16; Tables 4-5). By combining Mid-Marsh subclassess (BOMA and BOFL) we increased the overall and Mid-Marsh accuracy to 65% and 77%, respectively (Table 6). Using the empirically derived relationship between measured biomass samples, elevation and, the red-edge NDI (Equation 3; Figure 7), we extrapolated the biomass across the study area (Figure 17). We found that the High, Mid and Low-Marsh cover approximately 1.02, 1.58 and 1.42 km^2 with 951, 885 and 585 mT of plant material, respectfully (Table 6). Biomass analysis showed that the marsh edge (first 20 m) had a higher biomass compared to the Low and Mid-Marsh (Figure 17).

3.3.1 Maximum Likelihood Classification (MLC)

Our MLC classified the CASI imagery with an overall accuracy of ~67% (Table 3). Producer's accuracies are as follows: Bare (83%), Low-Marsh (49%), BOMA Mid-Marsh (41%), BOFL Mid-Marsh (44%), and

High-Marsh (75%). The MLC misclassified SCAM dominant Low-Marsh as Bare sediment and BOMA/SCAM co-dominant Mid-Marsh (Table 3). BOMA Mid-Marsh was primarily misclassified as SCAM dominant Low-Marsh (33%), bare sediment (10%) and lesser amounts of misclassification as BOFL and High-Marsh (7% each) (Table 3). BOFL dominated Mid-Marsh tended to be misclassified as BOMA/SCAM Mid-Marsh (35%) with lesser misclassification with High-Marsh (15%) (Table 3). High-Marsh has a higher producer's accuracy than other marsh assemblages (73.9%) (Table 3).

3.3.2 Decision Tree Classification

Through the DTC, we improved the overall accuracy to 77%, up 10% from the MLC results (Tables 3-5). Producer's accuracies are as follows: Bare (90%), Low-Marsh (62%), BOMA Mid-Marsh (47%), BOFL Mid-Marsh (66%), and High-Marsh (75%). Undifferentiated Mid-Marsh cover type yielded a producer's accuracy of (65%) (Table 6). High-Marsh and non-marsh cover-types saw little, if any, improvement between the MLC and the DTC because they were not specifically addressed with the DTC.

The Low-Marsh (SCAM) still tended to be misclassified as sediment (Figure 16; Table 5-6); however, misclassification as BOMA/SCAM dominated Mid-Marsh improved by 10%. The Low-Marsh DTC results tended to have solid patches with fewer random Low-Marsh pixels in the northern tidal flat, compared to the MLC results (Figure 16). BOMA/SCAM co-dominant Mid-Marsh DTC results had the lowest accuracy (48%) but improved by 7% from the MLC (Table 4-5). BOFL dominated Mid-Marsh (66%) had the largest improvement of all the marsh cover-types, up 12% from the MLC. Reclaimed BOFL pixels primarily came from the BOMA/SCAM cover-type.

3.3.3 Biomass Analysis

We found that biomass had the strongest relationship with imagery using a combination of Red-Edge Normalized Difference Index (RE-NDI) and elevation (Figure 7; Eqn 2; Appendix 4). We tested 12

alternative vegetation indices and found that the RE-NDI correlated best with biomass following the methods of Delegido (2013) (Appendix 4). This relationship was then used to extrapolate biomass across the delta (Figure 17). Here we used CASI's Band 22 (663-677nm), Band 25 (705-719nm), Band 31 (781-803nm) for red, red-edge, and NIR values respectively.

We found that the RE-NDI and elevation had a strong correlation with our biomass samples from the SOP sites. This relationship was used to predict biomass across the study area. We estimate that in 2014 marshlands had total of 2694 mT of biomaterial with 951, 885, and 858 mT within the Low, Mid and High-Marsh respectfully (Table 5). We found that biomass had a strong relationship with Fuller's (2015) binned percent cover data (Kendall's p-value =9.07E-6) (Figure 18). Biomass had a weak correlation (Kendalls p-value = 0.002) with Fuller's (2015) categorical stem density (Figure 19).

$$NDVI = \frac{NIR - Red}{NIR + Red} \quad \text{Eqn. 1}$$

$$RE_{NDI} = \frac{Red.Edge - Red}{Red.Edge + Red} \quad \text{Eqn. 2}$$

$$Biomass(g) = \frac{[12.96 \times NDI + 6.6607]^{\frac{1}{0.29}}}{Elevation} \quad \text{Eqn. 3}$$

4 Discussion

4.1 Side-on Photos (SOPs)

4.1.1 Plant Biophysical Characteristics

We found that SOP analysis is an effective method to predict vegetation height, biomass, vertical and, seasonal degradation of dominate bulrush species. These relationships provide an effective monitoring regime as photography and image analysis supplement sampling, drying and weighing of vegetation. We were unable to predict stem density or stem diameter using image analysis; yet, we argue that with

minor modifications to field sampling (e.g. thinner swath of vegetation, etc.), SOPs could improve stem density/diameter predications. We suspect that our SOP analysis was unsuccessful in estimating stem density because BOFL and BOMA have significant leaf material.

We used SOP data to assess vertical biomass/ surface area changes within the canopy (Figure 11). Leaves, stems and trapped vegetation material (broken stems) influence both surface area and biomass at our SOP sites. For example, the lower region, <25 cm, is influenced by trapped vegetation debris (broken stems from current and previous years) and exhibits a steep decline in biomaterial with height (Figure 11a-b). The mid region, 25 cm through 50 cm, is dominated by stem material for the current growing season and showed a lesser decline in plant material with height (Figure 11a-b). The high region, > 50 cm, is likely influenced by leafy material and showed stable plant material with increasing height (Figure 11a-b). BOMA sites were often co-dominated with SCAM and have a nuanced pattern compared to BOFL because SCAM does not have leaves in the mid to upper canopy (Figure 11a-b).

We suspect this loss of plant material in higher canopy in the Mid-Marsh to be a factor of: 1) the loss of leaf material; 2) the codominance of SCAM; 3) a larger influence of wave energy and stem breakage because BOMA dominant Mid-Marsh serves as the marsh edge during the winter season.

4.1.2 Seasonal Changes

Our seasonal SOP analysis showed a steady decline in vegetated pixels whereas biomass appeared relatively stable until February (Figure 12). Our seasonal vertical image analysis showed that the upper (>50 cm) canopy tended to lose plant material before the lower canopy (Figure 13). These patterns indicated a steady loss of leaf material through the winter months, concordant with our field observations. Thereby, stems were the dominant source of biomass and surface area during the late winter and early spring months.

If other workers continue research and monitoring efforts with the SOP analysis within similar wetland environments, we recommend a few alterations to the above methods: 1) Reduce the width of the photographed segment to 10 cm instead of 20 cm used in this study. We are confident that stem count and diameter can be calculated if the photographed segment thinner to reduce overlapping vegetation. 2) Lemien et al. (2015) and Rogers et al. (2015) incorporated a mirror at a 45-degree angle to produce a less destructive and more efficient method to capture plant characteristics. This method would provide a larger dataset (several images per site) that would be enough to validate the method and to predict characteristics at other sites. 3) Our study focused on the High, Mid and Low-Marsh. If this method is used to estimate biophysical characteristics that drive wave attenuation, we would recommend a focused sampling regime on the vegetation cover likely to be the most effective at attenuating energy, Mid Marsh in our case. At PSB, the Low-Marsh may attenuate wave energy when present; however, Low-Marsh is mostly decomposed by early November and not likely to influence winter erosion events.

4.2 Elasticity:

We argue that most wave attenuation occurred below 50 cm canopy height because: 1) there was more resistance to bending within the plants (Figure 15 e-f) and; 2) there was greater biomass and surface area during our study (Figure 11). The BOFL and BOMA exhibited strong, seasonally-insensitive, logarithmic relationships between bending strength and bending height (Figure 15 e-f). These logarithmic relationships may indicate two types of deformation, 1) internal deformation as the stem bends and 2) flexion at a basal pivot point. We suspect that internal deformation was dominant at angles lower than 30 degrees and/or at higher measurement heights (>75 cm), where deformation increases with no perceptible increase in bending force. For example, the force required to bend a stem is negligible (approx. 0g) at 100 cm for BOFL and 60 cm for BOMA, independent of season. Bending

strength and breakage was sensitive to cold temperatures because a November field investigation with freezing temperatures yielded anomalously high number of stems breaking (Figure 14).

The type of deformation is important because it is related to the amount of friction and potential wave attenuation. If the vegetation deforms with little resistance, then it will impose little friction; whereas, rigid stems would produce more friction to reduce wave energy. Therefore, at some critical angle and plant height, less than 30 degrees and lower then 75 cm, bulrush stems deform by flexion around a pivot instead of internally. At this point, stems physically resist the motion of water instead of attenuating flow through increased surface area. These measurements are discussed as analogy to force inflicted on a stem by water, we recognize that the two values may not be interchangeable. Water flowing through stems produces a force on all submerged vegetation not a single stem.

If future studies continue this work, we recommend pairing the elasticity measurements with wave sensor data. Wave sensor data would quantify wave attenuation for these vegetation assemblages and be able to relate wave attenuation with the strength of plants.

4.3 Remote Sensing:

4.3.1 Maximum-Likelihood Classification (MLC)

Our Maximum Likelihood Classification (MLC) acceptably delineated High-Marsh (75%) and Non-Marsh (85+%) cover types; however, Mid-Marsh (BOFL (41%) and BOMA (44%)) and the Low Marsh (49%) classified poorly. The High-Marsh and Non-Marsh cover types classified well because they have distinct spectral signatures (Appendix 2). The Mid-Marsh, arguably the most important in regards to winter wave hazard mitigation, required further analysis (DTC) and increased accuracy.

We suspect that this error within the Mid and Low-Marsh cover types is due to: 1) Very similar spectral signatures between bulrush species (Figure 5). For example, BOMA and BOFL being nearly identical plant

species, separated only by height, have statistically indistinguishable spectral signatures (Figure 5). 2) Plant species present in multiple assemblages. Being that SCAM is a dominant species in both the Low and Mid-Marsh assemblages, our MLC had difficulty separating the assemblages based on spectral signature. 3) By September, when the CASI imagery was taken, plant material has been coated with sediment. This sediment cover may have biased the spectral signatures. For example, Low-Marsh (SCAM dominated) tended to be misclassified with bare sediment (Figure 16; Table 3), indicating that sediment coating or thin plant cover (Figure 2) is biasing the SCAM spectral signature towards sediment. These mixed classes can be quite difficult to classify based only on spectral signature; especially if sediment makes up one cover type and covers the other.

4.3.2 Decision Tree Classification

Our DTC successfully improved the overall accuracy of our classification to 77%, 10% above the MLC, by focusing on the marsh cover-types. Mid-Marsh subclasses, BOFL (66%) and BOMA (47%), still classified poorly; however, did see the largest improvements. Moreover, we combined Mid-Marsh subclasses and improved the producer's accuracy up to 67%.

Mid-Marsh subclasses accuracies were increased by the incorporation of the LiDAR Bare Earth DEM (BE-DEM) data through the DTC. The Mid-Marsh is statistically distinguishable from the High and Low-Marsh cover-types (Table 1). Therefore, by incorporating this data we isolate wrongly classified High and Low-Marsh pixels and appropriately classify them as Mid-Marsh. Mid Marsh subclass (BOMA and BOFL) accuracy remain low, in part, because their ranges in the LiDAR BE dataset have considerable overlap (Table 1).

Here, we used the BE-DEM for our DTC. We found this data to be biased within marsh cover-types by ~0.40 m the assumed true elevation taken with RTKGPS (Appendix 1). A DEM corrected for the vegetation could potentially yield better results. We argue that a correction for the BE-DEM is not

necessary for this study because the bias is a product of elevation, stem height and desity. The biased BE-DEM has the potential to be a positive influence on our classification by increasing accuracy because vegetation species had more distinctive height ranges rather than elevation ranges (Table 1).

4.3.3 Biomass

Our model reasonably predicted biomass because of spatial patterns agree with our field observations, correlate with Fuller's (2015) categorical vegetation cover data, and exhibit similar spatial patterns as reported in the literature. Schalles et al (2013) and Hladik et al. (2013) found that marshland biomass was greatest at the marsh edge and along tidal channels due to higher sediment delivery and retention. Our biomass model predicts this pattern particularly in the northern zones (Figure 17).

Our predicted biomass showed a weak relationship with Fuller's (2015) categorical stem density data (Figure 19). Similarly, our SOP data showed a similar weak relationship between stem density and biomass (Figure 9). We suspect that this weak relationship is because of other biomaterial (leaves, dead stems, etc) that were present in biomass data but not accounted for in stem density measurements.

Were this analysis to be continued or expanded, we recommend a larger sampling size of biomass samples to provide a more statistically robust dataset to extrapolate biomass and account for interclass heterogeneity. We would focus on Mid and Low-Marsh because of their potential wave attenuation.

4.4 Port Susan Bay Marsh Structure and Vulnerability

To assess the relative spatial and temporal variability in biomass related to seasonal changes in species distribution and structure, we developed a normalized biomass metric mapped by marsh vegetation zone. The full summer biomass extent for each pixel of classified marsh was normalized by the highest biomass value found to create a relative biomass comparison across the study area. To explore the seasonal influences of senescence and SCAM deterioration, we then adjusted the lower marsh biomass

and mid-marsh biomass by 100% and 50%, respectively, to represent SCAM die-back that occurs across these zones. The resulting analyses show the biomass structure that can attenuate flow and waves relative to the maximum biomass in the system and the spatially explicit change through the early winter (Figure 20).

The normalized biomass map shows that large areas of the Low and Mid-Marsh generally exhibit 50 % of the biomass characteristic of the upper marsh. Areas like the north end of the marshes and central study area have cross-shore reaches of only 200-300 m with biomass only 15- 25% of the highest biomass in the system found can buffer waves approaching shore. By December and March, biomass in these areas decreases sufficiently to leave only 25-50% of the summer maximum biomass extent.

We observe that the largest decrease in biomass, 25% of summer maximum and a 50 m decrease in cross shore reaches, occurs within the BOMA Mid-Marsh in the regions north of the restoration area (Figure 20). In these vulnerable northern reaches BOFL Mid-Marsh and High Marsh are likely to be influential for decreasing daily erosive hydraulic energy and promote sediment retention and elevation gain in the later winter months (Jan- Mar).

Last, we coalesced our understanding of vegetation biophysical and wetland structural variability into a conceptual potential wave attenuation model (Figure 21). With this model we predict rapidly decaying SCAM (Low-Marsh) contributed to bed roughness and BOMA dominated Mid-Marsh produced hydraulic friction responsible for the highest wave attenuation during the early monsoon season (November and December). We hypothesize that as SCAM was fully incorporated into the tidal flat and BOMA dominated Mid-Marsh became patchy and sparse, BOFL dominated areas became critical for flow attenuation during the later portion of the monsoon season and early spring (December through March). According to our elasticity and vertical biomass studies, we estimated that the highest elasticity and biomass occurs within the first 50 to 75 cm of vegetation canopy from the marsh floor, BOMA and

BOFL respectively (Figure 13 and 15). This information indicates that BOFL would serve an important role to attenuate flow during storm events with high water level and, BOMA remains the most critical species for mitigating daily erosion.

5 Conclusions

Through this study, we isolated emergent plant biophysical characteristics (plant height, biomass, stem density and, stem diameter) using horizontal digital photographic methods described here as Side-on Photos (SOP). We found this methodology to be helpful in quantifying plant characteristics and investigating the seasonal degradation of bulrush species. We found our SOP analysis able to predict plant height and biomass (Kendall's Tau p-value 1.8×10^{-5} for both); while, stem diameter and stem density showed a weak relationship when comparing lab to image data (Kendall's p-value 0.04 for both).

SOPs were helpful to identify seasonal degradation patterns. Co dominant BOMA/SCAM sites showed an abrupt decrease in surface area by November; however, these sites did not show a significant decrease in biomass until February owing to SCAM's relatively low biomass. Mid-Marsh assemblages maintained their biomass until February when BOMA and BOFL stems became brittle tended to break.

We extrapolated marsh biomass across the delta through the experimentally defined relationship between elevation, Red Edge NDI and biomass samples. We validated our biomass analysis through a comparison with Fuller's (2015) categorical percent cover data. We found that the BOMA Mid-Marsh tended to exhibit higher biomass within the first 20 m of the marsh edge.

We successfully mapped biophysically distinct wetland assemblages using MLC and DTC classifications and achieved an overall accuracy of 77%. Our MLC did not capture the extent of plant assemblages owing to sediment coating, mixed pixels and similar spectral signatures. We integrated elevation (BE-DEM) and NDVI data using conditional statements in a DTC analysis and, improved the accuracy of our mapped assemblages by up-to 21% (BOFL).

BOMA dominated Mid-Marsh served as the winter marsh edge that is the first vegetation to come in contact with wave energy. SCAM dominated Low-Marsh decayed into the tidal flat by Mid November, whereas, Mid Marsh assemblages (both BOMA and BOFL dominated) maintained rigidity and density until degrading begins in February 2015. As such, BOMA dominated Mid-Marsh is likely to have the greatest influence on wave attenuation, in particular, the first 20 m where biomass is greatest. Generally, BOFL had more material strength, is taller, covered a higher elevation range, formed denser patches, had more biomass per stem, and trapped more basal debris than BOMA. BOFL likely played a significant role in wave attenuation during large storm events when erosive waves reach the higher elevations and later months as BOMA became sparse. Potential wave attenuation is likely to be greatest when wave-heights are between 50 and 75 cm above the marsh floor; because, the lower section of the canopy (<75 cm) contains the highest biomass/surface area and is where stems exhibit the highest structural strength.

Seasonal wetland structure and potential wave attenuation variability is critical information for coastal planners that seek a sustainable, low-impact alternative to protect coastlines and natural resources against increasing coastal hazards associated with SLR. Our conceptual model qualifies the current conditions and potential wave attenuation within Port Susan Bay. This information can be used to parameterize coastal flooding and wave models to quantify wetland protective services.

6 Works Cited

Anderson, M.E., and Smith, J.M., 2014, Wave attenuation by flexible, idealized salt marsh vegetation: Coastal Engineering, v. 83, p. 82–92, doi: 10.1016/j.coastaleng.2013.10.004.

Augustin, L.N., Irish, J.L., and Lynett, P., 2009, Laboratory and numerical studies of wave damping by emergent and near-emergent wetland vegetation: Coastal Engineering, v. 56, p. 332–340, doi: 10.1016/j.coastaleng.2008.09.004.

Chen, Q., and Zhao, H., 2012, Theoretical Models for Wave Energy Dissipation Caused by Vegetation: Journal of Engineering Mechanics, v. 138, p. 221–229, doi: 10.1061/(ASCE)EM.1943-7889.0000318.

Collins, B., and Sheikh, A., 2005, Historical reconstruction, classification and change analysis of Puget Sound Tidal Marshes: Washington Department of Natural Resources: Aquatic Resources Division.

Delegido, J., Verrelst, J., Meza, C.M., Rivera, J.P., Alonso, L., and Moreno, J., 2013, A red-edge spectral index for remote sensing estimation of green LAI over agroecosystems: European Journal of Agronomy, v. 46, p. 42–52, doi: 10.1016/j.eja.2012.12.001.

Finlayson, D., 2006, The geomorphology of Puget Sound beaches.: Puget Sound Nearshore Partnership, Washington Sea Grant Program, University of Washington 2006-02.\

Freeman, G.E., Rahmeyer, W.H., and Copeland, R.R., 2000, Determination of resistance due to shrubs and woody vegetation: DTIC Document.

Fresh, K., Dethier, M., Simenstad, C., Logsdon, M., Shipman, H., Tanner, C., Leschine, T., Mumford, T., Gelfenbaum, G., and Shuman, R., 2011, Implications of Observed Anthropogenic Changes to the Nearshore Ecosystems in Puget Sound. Prepared for the Puget Sound Nearshore Ecosystem Restoration Project. Techni-cal Report 2011-03: Cover photo: Washington Sea Grant,.

Fuller, R., 2015, Stillaguamish Estuary Monitoring Report Summary: Western Washington University.

Grossman, E., and Curran, C., In-Review, Sediment Transport Processes in Response to Estuary and Salmon Recovery Efforts and the SR530 (Oso) Landslide, Port Susan Bay, Washington 2013-2015: 2015-XXXX.

Hladik, C., Schalles, J., and Alber, M., 2013, Salt marsh elevation and habitat mapping using hyperspectral and LIDAR data: Remote Sensing of Environment, v. 139, p. 318–330, doi: 10.1016/j.rse.2013.08.003.

Hutchinson, I., 1988, The Biogeography of the Coastal Wetlands of the Puget Trough: Deltaic Form, Environment, and Marsh Community Structure: Journal of Biogeography, v. 15, p. 729, doi: 10.2307/2845336.

Jones, J., Swanson, F., Wemple, B., and Snyder, K., 2001, Effects of Roads on Hydrology, Geomorphology, and Disturbance Patches in Stream Networks: Conservation Biology, v. 14.

Kirwan, M.L., Guntenspergen, G.R., D'Alpaos, A., Morris, J.T., Mudd, S.M., and Temmerman, S., 2010, Limits on the adaptability of coastal marshes to rising sea level: ECOGEOMORPHIC LIMITS TO WETLAND SURVIVAL: Geophysical Research Letters, v. 37, p. n/a–n/a, doi: 10.1029/2010GL045489.

Koch, E.W., Barbier, E.B., Silliman, B.R., Reed, D.J., Perillo, G.M., Hacker, S.D., Granek, E.F., Primavera, J.H., Muthiga, N., Polasky, S., Halpern, B.S., Kennedy, C.J., Kappel, C.V., and Wolanski, E., 2009, Non-linearity in ecosystem services: temporal and spatial variability in coastal protection: Frontiers in Ecology and the Environment, v. 7, p. 29–37, doi: 10.1890/080126.

Lemein, T., Cox, D., Albert, D., and Mori, N., 2015, Accuracy of optical image analysis compared to conventional vegetation measurements for estimating morphological features of emergent vegetation: Estuarine, Coastal and Shelf Science, v. 155, p. 66–74, doi: 10.1016/j.ecss.2014.12.051.

Mendez, F., and Losada, I., 2004, An empirical model to estimat the propagation of random breaking and nonbreaking waves over vegetation fields: Coastal Engineering, v. 51, p. 103–118.

Moller, I., 2006, Quantifying saltmarsh vegetation and its effect on wave height dissipation: Results from a UK east coast saltmarsh: Estuarine, Coastal and Shelf Science, v. 69.

Moffett, K.B., and Gorelick, S.M., 2013, Distinguishing wetland vegetation and channel features with object-based image segmentation: International Journal of Remote Sensing, v. 34, p. 1332–1354, doi: 10.1080/01431161.2012.718463.

Mullarney, J.C., and Henderson, S. H., 2010, Wave-forced motion of submerged single stem vegetation: Journal of Geophysical Research, v. 115, doi: 10.1029/2010JC006448.

Rogers, J.N., Parrish, C.E., Ward, L.G., and Burdick, D.M., 2015, Evaluation of field-measured vertical obscuration and full waveform LiDAR to assess salt marsh vegetation biophysical parameters: Remote Sensing of Environment, v. 156, p. 264–275, doi: 10.1016/j.rse.2014.09.035.

Schalles, J., Hladik, C., Lynes, A., and Pennings, S., 2013, Landscape Estimates of Habitat Types, Plant Biomass, and Invertebrate Densities in a Georgia Salt Marsh: Oceanography, v. 26, p. 88–97, doi: 10.5670/oceanog.2013.50.

Seliskar, D., Gallagher, J., 1983, The ecology of tidal marshes of the Pacific Northwest coast: A community profile: U.S. Fish and Wildlife Service.

Shepard, C.C., Crain, C.M., and Beck, M.W., 2011, The Protective Role of Coastal Marshes: A Systematic Review and Meta-analysis (J. Clifton, Ed.): PLoS ONE, v. 6, p. e27374, doi: 10.1371/journal.pone.0027374.

Simenstad, C., Ramirez, M., Burke, J., Logsdon, M., Shipman, H., Tanner, C., Toft, J., Craig, B., Davis, C., Fung, J., Bloch, and Fresh, K., 2011, Histoical Change and Impairment of Puget Sound Shorelines: Atlas and Interpretation of Puget Sound Nearshore Ecosystem Restoration and Analysis: Puget Sound Nearshore Ecosystem Restoration Project 2011-01.

Small, C., and Nicholls, R.J., 2003, A global analysis of human settlement in coastal zones: Journal of Coastal Research,, p. 584–599.

Tabor, R. W., Booth, D. B., Vance, J. A., and Ford, A. B., 2002, *"Geologic Map of the Sauk River 30- by 60- minute quadrangle, Washington"*, U.S. Geological Survey, Miscellaneous Investigations map I-2592, 2 sheets and pamphlet, scale 1:100,000.

Tackenberg, O., 2006, A New Method for Non-destructive Measurement of Biomass, Growth Rates, Vertical Biomass Distribution and Dry Matter Content Based on Digital Image Analysis: Annals of Botany, v. 99, p. 777–783, doi: 10.1093/aob/mcm009.

Thom, R., and Hallum, L., 1990, Long-term changes in the areal extent of tidal marshes, eelgrass meadows and kelp forests of Puget Sound.: University of Washington, Wetland Ecosystem Team, Fisheries Research Institute, School of Fisheries.

Yang, S.L., Shi, B.W., Bouma, T.J., Ysebaert, T., and Luo, X.X., 2011, Wave Attenuation at a Salt Marsh Margin: A Case Study of an Exposed Coast on the Yangtze Estuary: Estuaries and Coasts, v. 35, p. 169–182, doi: 10.1007/s12237-011-9424-4.

Zehm, A., Nobis, M., and Schwabe, A., 2003, Multiparameter analysis of vertical vegetation structure based on digital image processing: FLORA, v. 198, p. 142–160, doi: 10.1078/0367-2530-00086.

7 Tables

Table 1. Elevation and NDVI statistics for primary bulrush species and bare sediment. These values are derived from the training ground truth points with a 5 meter radius around ground truth points. Data includes north zone south zone and the restoration site. Note: the elevation statistics for this study were derived from the 2014 Bare Earth LiDAR DEM. We estimate the BE DEM to over predict the marsh floor elevation by approximately 0.4 m on average (Appendix 1). All elevation and tidal ranges provided here are in NAVD88.

	LiDAR Bare-Earth DEM				NDVI				Elevation (Fuller (2015))			
	min	max	mean	SD	min	max	mean	SD	min	max	median	SD
BOFL	2.31	3.47	2.76	0.26	0.037	0.711	0.328	0.173	-	-	-	-
BOMA	1.48	3.14	2.41	0.36	-0.003	0.6.75	0.217	0.117	1.7	2.7	2.2	-
SCAM	0.48	2.76	1.74	0.46	-0.358	0.438	0.105	0.092	1.2	1.99	1.6	-
Tide Flat	0.96	2.91	1.69	0.33	-0.034	0.398	0.050	0.047	**MHHW**	**MHW**	**MSL**	-
Tides	-	-	-	-	-	-	-	-	2.77	2.50	1.37	-

Table 2. Statistics of the elasticity regression analysis of BOFL and BOMA. Regressions use measurement height (X) to derive bending force (Y) to 30 degrees with respect to month.

BOFL

30 degrees			
	Equation	Adj-r^2	P-value
All	ln(Y) = -1.48*ln(X) + 9.57	0.64	2.20E-16
Oct	ln(Y) = -1.60*ln(X) + 10.29	0.75	2.20E-16
Nov	ln(Y) = -1.08*ln(X) + 7.35	0.52	2.20E-16
Dec	ln(Y) = -1.63*ln(X) + 10.25	0.76	3.41E-16
Jan	ln(Y) = -1.53*ln(X) + 10.11	0.66	2.20E-16
Feb	ln(Y) = -1.53*ln(X) + 9.97	0.66	8.61E-14
Mar	ln(Y) = -1.39*ln(X) + 9.10	0.63	3.02E-16

BOMA

30 degrees			
	Equation	Adj-r^2	P-value
All	ln(Y) = -1.44*ln(X) + 8.46	0.46	2.20E-16
Oct	ln(Y) = -1.17*ln(X) + 7.28	0.19	4.37E-02
Nov	ln(Y) = -1.37*ln(X) + 8.11	0.57	2.20E-16
Dec	ln(Y) = -1.37*ln(X) + 8.23	0.47	3.96E-12
Jan	ln(Y) = -1.48*ln(X) + 7.83	0.47	1.53E-09
Feb	ln(Y) = -1.27*ln(X) + 8.15	0.26	3.36E-05
Mar	ln(Y) = -1.48*ln(X) + 8.91	0.42	9.11E-10

Table 3. Confusion Matrix of Maximum Likelihood Classification (MLC). Values are in number of pixels and accuracies are in percent. Each GPS ground truth point was converted into a circle polygon with a radius of 5 m and thus represent approximately 80 pixels.

	Testing Ground Truth Areas									
MLC	Blackberries	Beachwood	Trees	High-Marsh	Bare	BOFL	BOMA/SCAM	SCAM	Total	User's Accuracy (%)
Blackberries	1746	7	20	-	-	-	-	-	1773	98.5
Beachwood	17	1087	-	59	-	-	22	4	1189	91.4
Trees	6	-	279	1	-	-	-	-	286	97.6
High-Marsh	34	127	2	1567	3	237	209	69	2248	69.7
Bare	-	-	-	7	2418	25	298	560	3308	73.1
BOFL	-	45	9	283	25	665	220	74	1321	50.3
BOMA/SCAM	-	-	-	170	26	531	1199	310	2236	53.6
SCAM	-	-	-	5	446	54	994	971	2470	39.3
Total	1803	1266	310	2092	2918	1512	2942	1988	14831	
Producer's Accuracy (%)	96.8	85.9	90.0	74.9	82.9	44.0	40.8	48.8		
Overall Accuracy (%)	**67.0**									

Table 4. Confusion matrix of Decision Tree Classification (DTC). Values are in number of pixels and accuracies are in percent. Each GPS ground truth point was converted into a circle polygon with a radius of 5 m and thus represent approximately 80 pixels.

	Testing Ground Truth Areas									
DTC	Blackberries	Beachwood	Trees	High-Marsh	Bare	BOFL	BOMA/SCAM	SCAM	Total	User's Accuracy (%)
Blackberries	1746	7	20	-	-	-	-	-	1773	98.5
Beachwood	17	1087	-	59	-	-	22	4	1189	91.4
Trees	6	-	279	1	-	-	-	-	286	97.6
High-Marsh	34	127	2	1564	-	237	209	69	2248	69.6
Bare	-	-	1	8	2622	12	242	545	3308	79.3
BOFL	-	45	3	317	-	993	223	6	1321	75.2
BOMA/SCAM	-	-	5	115	25	270	1385	130	2236	61.9
SCAM	-	-		28	271	-	861	1234	2470	50.0
Total	1803	1266	310	2092	2918	1512	2942	1988	14831	
Producer's Accuracy (%)	96.8	85.9	90.0	74.8	89.9	65.7	47.1	62.1		
Overall Accuracy (%)	**73.6**									

Table 5 Confusion matrix of Decision Tree Classification (DTC) where Mid-Marsh classes (BOMA and BOFL dominated) have been combined. Values are in number of pixels and accuracies are in percent. Each GPS ground truth point was converted into a circle polygon with a radius of 5 m and thus represent approximately 80 pixels.

	Testing Ground Truth Areas								
DTC	Blackberries	Beachwood	Trees	High-Marsh	Bare	Mid-Marsh	SCAM	Total	User's Accuracy (%)
Blackberries	1746	7	20	-	-	-	-	1773	98.5
Beachwood	17	1087	-	59	-	22	4	1189	91.4
Trees	6	-	279	1	-	-	-	286	97.6
High-Marsh	34	127	2	1564	-	446	69	2242	69.8
Bare	-	-	1	8	2622	254	545	3430	76.4
BOMA/SCAM	-	45	8	432	25	2871	136	3517	81.6
SCAM	-	-		28	271	861	1234	2394	51.5
Total	1803	1266	310	2092	2918	4454	1988	14831	
Producer's Accuracy (%)	96.8	85.9	90.0	74.8	89.9	64.5	62.1		
Overall Accuracy (%)	**76.9**								

Table 6. Estimates of the areal extent and biomass of cover types from the DTC land-cover analysis.

		Biomass Analyses				
Cover Type	**Area (sq-m)**	**Total Biomass (mT)**	**Min (kg/sq-m)**	**Max (kg/sq-m)**	**Mean (kg/sq-m)**	**STD (kg/sq-m)**
High Marsh - undifferentiated	**1.02E+06**	**1083.78**	**-**	**64.46**	**1.06**	**0.44**
Mid Marsh	**1.58E+06**	**925.30**				
BOFL	5.36E+05	315.67	0.12	3.35	0.59	0.25
BOMA/SCAM	1.04E+06	609.62	0.10	5.42	0.59	0.16
SCAM	**1.42E+06**	**1108.22**	**0.09**	**17.47**	**0.78**	**0.32**
Bare - undifferentiated	**2.42E+06**	**1377.47**	**-**	**103.86**	**0.57**	**0.24**
Other	**1.08E+05**	**149.42**				
Blackberries	3.76E+04	81.61	0.14	5.00	2.18	0.67
Beachwood	5.47E+04	35.50	-	57.58	0.65	1.27
Trees	1.60E+04	32.32	-	8.34	2.05	0.78
Total Study Area	**6.55E+06**	**4644.19**				

8 Figures

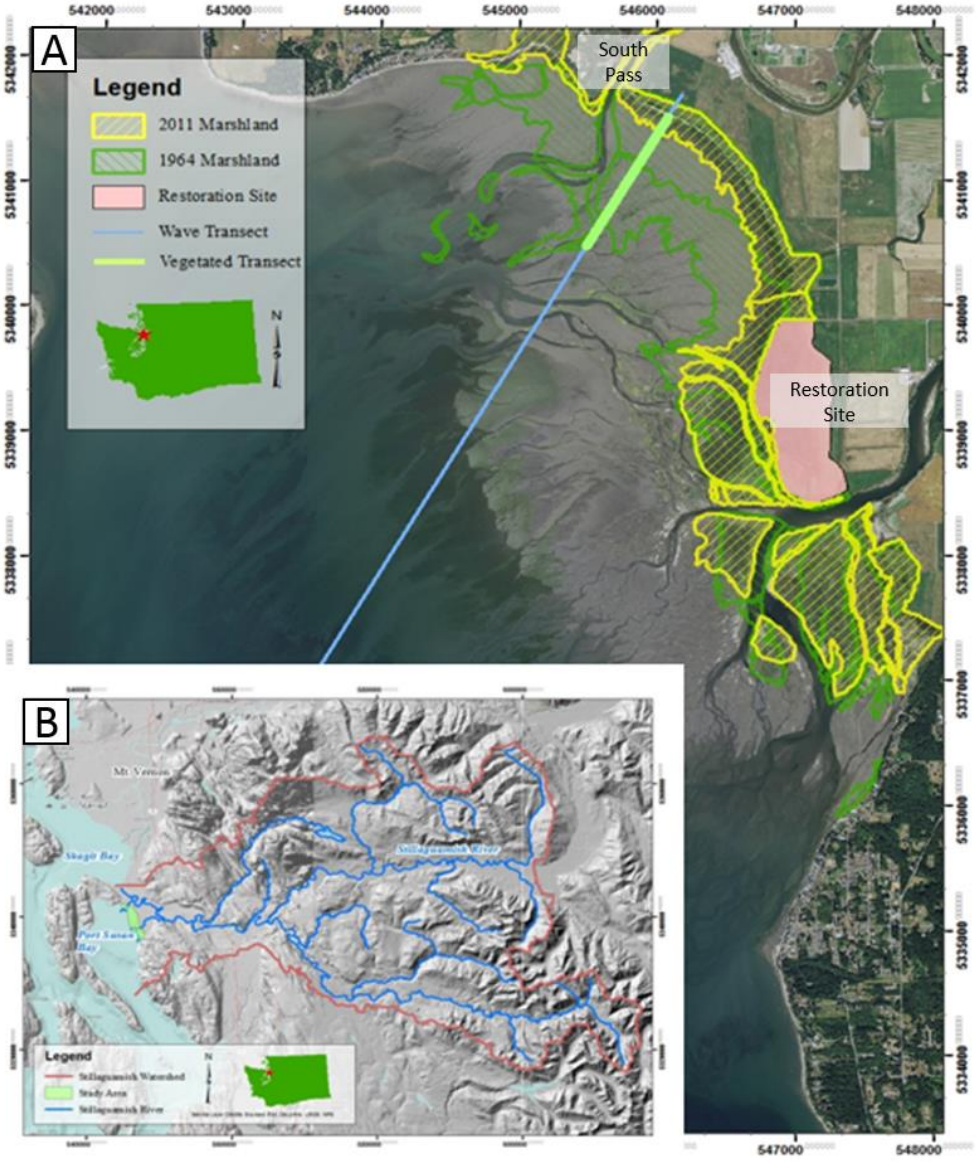

Figure 1. Map showing study area of Port Susan Bay. A) Historical wetland extent (yellow, 2011; green ,1964) reconstructed from aerial photography and indicates up to 1km of marsh retreat since 1964 (Grossman and Curran, in review). Also shown is a representative cross-shore transect (blue line) of predominant wave approach with extent that historical vegetation of 1964 would influence wave energy reaching northern PSB. Pink area represents a recent restoration effort by The Nature Conservancy. B) Reference map detailing the extent and topography of the Stillaguamish River catchment.

Figure 2. Annotated picture of channel bank on southern island. Shows SCAM dominated Low-Marsh interclass heterogeneity (mixed cover-types) with respect to stem density. This image shows a mixed cover-type (SCAM with bare sediment) and a non-mixed cover-type (SCAM).

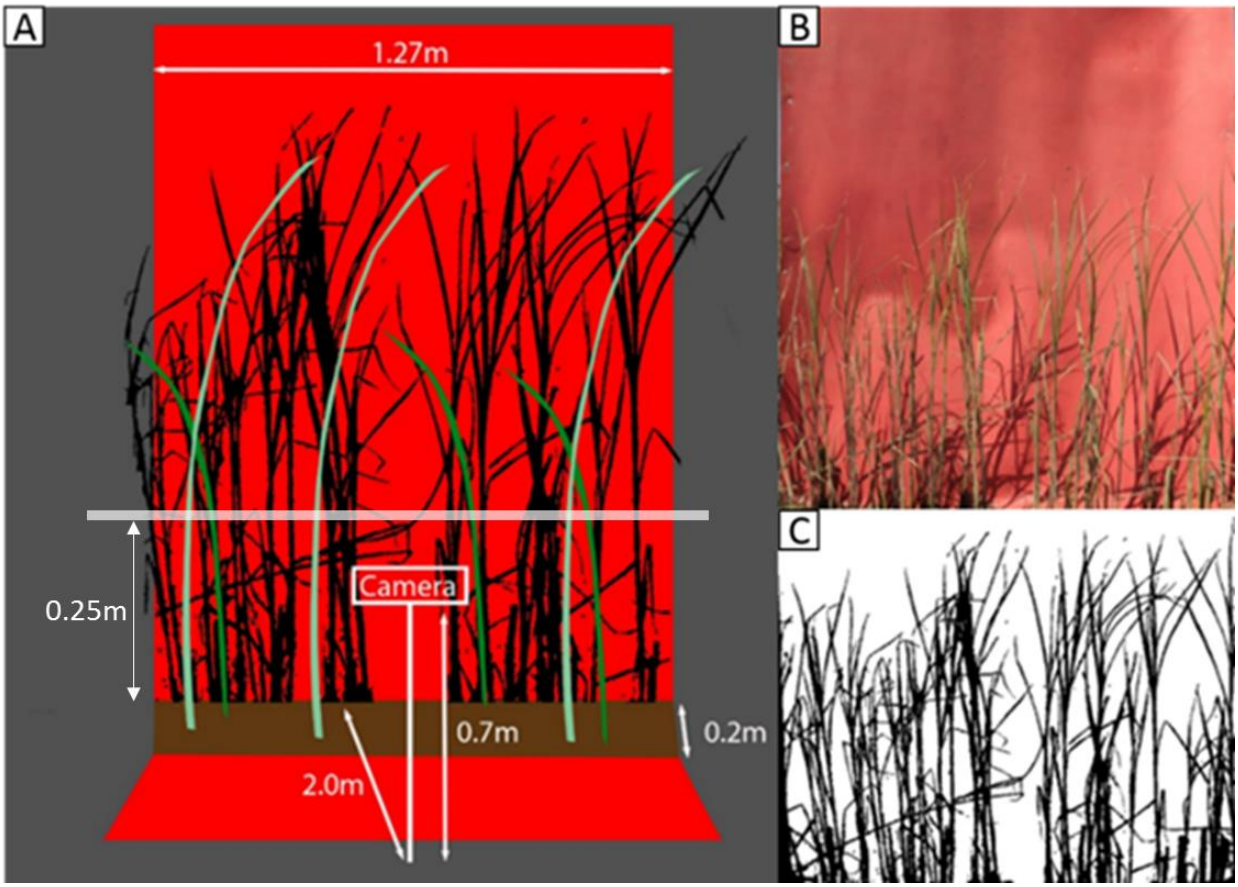

Figure 3. A) Schematic of Side-On Photo setup. Representative strip of vegetation was sectioned off (0.2 m by 1.3 m) vegetation with a red backboard (~2 m x 1.27 m) and a red tarp on the ground surface. Camera was centered 2 m from the backboard at a

height of 0.7 m. Stem density was assess using a 1 cm tall row of pixels at 0.25 m above the marsh floor. B) Unaltered image of emergent bulrush (BOMA) to be processed through ENVI and SideLook (VESTA) C) Binary image of bulrush (BOMA) used for processing in SideLook.

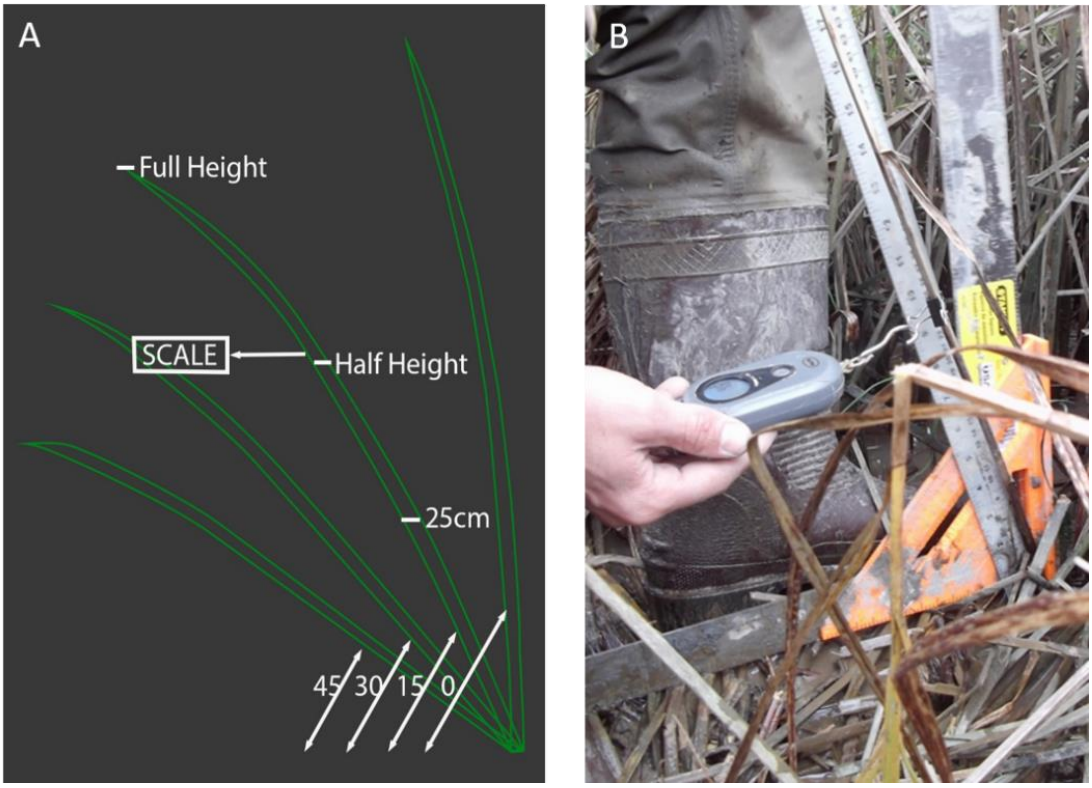

Figure 4. A) Schematic of in-situ elasticity measurements. Each stem had a total of 9 measurements: 3 heights (height, half height and, 25 cm) by 3 angles (15, 30, 45 degrees measured from initial position) measurements. Initially stems were approximately vertical (~90 degrees) from the marsh surface. B) Photo of data collection.

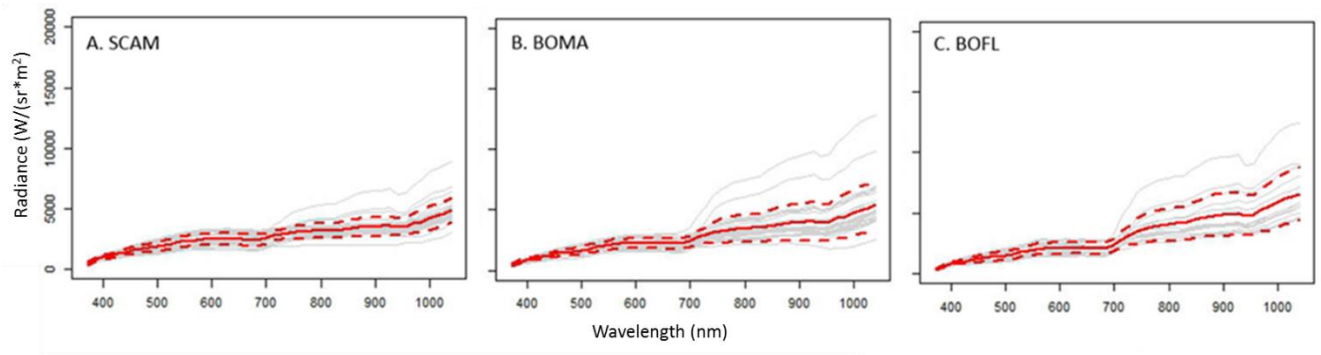

*Figure 5. Spectral signatures for emergent Mid-Marsh vegetation species: A) SCAM (*Schoenoplectis americanus*); B) BOMA (*Bulboschoenus maritimus*), C) BOFL (*Bulboschoenus fluviatilis*). Solid red line is the mean spectral signature; dashed redlines are one standard deviation; solid light gray lines are individual spectral signatures. Note: CASI spectral signatures are the average for a defined region of interest. There may be some misclassified BOFL spectral signatures as BOMA. At the beginning of this study, BOFL and BOMA were considered the same species.*

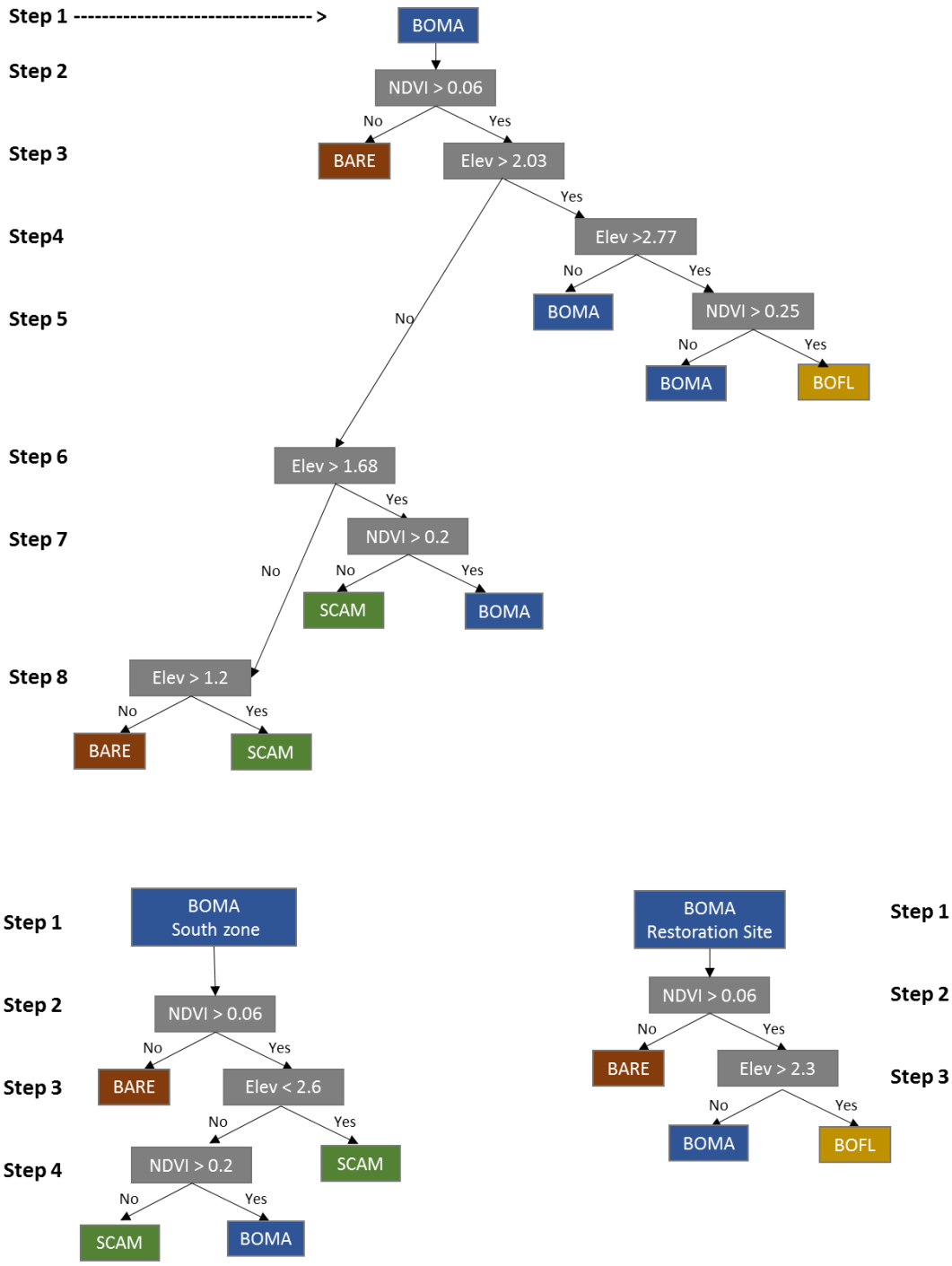

Figure 6. Decision Tree diagrams to isolate BOFL. Decision trees were initially created using data in Table 1 for the north zone, where a pixel would only be reclassified if it fell out of the standard deviation of two or more classes. Decision trees were altered to account for spatially dependent elevation (South Zone and Restoration Site) (Appendix 3).

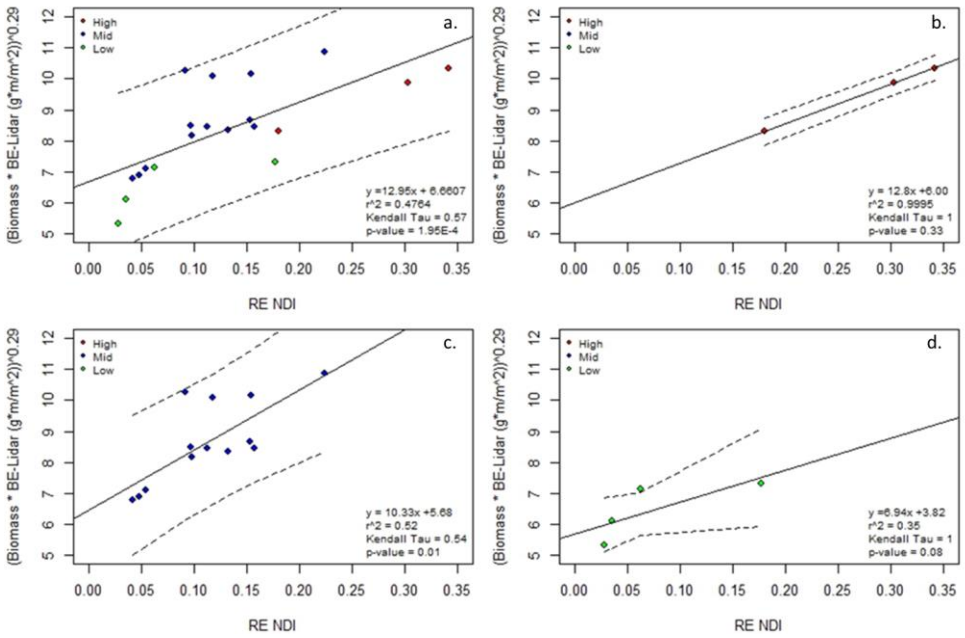

Figure 7. Plots detailing the linear model fit from the transformed biomass, elevation data, and Red-Edge Normalized Difference Index (RE NDI). A) Scatterplot detailing model for all marsh assemblages. These data are correlated with a Kendall's Tau =0.5789 and p-value = 0.00019. Our linear model: $Y = [12.96(X) + 6.6607]^{1/0.29}$ has an adjusted $r^2 = 0.4764$. Red, blue and green points represent High, Mid and, Low-Marsh respectively. Dashed lines represent 95% confidence. Figure 7b – d are scatterplots and linear regressions of isolated High, Mid and, Low-Marsh assemblages, respectively.

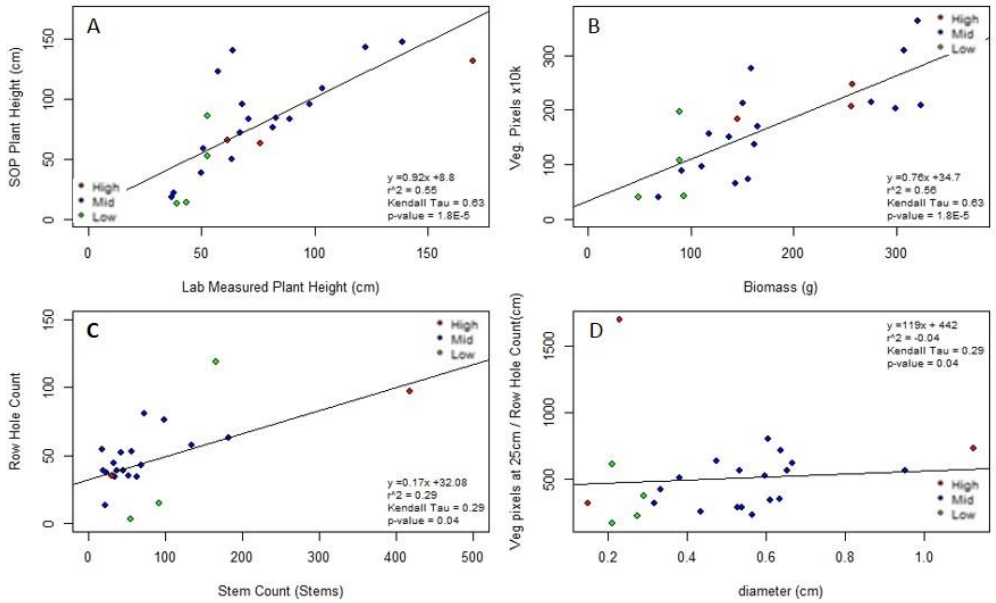

Figure 8. shows several comparisons of SOP derived parameters to lab measured values. a) Plot detailing the relationship between Mean-Max Vegetated pixels, the averaged maximum of vegetated pixels of a SOP image, with lab-measured average plant height excluding plant fragments. b) Scatter plot comparing total vegetated pixels with lab measured biomass. c) Scatterplot showing Row-Hole Count, contiguous white space between vegetated pixels for a 1 cm row of pixels at 25 cm above the marsh floor, compared to lab measured stem count. d) Scatter plot comparing the ratio of vegetated pixels at 25 cm above the marsh floor over Row Hole Count with respect to measured stem diameter.

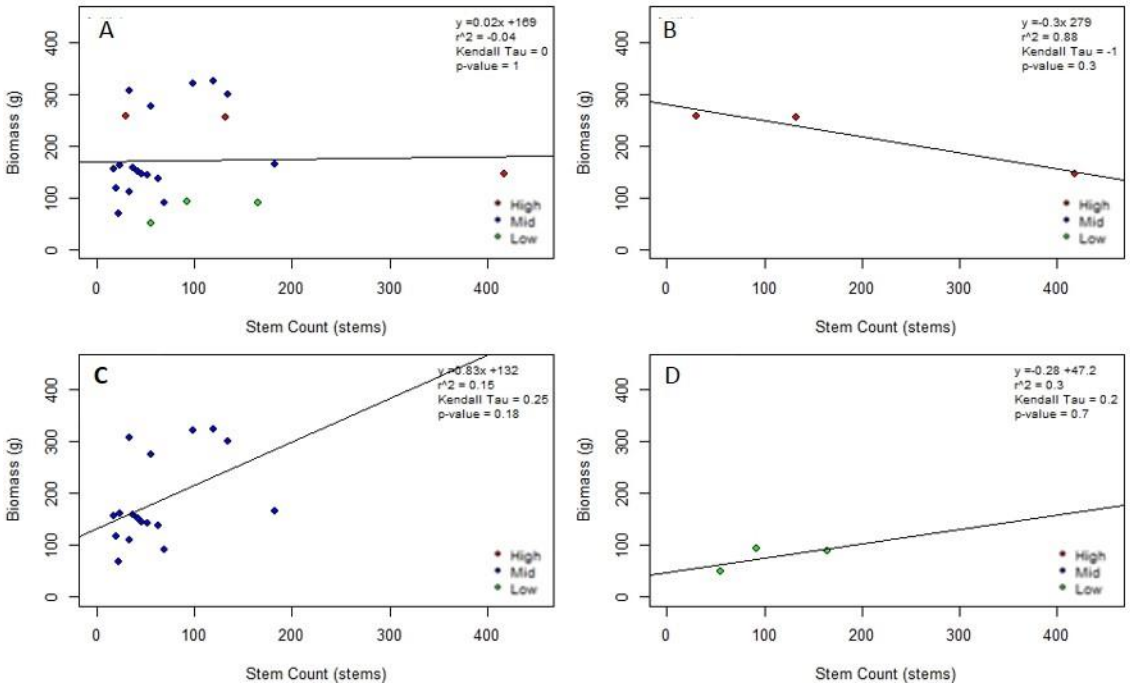

Figure 9. Plots comparing lab measured biomass to lab measured stem count with respect to assemblage. A) shows biomass with respect to stem count for combined marsh assemblages; B) High-Marsh assemblage; C) Mid-Marsh assemblage; D) Low-Marsh assemblage.

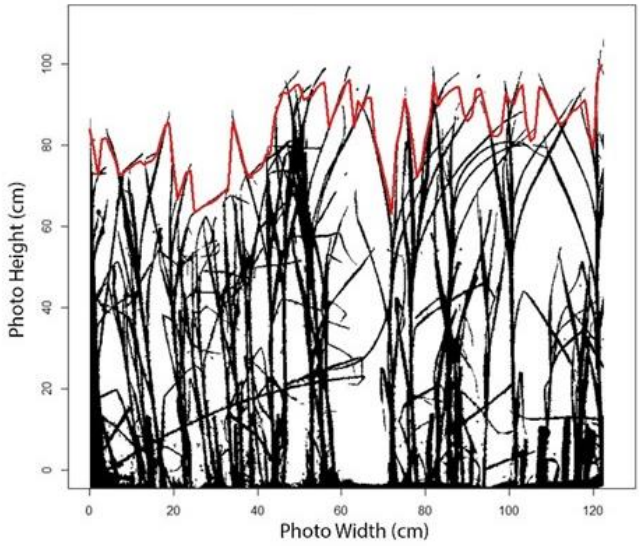

Figure 10. Plot showing the average plant height by the width of the photograph. Height is averaged for every 1 cm column. Binary image underlain the plot shows qualitative accuracy. Data is from Site 002, a BOMA dominated Mid-Marsh site, Located at the marsh edge in the northern study area.

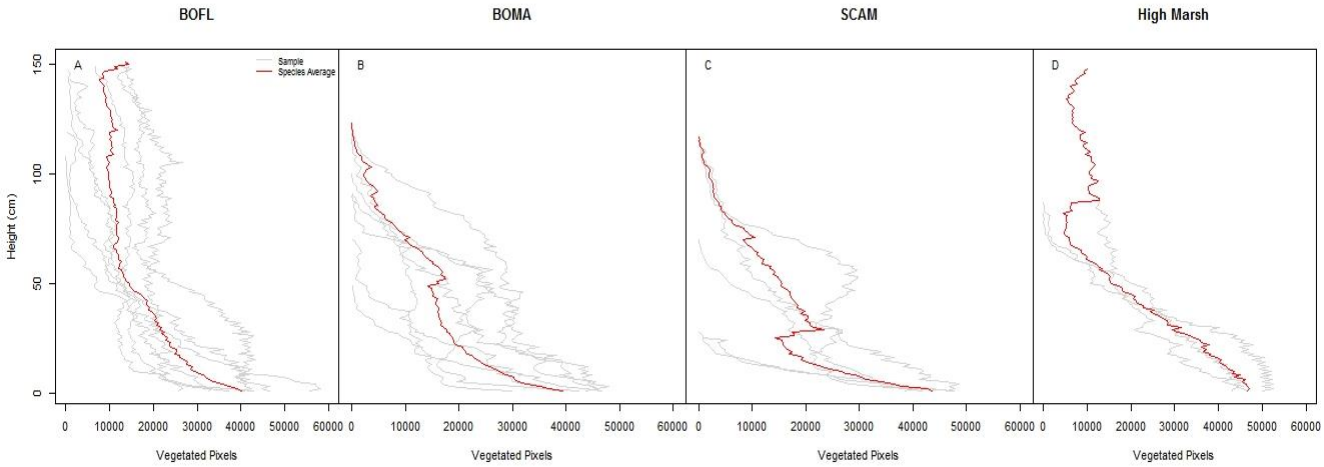

Figure 11. Plots detailing vertical biomass, using vegetated pixel count per 1 cm row as analog, with respect to assemblage/dominant species. Grey lines show data from a single SOP image; red lines describe the average of all SOP images separated by cover-type: A) BOFL; B) BOMA; C) SCAM, D)High-Marsh, respectively.

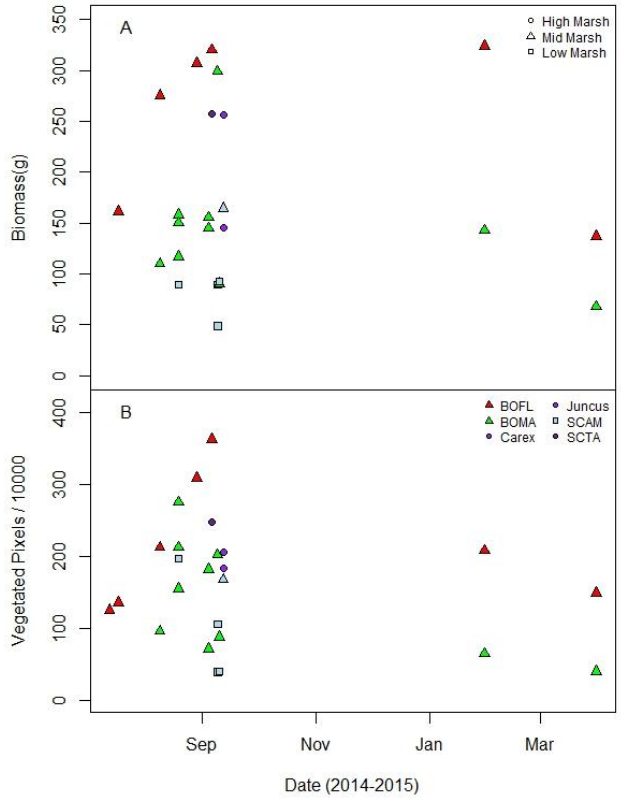

Figure 12. Temporal analysis of (A) biomass and (B) SOP vegetated pixels through the sampling season, Fall 2014 to Spring 2015.

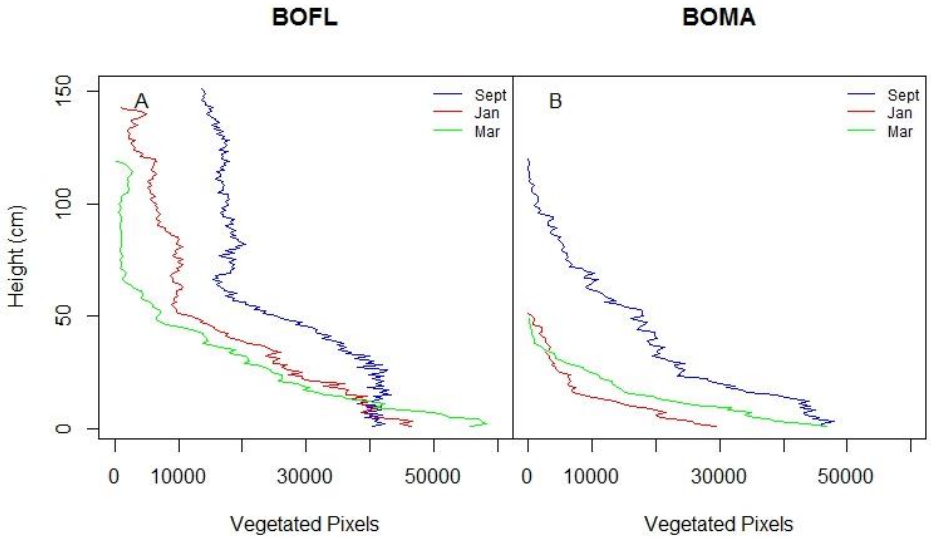

Figure 13. Seasonal changes in vertical vegetation structures at elasticity measurement sites (Site 22 and 20; BOFL and BOMA respectfully): A) BOFL cover-type; B) BOMA cover-type.

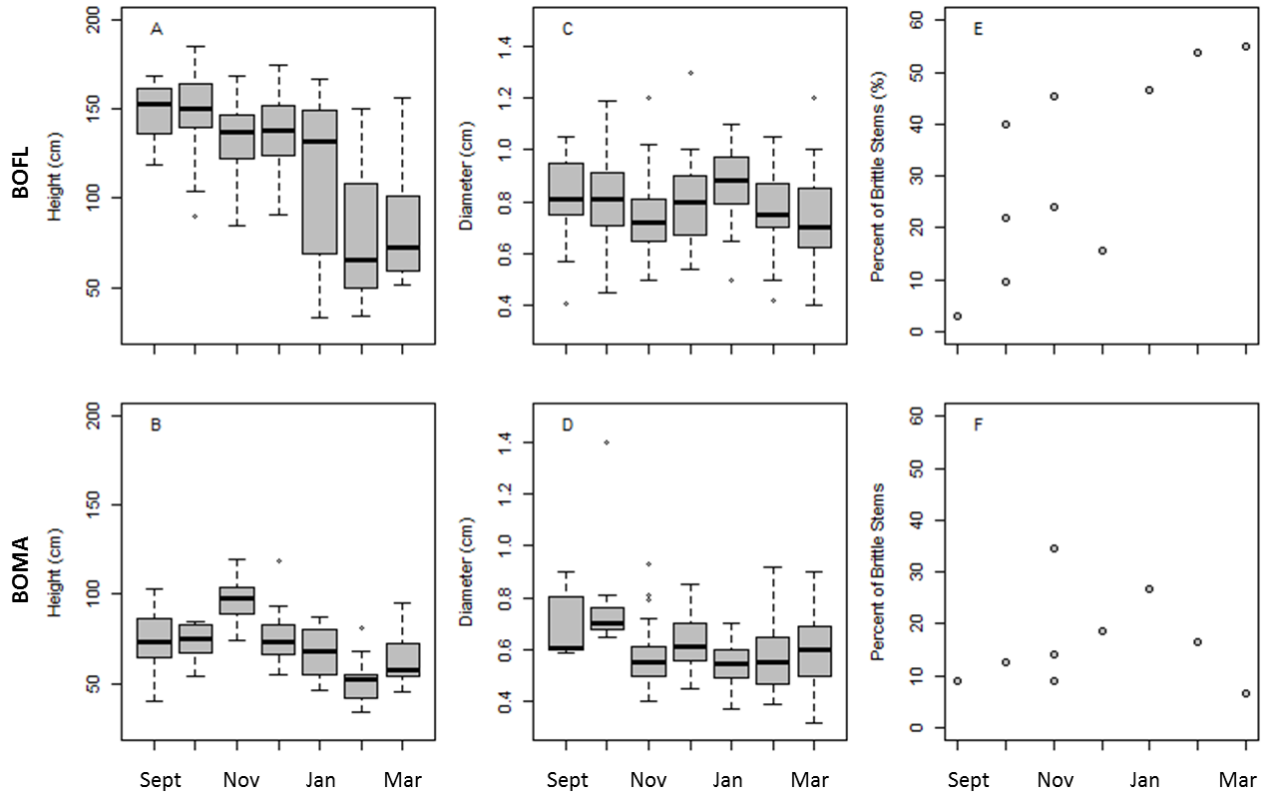

Figure 14. Temporal changes in plant characteristics height, diameter and brittleness for BOMA (Site 20) and BOFL (Site 22). Data was collected biweekly to monthly beginning in September through March. A) Boxplot detailing monthly changes in plant height for BOFL; B) Boxplot detailing monthly changes in plant height for BOMA; C) Boxplot of monthly stem diameter in BOFL;

D) Boxplot of monthly stem diameter for BOMA; E) Percent of BOFL stems that broke during elasticity measurements by month; F) Percent of BOMA stems that broke during elasticity measurements by month.

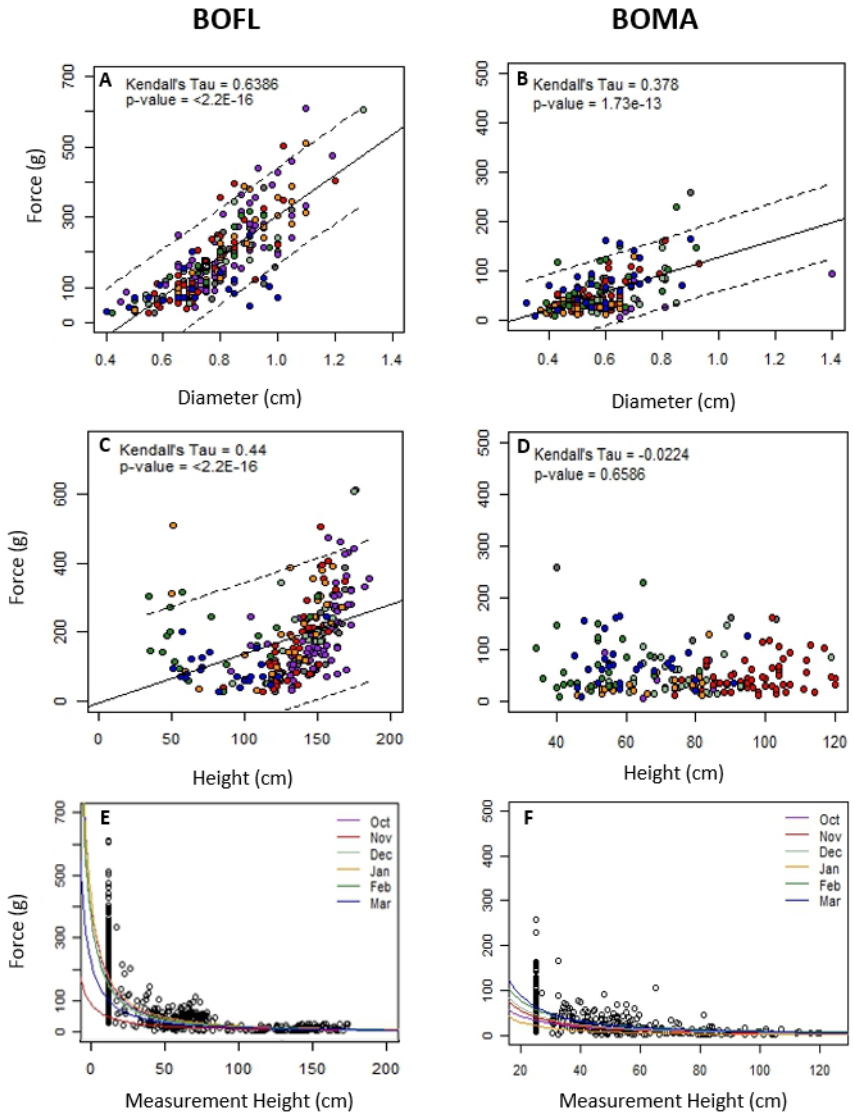

Figure 15. Plots detailing the seasonal relationships of force (at 25 cm to 30 degrees) to diameter, total plant height and measurement height (contains force data for plant height, half height, and 25 cm bent to 30 degrees) in both BOFL and BOMA. A) Scatter plot of bending force vs stem diameter for BOFL; B) Scatter plot of bending force vs diameter in BOMA; C) Scatter plot of bending force with respect to total stem height in BOFL; D) Scatter plot of bending force with respect to total stem height in BOMA; E) Scatter plot of bending force as a function of measurement height by month in BOFL; F) Scatter plot of bending force as a function of measurement height by month in BOMA. October(purple), November (red), December (pale green), January (dark yellow), February (dark green), March (blue). See Appendix 6 for a more detailed analysis of the elasticity data.

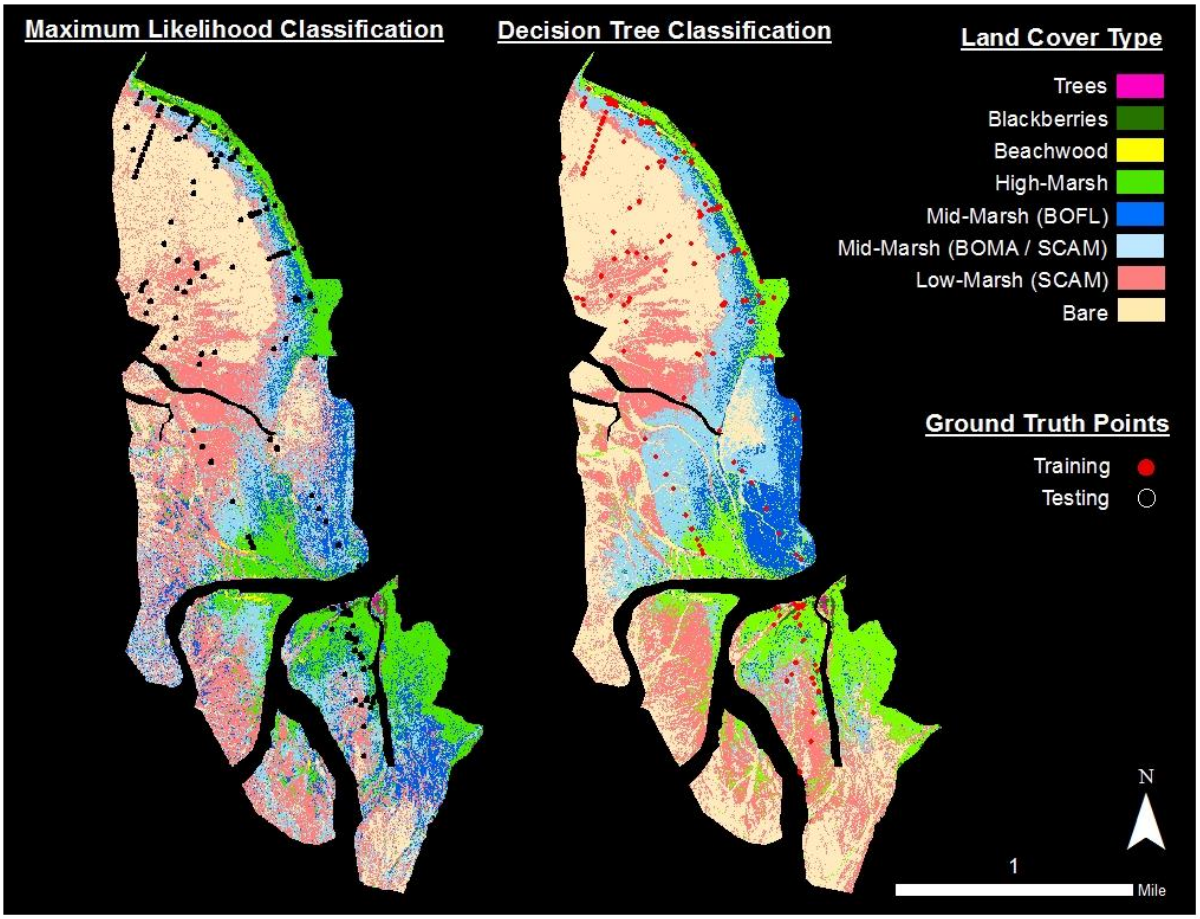

Figure 16. Maps of Maximum Likelihood Classification (MLC) and Decision Tree Classification focused on isolating bulrush species. Black and Red dots represent ground truth points with a 5-meter buffer.

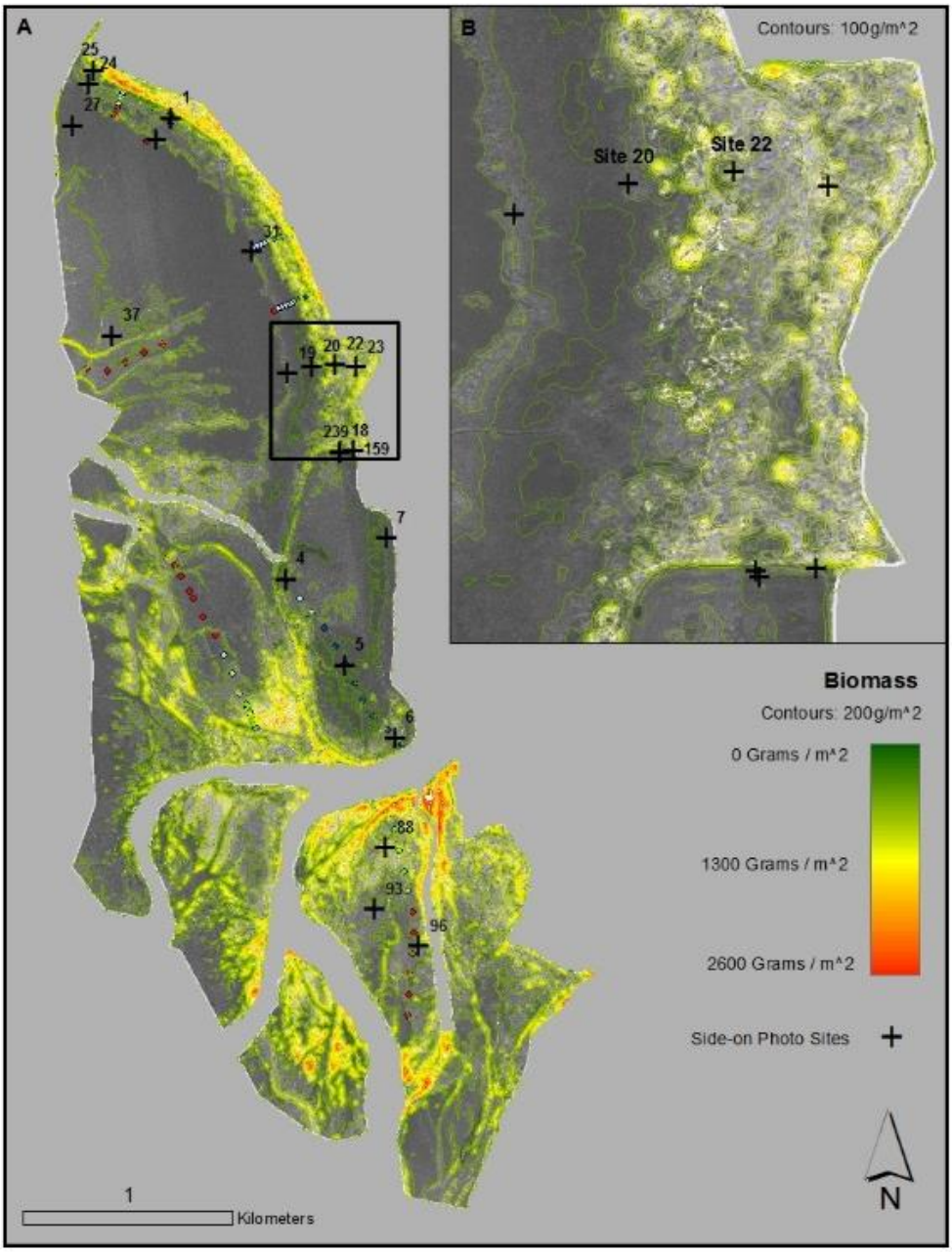

Figure 17. Map displaying the biomass grid and contours derived from the linear model (Eqn. 3). This map shows relative biomass per square meter across the emergent vegetation defined by the DTC (Figure 3). Maximum biomass is shown here as 2.6kg/m², this is over two standard deviations above the mean for High-Marsh (Table 5). Our model predicts values up to ~100kg/m² that are anomalous or for non-marsh cover-types (Table 5). High-Marsh vegetation sampling points were taken from clumps of Juncus, Carex, and softstem bulrush where the majority of the High-Marsh assemblages is dominated by low (0.1 to 0.5 m high) grass species. This may lead to an over estimate of biomass within the High-Marsh.

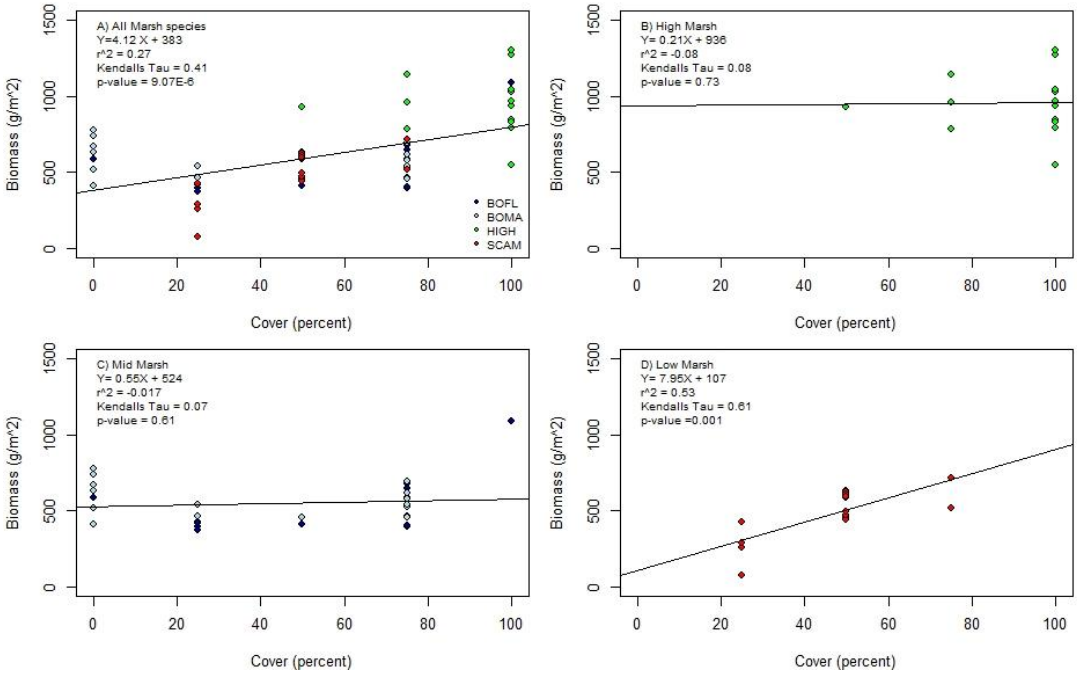

Figure 18. Validation analysis for estimated biomass spatial extrapolation by comparison with Fuller's (2015) categorical percent cover data. We dissected the data by marsh assemblage: A) All marsh assemblages; B) High-Marsh assemblage; C) Mid-Marsh assemblage; D) Low-Marsh assemblage.

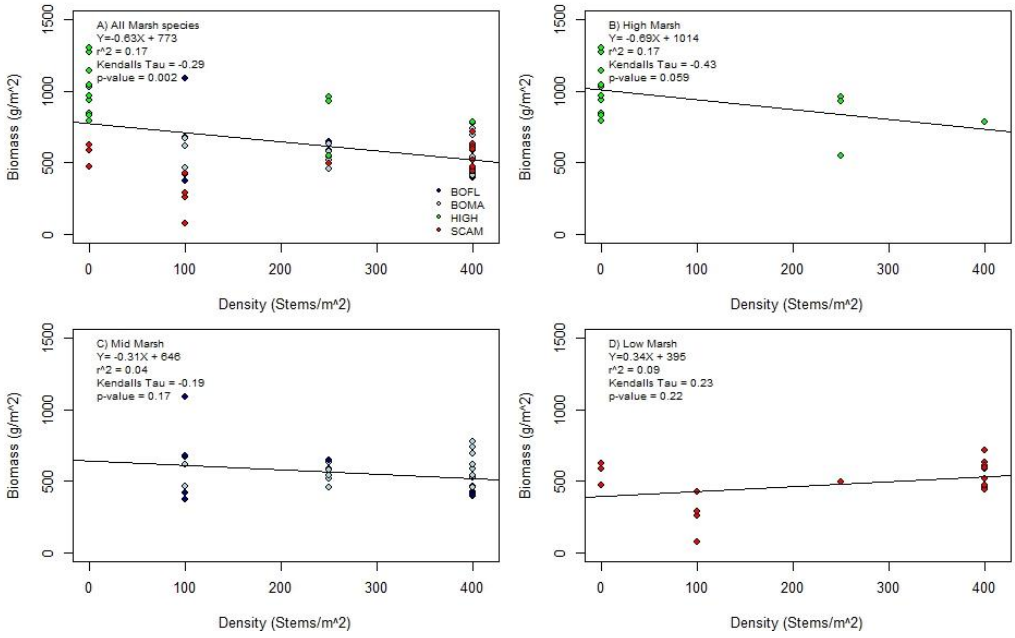

Figure 19. Validation analysis for estimated biomass spatial extrapolation by comparison with Fuller's (2015) categorical stem density data. We dissected the data by marsh assemblage: A) All marsh assemblages; B) High-Marsh assemblage; C) Mid-Marsh assemblage; D) Low-Marsh assemblage.

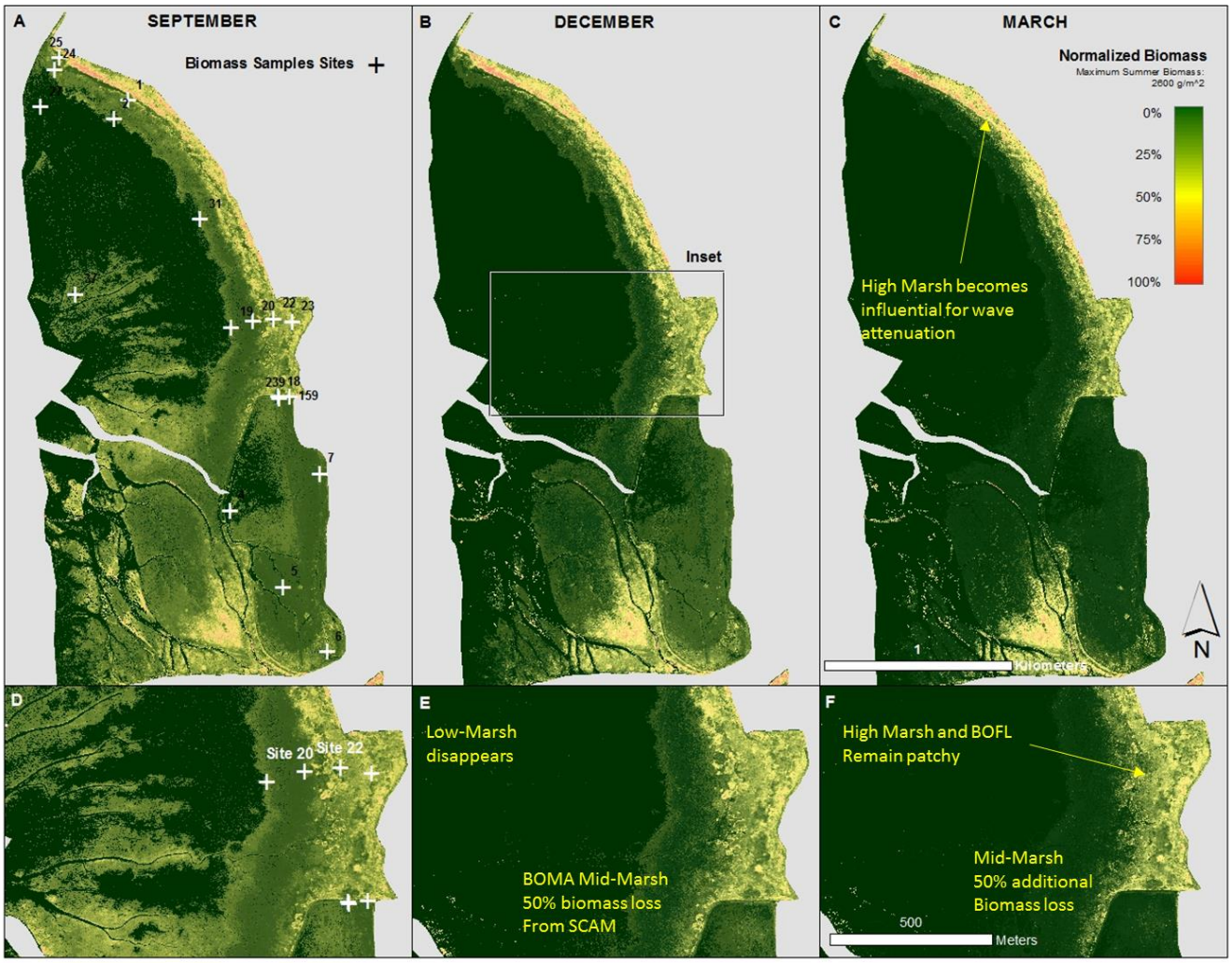

Figure 20. A) Map displaying the normalized biomass grid derived from the linear model (Eqn. 3) for peak biomass (September) normalized by the biomass maximum. Maximum biomass is shown here as 2.6kg/m^2, this is over two standard deviations above the mean for High-Marsh. Our model predicts values up to ~100kg/m^2 that are anomalous or for non-marsh cover-types. High-Marsh vegetation sampling points were taken from clumps of Juncus, Carex, and softstem bulrush where the majority of the High-Marsh assemblages is dominated by low (0.1 to 0.5 m high) grass species. This may lead to an over estimate of biomass within the High-Marsh. B) Our estimate biomass conditions for December where SCAM has fully degraded and been incorporated into the marsh floor. Here we assume the Low-Marsh is comprised of 100% SCAM and the Mid Marsh 50% SCAM. C) Our estimates for March biomass. Here we assume that BOMA and BOFL have lost approximately 50% of their peak biomass from data presented in Figure 12. Therefore, BOMA dominated Mid-Marsh is 25% of September estimates.

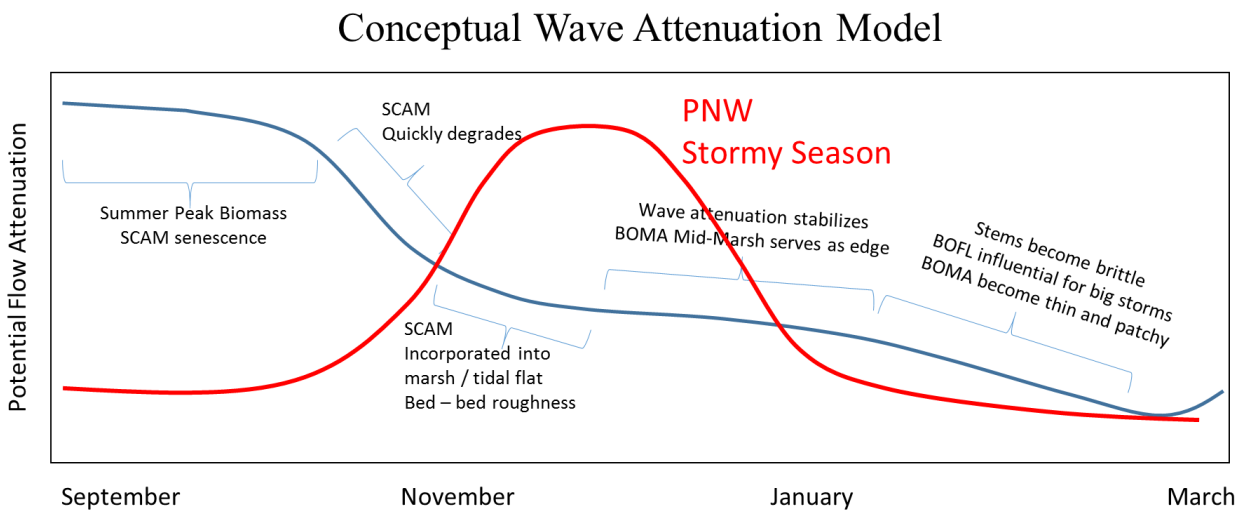

Figure 21. Conceptual wave attenuation model detailing seasonal and spatial wetland variability. Blue line shows relative seasonal wave attenuation responding to vegetation biophysical changes. Potential wave attenuation represents seasonal decreases in biomass. Here, 100% of SCAM biomass has been incorporated into the tidal flat by December which results in a 100 and 50% loss in biomass in the Low and BOMA dominated Mid-Marsh by December. After December the BOMA Mid Marsh and continues to degrade slowly and is reduced to 25% of peak biomass by March. Red line shows contemporary and idealized monsoon season for the Pacific Northwest (PNW) and our study area, where the study area receives the majority of the erosive storm events during November through January.

Chapter 2

Title: Winter sediment dynamics in a Pacific Northwest tidal marsh, Port Susan Bay: role of vegetation

Keywords:

Tidal marsh, sedimentation, vegetation, flow attenuation, Puget Sound, Port Susan Bay

Abstract:

The role of coastal or estuarine vegetation is conceptually understood to provide protective services such as wave attenuation, sediment retention, flood-water storage, etc. Information quantifying the extent that they protect shorelines through flow attenuation and sediment retention is valuable to resource managers interested in utilizing wetlands as "green infrastructure." Some studies have found that wave energy decreases exponentially with distance across marshlands and varies with site morphology and species-specific plant characteristics (Yang et al., 2011). Sediment deposition may exhibit similar patterns; however, sediment, geomorphic and habitat models seldom integrate site-specific biophysical plant parameters into change analyses. Our goal is to investigate sediment dynamics with respect to vegetation assemblage to characterize: 1) the rate, distribution and composition of sediment deposits; 2) effectiveness of wetlands to retain sediment; 3) contribution to the sediment budget of sediment coated vegetation; 4) suspended sediment dynamics and availability, e.g. tidal channels, along shore and cross-shore, and their relationship with river and wind patterns. Our study was conducted within a vulnerable Pacific Northwest estuary, Port Susan Bay in Washington State, where tidal marsh has retreated up to 1 kilometer over the past fifty years. Port Susan Bay serves as the mouth of the Stillaguamish River that was influenced by a catastrophic landslide, the Oso Mudslide (SR530 Landslide), in Marsh 2015 prior to this investigation. Results showed that the highest winter sediment deposition occurred in the High to Mid-Marsh boundary, up to 300 m inland of the marsh edge, where bulrush species were determined to have the highest biomass by an associated vegetation

study (Chapter 1). We estimated that sediment retained in the northern marsh is up to 2.5% of the total sediment delivered to the delta by the Stillaguamish river. Sediment coating vegetation may contribute up to 0.5% of the northern marsh sediment budget. Turbidity of a tidal channel is closely related to turbidity and discharge responses from the Stillaguamish River, the assumed primary sediment source. The northern marsh turbidity indicated an episodic and delayed (~2 days) sediment response to the river and showed relationships to regional winds that generate waves. Longshore turbidity patterns indicate that sediment is delivered uniformly to our study area. Cross-shore pattern exhibited an increase in turbidity inland corresponding to regions with the greatest deposition. Based on turbidity patterns, sediment trap data and field observations, we speculate that during the study (winter of 2014-15) hydraulic energy was high enough to erode the marsh edge, suspend sediment from associated tidal flat, and transport material approximately 300 m inland to the High/Mid-Marsh boundary. These results inform restoration efforts to restore marshland and associated sediment supply, as well as, the scientific understanding of marshland vulnerability and adaptability to climate change and sea-level rise.

1 Introduction and Background

Coastal lowlands provide many ecosystem services important to human populations, such as essential salmon habitat, productive agricultural land, and barrier for coastal hazards such as flooding events and erosion (Koch et al., 2009). Coastal wetlands have been shown to be important for buffering impacts to vulnerable lowlands by attenuating wave energy, encouraging shoreline stabilization and, allowing for flood water storage (Shepard et al., 2011). Human modifications, i.e. engineering and/or agricultural efforts, of coastal hydrology and sediment transport have resulted in a loss of wetland land-cover and protection within the Puget Sound (Bortelson, 1980). SLR projections, today's 100 year marine overwash event becoming a 10 yr event with 1 ft rise in sea level (Trebaldi, 2012), are leading coastal managers to consider alternative approaches to coastal protection. Within the pacific northwest (PNW), storm surges and coastal flooding are predicted to increase with SLR compounded by shifts in seasonal precipitation

patterns, peak stream discharge and, sediment delivery (Huppert et al., 2009). SLR and increased storm events amplify the need for effective and cost efficient engineering solutions to protect coastal communities and wetland resources (Shepard et al., 2011).

Coastal wetland restoration can be a long-term and cost-effective mitigation strategy to supplement (or replace) traditional engineered flood protection, i.e. levees and dikes (Shepard et al., 2011). Historically, estuarine habitat restoration was seldom considered in coastal protection planning because predictive models that evaluate vegetation protective-capacity require improved vegetation biophysical data. An improved understanding of the role and adaptability of estuarine wetlands can help guide decisions that protect and enhance ecosystem services.

Wetlands have been shown to accrete and migrate inland at a rate equal to SLR if supplied with sufficient sediment (Shepard et al., 2011); however, because of human modifications to stream flow, contemporary sediment delivery to wetlands today varies considerably from historical sediment loads (Curran et al. 2016; Czuba et al., 2011). Some streams deliver less sediment due to reservoir impoundment, others deliver more sediment due to fluvial and coastal engineering efforts (Grossman et al., 2011) and forest management practices (Jones et al., 2001). Important to marshes is the extent, connectivity and, retention of fluvial sediment affected by levees and shoreline armoring (Grossman et al., 2011). At the interface of terrestrial, marine and climatic forces, coastal wetlands play an integral role in coastal resilience because they attenuate flow, trap sediment and, adapt to local sea level changes. Here, we seek to understand the role and ability of wetland vegetation to retain sediment.

1.1 Site Description:

This study focused in the northern marsh regions of Port Susan Bay (PSB), a temperate estuary located in the Salish Sea of Washington State. PSB serves as the mouth and delta for the Stillaguamish River. The vulnerable PNW estuary that has experienced up to 1 kilometer of marsh loss (retreat) since 1964

(Figure 22). PSB was selected to investigate sediment deposition patterns within a dynamic wetland that has been the focus of restoration efforts (The Nature Conservancy), on-going sediment budget studies (Grossman and Curran, in review) and serves as an important environment for salmon resources and bird habitat. This study aims to isolate characteristics that enhance resilience and to help test the performance of the 2012 PSB estuary restoration to regain connectivity and sediment supply.

The Stillaguamish River begins in the North Cascades dominated by high-relief bedrock and, quickly reaches the Puget Lowlands dominated by glacio-fluvial and lahar deposits from Glacier Peak (Tabor et al., 2002). The associated watershed occupies approximately 1800km^2 where flow is dominated by rainfall and snowmelt (no glacial influence) with a mean annual discharge of approximately 85 m^3/s (3000cfs) (Grossman and Curran, in review).

Glacier Peak lahars have had a significant influence on the fluvial and deltaic morphology of the Stillaguamish River. The Sauk River is thought to have been diverted north to The Skagit River by a lahar dated at 5kya (Tabor et al., 2002) and, the formation of the deltaic fan is associated with Glacier Peak lahar deposits (Tabor et al., 2002). The Stillaguamish River valley recently came under national spotlight because of the tragic 2014 Oso Landslide that was sourced from a 300 m tall terrace of unconsolidated glacio-fluvial and lacustrine deposits. A recent study estimates that the catastrophic landslide increased the river's sediment load 50% during the first two years following the slide (Grossman and Curran, in review) likely increasing sediment load to the study area.

PSB experiences a temperate maritime climate with a winter monsoon season responsible for the majority of the ~30 in of mean annual precipitation and dry summers; temperatures remain temperate rarely dropping below freezing and above 80^{o}F (Grossman and Curran, in review). The dominant wind direction affecting the delta is from the south-southwest with a fetch of 35-50 km (Grossman and Curran

in review) (Figure 22). Tidal range and regime is generally mesomareal and semi diurnal for PSB with a tidal range from 2.44 m and -0.27 of MLLW.

PSB is dominated by three general marsh types that influence resilience:

1) High-Marsh is above Mean High Water (MHW) (>2.5 m NAVD88) and is dominated by graminoid (grass), sedge, and rush species. Inundation occurs during unusually high tides (Fuller, 2015).
2) Mid-Marsh exists below MHW (2.5 m > X > 2.0 m) and is dominated by bulrush species (Fuller, 2015). The Mid-Marsh plays a key role in winter sediment accumulation and wave attenuation because it serves as the winter marsh edge. Mid-Marsh is dominated by three bulrush species.
    a. BOMA (*Bulboschoenus maritimus*) – Hip to waist height (mean ~ 0.75 m), semi-rigid stems, ~3 bladed leaves up to 2ft in length.
    b. BOFL (*Bulboschoenus fluviatilis*) – Chest to head height (mean ~1.5 m), semi-rigid stems, ~3 bladed leaves up to 2.5 ft in length.
    c. SCAM (*Schoenoplectis americanus*) – Knee to hip height (mean ~0.5 m), semi-flexible stems, no significant leaves.

The Mid-Marsh is further separated into two sub categories:

    1. Upper Mid-Marsh is dominated by BOFL and creates a continuous band within the study area (between the restoration site and South Pass), the northern section of the delta (Fuller, 2015).
    2. Lower Mid-Marsh is co dominated (50-50) by SCAM and BOMA. The lower Mid-Marsh serves as the winter marsh edge.

3) The Low-Marsh (1.3 < X > 2 m) is dominated largely by SCAM and has low species richness (Fuller, 2015). Low-Marsh Vegetation density (78 ± 156 stems/m^2) varied widely with space and time

(Fuller, 2015). SCAM tended to be coated with sediment and showed signs of senescence by early fall (September) and had degraded into the marsh / tidal flat surface by winter (Mid-November).

2 Methods:

We used a combination of sediment tile traps, Sediment Erosion Bars (SEBs) and turbidity sensors to study accretion, particle size, erosion and suspended sediment dynamics respectively. These methods were employed along 5 cross-shore transects across the northern PSB to examine the role of vegetation on sediment retention patterns (Figure 22). Field work was conducted between December 2014 and April 2015. We defined the study area with a polygon that surrounded the sampling area. Seaward extent was defined by approximately 15 m southwest of the marsh edge. Landward extent was defined by the beachwood/ shrub boundary or grass dominated area. These definitions were adopted in order to isolate the Mid-Marsh as defined by Fuller (2015).

Transects numbered 1 through 5 (South to North) contained 5 sampling sites that were ecologically defined by wetland assemblage. Site 1 was located in the High-Marsh surrounded by grass-like plant species with sparse patches of BOMA or BOFL. Site 2 was located at the beginning of bulrush dominated marsh, often located in a BOFL patch. Site 3 was located in the center of the vegetated transect often co-dominated by SCAM and BOMA. Site 4 was placed 5 m inland of the marsh edge also co-dominated by SCAM and BOMA. Site 5 was located 10 m seaward of the marsh edge.

2.1 Sediment Traps:

Flat surface sediment traps provide information about the weight and type of material being deposited, e.g. sediment size, organic fraction. These sediment traps are a common method to measure sediment accumulation within tidally influenced wetlands (Steiger et al., 2003). This method involves the installation of tiles flush to the marsh surface (Nolte et al., 2013 and Steiger et al., 2003). On recovery, sedimentation rates can be estimated through the thickness and total weight accumulated (Nolte et al.,

2013 and Steiger et al., 2003). We used small detachable ceramic tiles (10 cm x 10 cm) anchored flush to the marsh surface with a 0.5 m length PVC pipe. Tile traps were deployed at each of the 25 sites. At each site 3 tiles were placed within a 0.25 m^2 area following protocols of Thomas and Ridd (2004). We used the roughened (bottom) surface of the tile to mimic a rough marsh surface. Sediment traps were installed between December 8 and 11 of 2014 and samples were collected between March 24 and April 3 of 2015. The median deployment time was 16 weeks (4 months).

We measured the thickness of sediment accumulation on the tiles during sampling; 3 measurements were taken per tile, 9 measurements were taken per site (3 tiles per site) and were averaged to estimate average sediment accumulation. We sampled the tile with the median deposit thickness at each site. If one or more of the tile traps were discarded due to breakage, the tile with the maximum amount of deposit was collected. Samples were marked, double bagged and sent to the USGS Pacific Coastal and Marine Science Center Sediment Lab for weight, organic fraction and sediment particle size analysis. All sampled traps were replaced for future monitoring projects. Tile trap data were extrapolated across the study area by Theissen Polygons and Inverse Distance Weighted (IDW) techniques, common methods to extrapolate point data across an area. Theissen Polygons divide an area into polygons based on the equidistance line between point data sources. Theiessen Polygons extrapolates data that point data is representative of the contiguous polygon. IDW algorithm generates a grid and through an algorithm interpolates cell values based on distance from the original point data source. Here we used the standard parameters within the ArcGIS 10.3 software: output cell size of 1 m, distance exponent of 2.

2.2 Vegetation Sampling

To quantify sediment trapped on vegetation, we collected plant samples during December 2014 and February 2015. Samples taken in December involved sampling the marsh edge sites (Site 4) for all transects and mid and upper marsh (Sites 3 and 1) on Transect 3. At each site, five stems (BOMA or BOFL) were selected, cut and bagged. December samples were carefully cut into 10 cm segments and

removed of leaves in the lab. For each site, a random subsample of five stem segments was chosen for analysis.

In February, repeat sampling was taken at Site 1, 3 and 4 for Transect 3. Similar to December, five stems were carefully cut and bagged. Stem samples were cut into 3 -10 cm long segments in the field: Low (marsh floor to 10 cm), Mid (20 cm to 30 cm), High (40 cm to 50 cm). February sampling required stem samples to be 50 cm tall or greater.

Inorganic sediment was isolated from organics through Loss on Ignition (LOI) where samples were burned in an anaerobic oven at 450^{o}C for 4 hours. Samples were left to dry for one week prior to burning. Samples were weighed (Mt), skinned (we removed outer layers to lessen combusting organic material; interior of stem samples were discarded), oven dried (100^{o}C) for 24 hours, weighed (Ms), burned and weighed (Mss) again. These samples should be a measure of the sediment accumulated on plant surfaces over the growing and wintering season.

We estimate the contribution of sediment that has accumulated on vegetation to the entire sediment budget using Equation 1. Sediment flux is a function of accumulated sediment (Mss), average height of vegetation(Ht), stem density(ρ_{Veg}), and assemblage area.

$$Sediment\ Flux\ \left(\frac{g}{m^2}\right) = Mss\left(\frac{g}{stem}\right) \times \frac{Ht(cm)}{10(cm)} \times \rho_{Veg}\left(\frac{stem}{m^2}\right) \quad \text{Eqn. 4}$$

2.3 Turbidity and Suspended Sediment Concentration:

The Suspended Sediment Concentration (SSC) in tidally inundated coastal wetlands represents the maximum potential sediment retained within a given marsh (Nolte et al., 2013). SSC is an important variable in calculating sediment budgets and parameterizing sedimentation models but, does not quantify deposition or net accumulation rates (Nolte et al., 2013). Optical turbidity sensors are able to measure continuous turbidity in the water column and rely on calibration to calculate SSC.

We conducted three deployments using YSI optical backscatter turbidity sensors (YSI 600 – 6138 series) (Table 7). The first deployment in February 2015 was conducted alongside a USGS maintained DTS-12 turbidity sensor. The DTS sensor had established the relationship between turbidity and the SSC at the USGS station at the channel entrance to the 2012 restoration site (Figure 23). This provided a means to develop a turbidity-SSC rating for the YSI based on correlation with the DTS-12. The second installment (March 1 through March 20) monitored variability in turbidity alongshore at the marsh edge (Site 4) on Transects 3 and 5 (Figure 23). The third installment (March 20 through April 18) monitored turbidity variability in the cross-shore direction from the marsh edge at Site 4, 3 and 1 on Transect 3 (Figure 23). All turbidity data was processed to remove data when the sensors were not submerged.

We compared our turbidity sensor data to wind data from four local weather stations. We analyzed wind average from Padilla Bay (PB), West Point (WP), Smith Island (SI) and Hein Bank (HB) weather stations (Figure 23).

2.4 Sediment Erosion Bars

We installed Sediment Erosion Bars (SEBs) to measure sediment deposition or erosion at two sites, Transect 3 Sites 4 and 5 (T3.4 and T3.5). SEBs were placed 15 m on either side of the marsh edge and included the installation of three vertical poles that form an equilateral triangle after Van Wijnen and Bakker (2001); where, a 1.5 m PVC is driven into the ground and leveled. The PVC poles serve as a base for a removable aluminum bar with equally spaced holes through which measurements are taken with a thin metal pin (Van Wijnen and Bakker, 2001) (Figure 24). Erosion or accretion was measured using a small pin inserted through predrilled holes in the top bar until they reached the marsh surface (Nolte et al., 2013). We chose SEBs over other sedimentation/erosion measurement techniques because they are cost-effective approaches and unlikely to alter the hydrodynamics (Nolte et al., 2013). SEBs were installed and measured in January 2015 and measured again in February and March 2015. SEBs can only detect changes greater the 0.5 cm in surface morphology.

3 Results

3.1 Sediment Budget

Our tile trap data showed that the greatest sediment deposistion occurs seaward of the Mid to High-Marsh transition at Sites 2 and 3 for most cross-shore transects (Figure 25). Longshore analysis of our data indicated that the majority of depostion occurs in the middle of the study area and lower deposistion at the north and south ends (Figure 25b). Overall deposits were composed of 97.4% detrital fines (< 0.0625 mm), 1.15% sand and 1.16% organic material (TOC). There did not appear to be a difference in percent volume or composition of deposits between the sampling sites on either side of the marsh edge (Sites 4 and 5); however, deposition increased with distance inland of the marsh edge and towards the center of the study area (Figure 25-26). Maximum deposition occured on the Mid-High-Marsh transistion about 300 m inland of the marsh edge (Figure 25).

We estimated a total of ~12500 metric Tonnes (mT) of sediment deposited during the winter across our study area based on Theissen Polygon interpolation and ~11200 mT using IDW interpolation (Table 8). Over the period December 8, 2014 through April 3, 2015 these amounts may represent ~111 mT/day and 100 mT/day, resepctively (Table 8). These rates represent between 2.2 and 2.5% if the total sediment delevered by the river over that time (Grossman and Curran (in review)) (Table 8).

Overall, the average deposit contains about 1.15% of sand by weight. Percent of sand deposits increase towards the northern regions of the study area (Figure 27b) with no clear trends cross-shore (Figure

27a). Longshore percent sand variablity showed an indisinct and inconsitent pattern (Figure 27c); however, variablity in percent sand increased toward the northern most transects (Figure 27d).

On average, these tile trap data have a slightly higher organic fraction (percent TOC) inland (Site 1 and 2) and south (Figure 27). TOC variablity is highest within the High-Marsh (Site 1) and has the least variablity within the bare tidal flats (Site 5) (Figure 28C) .

3.1.1 Sediment Accumulation on Vegetation

We estimate approximately 53 mT of inorganic material accumulated on plant stems accounting for 0.5% of the total sediment budget for the northern marsh (Table 9). We are to unable to define a distinct spatial, vertical or temporal pattern in sediment accumulation on vegetation (Figure 29). The mass of material after our LOI processing (Mss) does show a significant relationship between the total stem segment weight (Mt) and a weak relationship to stem surface area (SA) (Figure 29b and d).

3.2 Turbidity and Suspended Sediment Concentration

During the first deployment, January 25th to March 1, 2015, YSI 6000 turbidity sensors were deployed in the channel to the restoration area alongside the DTS turbidity sensor maintained by the USGS (Figure 22). The DTS showed correlation to suspended sediment concentration (Grossman and Curran, in review), and showed a strong relationship to both YSI turbidity sensors (Turb 1 and Turb 3) used here (Figure 30). There was no significant storm event resulting in relatively low turbidity values in both the DTS and the Turb 3 sensors during this deployment (Figure 30a). Turbidity values from the YSI sensors were generally lower than the DTS which may be the result that the YSI sensors were installed at the edge of the channel, ~0.5 m above the DTS installed on the channel bed. In Figure 31, turbidity values of the DTS and YSI sensors deployed in the restoration channel showed a relationship with the Stillaguamish River turbidity and gauge height. For example, February 2, 2014 there was an increase in

turbidity within the channel (DTS and YSI-Turb1 sensors) that appeared to have a positive and nearly immediate response to the Stillaguamish River turbidity (Figure 31c-d).

The second deployment, March 1 to March 21, 2015, turbidity sensors were placed at the marsh edge on Transects 3 and 5 (Sites T3.4 and T5.4) to study alongshore dynamics. Turbidity in the estuary restoration channel showed a strong relationship to river turbidity and discharge (Figure 32). The relationship between river and the nearshore marsh sensors is more complex than the channel (Figure 32). Turbidity measurements were relatively uniform alongshore that suggests equal delivery to the marsh edge (Figure 32 e-f).

The third deployment, March 21 to April 20, 2015, involved the placement of YSI sensors on Transect 3 (sites T3.1, T3.3, T3.4) to assess cross-shore suspended sediment dynamics. The sensor placed within the center of the Mid-Marsh (T3.3) had consistently higher turbidity than the marsh edge (T3.4) and the High-Marsh (T3.1) (Figure 33). There were no significant rain events during this deployment.

Turbidity showed a variable relationship with wind speed and turbidity within the restoration channel does not appear to be influenced by wind. For example, on 3/14 and 3/20 there was an increase in marsh turbidity and wind speed observed at several wind sensors (SI and WP) (Figure 31f and Figure 34c); but, on 3/23 and 3/28 there was an increase in turbidity with no apparent increase in wind speed. These events occurred approximately 1 day after increases in turbidity within the river (Figure 32a-d). Within the tidal channel leading to the restoration area, on February 2, 2014 there was an increase in channel turbidity (DTS and YSI-Turb1 sensors) that appears to have a positive and nearly immediate response to the Stillaguamish River turbidity (Figure 31c-d); however, local wind stations do not show high wind speeds during this time (Figure 34b).

3.3 Sediment Erosion Bars:

The SEB data showed some accretion and erosion between January 11 and March 21 of 2015 at T3.4 (marsh) and no changes in elevation at the tidal flat site (T3.5) (Figure 35). At T3.4, we observed up to 2 cm of accretion and 3 cm of erosion at bar lengths 140 cm and 230 cm, respectively (Figure 35). SEB support bars were located at bar lengths 0, 115 and 230 cm, respectively. We observed during field visits micro topography at the marsh edge where plateau forms (bar length 115 to 200 and 250 to 300 cm) were often vegetated and lower areas (bar length 200 cm to 250 cm) were bare small channels (Figure 35a and Figure 34). This pattern was representative of the micro-topography within the first 50 m of the marsh edge. T3.5 showed little micro- topography that was characteristic of the tidal flat.

4 Discussion

4.1 Sediment Budget

The highest during our study deposition occurred at the Mid/High-Marsh boundary (Sites T1.3, T2.2, T3.2, T3.3, T4.2; Figure 25 -26). Here the vegetation changes from an emergent marshland dominated by bulrush to a rarely inundated, slightly elevated, grass and sedge dominated wetland (Chapter 1). We interoperate deposition at the Mid/High-Marsh transition, along with field observations of ripple marks oriented parallel to the shoreline/marsh edge, as sediment being transported from the nearshore and deposited, in part, as a result of bed / saltation load (Figure 37). Small developing tidal channels at the marsh-edge likely increase bed roughness and contribute to wave attenuation. Ripple marks and developing channels are indicators of relatively higher hydraulic energy than the tidal marshlands that depend on accumulation from sediment falling out of suspension.

Sand content patterns reflect variable hydraulic energy with the assumption that higher energy would yield higher sand content by winnowing fines proportion. The higher sand content within the northern transects (T4 and T5) indicate: 1) that the Old Stilly Slough, northern edge of the study area, serves as a

source of sandy material for the marsh and that, 2) that hydraulic energy is highest at the northern reaches of our study area. This is consistent with the high exposure of northern reaches to the greatest fetch of predominant winter waves. We hypothosize that regions of strong wave attenuation due to vegetation would exhibit a decrease in sand content landward. Our study does not show this pattern which may indcate that there is sufficient energy to transport sand uniformly through the relatively narrow and uniformly sloping marsh.

Total organic carbon (TOC) can be used to quantify biomatter is within a sediment sample and can further indicate if deposition is influenced by accretion and decomposition of plant material or by detrital processes (Mitsch and Gosselink, 2015). Total organic content (TOC) was relatively low (< 5%), consistent with other studies (Grossman et al., 2011) . TOC patterns indicate higher content to the south and inland (Figure 28). High TOC may indicate: 1) a relativly low energy environment that allows light organic material to be accreted; 2) a relatively high, intial and, local, biomass. Inland and southern reaches have a higher wetland biomass and may be exhibit more accretion of plant material (Chapter 1).

4.1.1 Sediment Accumulation on Vegetation

We predict that the accumulated sediment on vegetation may contribute up to 0.5 % and 53 mT of the overall sediment budget. Suspended sediment delivered by tides and waves adhered to bulrush stems seemingly would vary with surface area; however, our measurements suggest is a strong relationship between inorganic material (Mss) and stem segment biomass (Mt) and a lesser relationship with surface area (Figure 29b and d). We speculate that the relationship between Mss and SA is biased by the LOI approach which produces ash. LOI is a method used most often to calculate the fraction of carbon within a sediment sample and not the fraction of sediment on a plant sample as we have performed here. One possibility is that the amount of ash from the stem is not insignificant as often assumed in sediment studies and therefore biasing our results.

Vertical and temporal analyses are equally unclear (Figure 29c and 29e). We speculate that Mss values should increase with number of inundations with more accumulation at the base of plants and later in the season. However, it is possible that increased inundation speeds the degradation and rotting processes and therefore less likely to retain sediment. Future studies should reconsider using LOI analysis to determine sediment accumulation on emergent plant species. Future studies may also consider a larger sample set, earlier season, and more frequent sampling to determine if there is a spatial, vertical or temporal pattern.

4.2 Sediment Dynamics from Turbidity Sensors

Our turbidity sensors indicated that the suspended sediment concentration (SSC) within estuary restoration channel closely correlated with turbidity/discharge of the Stillaguamish River in magnitude and timing. This relationship indicated that the Stillaguamish River was the primary source of sediment for the restoration area.

Turbidity across the nearshore and northern marsh sites showed variations in response to both the river input of sediment and wind events that generate waves. The intermittent 1-2 day delay between northern marsh and river turbidity peaks suggests flux from the river likely takes a circuitous route to reach the marshes, 2-4 cycles of flood and ebb tides given the semi-diurnal tidal regime. Elevated turbidity in the northern nearshore and marshes associated with high wind events suggested waves suspend and transport sediment from the tidal flats (Figure 33-35). A standard sediment delivery event required inundation from tides and wind-driven waves to remobilize sediment. If tides remained high during a sediment moving event within the Stillaguamish River then the northern marsh may experience a direct, albeit delayed by 1-2 days, relationship with the assumed primary sediment source for the delta. The relatively uniform turbidity alongshore during high river delivery and wave events may be a result of the elevated sediment flux associated with the 2014 Oso landslide.

Cross-shore turbidity on Transect 3 showed the highest turbidity concentrations within the middle of the Mid-Marsh and coinciding with the highest sediment accumulation from tile trap data (Figures 25 and 34). This pattern suggests the highest potential sedimentation was ~300 m landward of the marsh edge where the reduction of tidal current velocities would facilitate sedimentation. During a storm event material was likely excavated from the tidal flat and marsh edge and then transported and deposited within the central Mid-Marsh.

4.3 Marsh Migration and Bed Roughness

Although the SEB data did not indicate significant accretion, erosion, or marsh migration, we acknowledge that the sampling period was relatively short. The power of the SEB measurements are to be realized through continued monitoring. Even so, variations of up to 3 cm over the few months are high; though it remains uncertain if the highest erosion was effected by support bars. Accretion patterns, albeit less than 1 cm in places, may be the result of the high input of sediment associated with the Oso slide. The SEBs provide salient information characterizing the greater surface roughness within the wetland compared to the tidal flat. This surface roughness may indicate the formation of tidal channels and rivulets and thus an overall erosion pattern at the marsh edge. Moreover, surface roughness produces obstacles and friction that decrease hydraulic energy and may contribute to the deposition directly landward.

5 Conclusions

This study investigated and compared sediment dynamics to ecologic, climatic and geomorphic influences within a vulnerable temperate estuary within the Pacific Northwest (Figure 38). Here, we estimate the total sediment deposition during the 2014-15 winter to be between ~6400 and ~7100 m^3 with highest deposition occurring within the High-Mid-Marsh that was dominated by chest to head height bulrush (BOFL). The northern marsh is estimated to retain up to 2.5% of the average daily

sediment delivered by the Stillaguamish River. We estimated the influence of sediment that has adhered to vegetation to contribute up to 0.5% to the sediment budget. Sand content increased toward the north and TOC increased towards the south. These patterns may indicate increasing hydraulic energy associated with wind generated wave activity towards the north. Turbidity data within the restoration tidal channel showed a strong and closely timed relationship with river sediment and responses. Turbidity within the northern marsh indicated that SSC is uniform along the marsh edge and increased landward where deposition is highest. The cross-shore turbidity patterns and presence of ripples in muddy sands within the high marsh are consistent with transport landward by bed-load and suspended load associated with wind-driven waves. Moreover, marsh turbidity showed a delayed relationship to the river and pronounced responses to high wind and assumed wave events. Our comparative analysis with wind data indicated that wind-driven waves may be the dominant influence remobilizing sediment from the contiguous tidal flat enabling deposition within the wetland. The amount of sediment estimated to accumulate during the study, while only a fraction of the river load, is likely biased high over normal years in response to the increase in delivery from the Oso Landslide.

6 Works Cited

Bortleson, G. C., M. Chrzastowski, and A. K. Helgerson, 1980, Historical changes of shoreline and wetland at eleven major deltas in the Puget Sound region, Washington. U.S. Geological Survey, U. S. Dept. of, Justice, U.S. Bureau of Indian, Affairs, Reston, Va.

Curran, C.A., Grossman, E.E., Mastin, M.C., Huffan R.L., 2016, Sediment load and distribution in the lower Skagit River, Skagit County, Washington: U.S. Geologic Survey Scientific Investigations Report 2016-5106.

Czuba, J.A., Magirl, C.S., Czuba, C.R., Grossman, E.E., Curran, C.A., Gendaszek, A.S., and Dinicola, R.S., 2011, Sediment load from major rivers into Puget Sound and its adjacent waters: U.S. Geological Survey Fact Sheet 2011–3083, 4 p.

Fuller, R., 2015, Stillaguamish Estuary Monitoring Report Summary: Western Washington University.

Grossman, E.E., George, D.A., Lam, A., 2011, Shallow stratigraphy of the Skagit River Delta, Washington, USA derived from sediment cores. USGS Open File Report 2011-1194, p 123.

Grossman, E., and Curran, C., In-Review, Sediment Transport Processes in Response to Estuary and Salmon Recovery Efforts and the SR530 (Oso) Landslide, Port Susan Bay, Washington 2013-2015: 2015-XXXX.

Huppert, D.D., Moore, A., Dyson K., 2009, Impacts of climate change on the coasts of Washington State. Washington Climate Change Impacts Assessment: Evaluating Washington's future in a changing climate. In press

Jones, J., Swanson, F., Wemple, B., and Snyder, K., 2001, Effects of Roads on Hydrology, Geomorphology, and Disturbance Patches in Stream Networks: Conservation Biology, v. 14.

Koch, E.W., Barbier, E.B., Silliman, B.R., Reed, D.J., Perillo, G.M., Hacker, S.D., Granek, E.F., Primavera, J.H., Muthiga, N., Polasky, S., Halpern, B.S., Kennedy, C.J., Kappel, C.V., and Wolanski, E., 2009, Non-linearity in ecosystem services: temporal and spatial variability in coastal protection: Frontiers in Ecology and the Environment, v. 7, p. 29–37, doi: 10.1890/080126.

Nolte, S., Koppenaal, E.C., Esselink, P., Dijkema, K.S., Schuerch, M., Groot, A.V., Bakker, J.P., and Temmerman, S., 2013, Measuring sedimentation in tidal marshes: a review on methods and their applicability in biogeomorphological studies. Journal of Coastal Conservation 17: 304–325.

Steiger, J., Gurnell, A. M., and Goodson, J. M., 2003, Quantifying and characterizing contemporary riparian sedimentation, River Res. Appl., 19, 335–352, doi:10.1002/rra.708.

Shepard, C.C., Crain, C.M., and Beck, M.W., 2011, The Protective Role of Coastal Marshes: A Systematic Review and Meta-analysis (J. Clifton, Ed.): PLoS ONE, v. 6, p. e27374, doi: 10.1371/journal.pone.0027374.

Tabor, R. W., Booth, D. B., Vance, J. A., and Ford, A. B., 2002, Geologic Map of the Sauk River 30- by 60- minute quadrangle, Washington, U.S. Geological Survey, Miscellaneous Investigations map I-2592, 2 sheets and pamphlet, scale 1:100,000.

Tebaldi, C., Strauss, B. H., and Zervas, C. E., 2012, Modelling sea level rise impacts on storm surges along US coasts. Environmental Research Letters, 7(1), 014032.

Thomas, S. and Ridd, P.V., 2004. Review of methods to measure short time scale sediment accumulation. Marine Geology, 207(1), pp.95-114.

van Wijnen, H.J., and Bakker, J.P., 2001, Long-term surface elevation change in salt marshes: a prediction of marsh response to future sea-level rise. Estuarine Coastal and Shelf Science 52: 381–390.

7 Tables

Table 7. Table detailing the inundation frequency of turbidity sensors during deployments. Inundation frequency was calculated as the ratio of the number of wet values over the total sample number.

Site - Sensor	Inundation Frequency (%)	Begin date	End Date	Sample Number	Elevation (m)	Highest tide (m)
PSB1 – Turb1	99.1	1/29/2015	2/6/2015	2220	0.10	3.56
PSB1 – Turb3	100	2/14/2015	3/1/2015	3597	0.10	3.24
T5.4 – Turb3	32.6	3/1/2015	3/20/2015	5363	2.08	3.27
T3.4 – Turb1	24.9	3/1/2015	4/18/2015	14245	1.99	3.41
T3.3 – Turb3	22.0	3/20/2015	4/18/2015	4318	2.74	3.41
T3.1 – Turb2	0.44	3/20/2015	4/18/2015	8135	3.35	3.41

Table 8. Summary of sediment budget for the study area. Volume deposits calculated using Thiessen Polygons and Inverse Distance Weighted (IDW) technique. Sediment density is assumed to be 1.75 g/cm ^{3}. Daily Rate assume an average study time of 112 days. Grossman and Curran (in review) investigated the sediment yield for the Stillaguamish River estimating 2.6 Million Metric tonnes of material being delivered to the delta between 11/15/2013 and 6/15/15 (577 days).

	Thiessen Polygons	IDW	Grossman and Curran (in review)
Total deposit volume(m^3)	7116.86	6412.60	
Total deposit mass (mT)	12454.51	11222.04	2.6×10^6
Volumetric Rate (m^3 /day)	63.54	57.27	
Deposited Mass Rate (mT/day)	111.20	100.20	4506.06
Percent of River Sediment yield (%)	2.4	2.5	100

Table 9. Sediment budget and flux results for study area. Average mass of sediment (Mss) derived from LOI analysis of all samples. Sediment flux (g/m^2) calculated from detrital accretion on vegetation using Equation 1. Bulrush density and height data were provided by Fuller (2015) for their defined Zone 4 and Zone 5. Total sediment flux is calculated by multiplying sediment flux over the study area (530458 m^2). Here we assume a bulk density of 1.75g/cm^3

Habitat Zone	Zone 4	Zone 5	Average
Bulrush Density (stems/m^2) (Fuller, 2015)	114	100	107
Vegetation Height (cm) (Fuller, 2015)	83	78	81
Average Mss (g/10 cm stem segment)			0.116
Sediment Flux (g /m^2) (Eq. 1)			100.756
Total Sediment Flux (metric ton)			53.446
Estimated Volume Flux (m^3)			30.541
Volumetric percent sediment budget			0.2-0.3%
Weight percent of sediment budget			0.5-0.6%

8 Figures

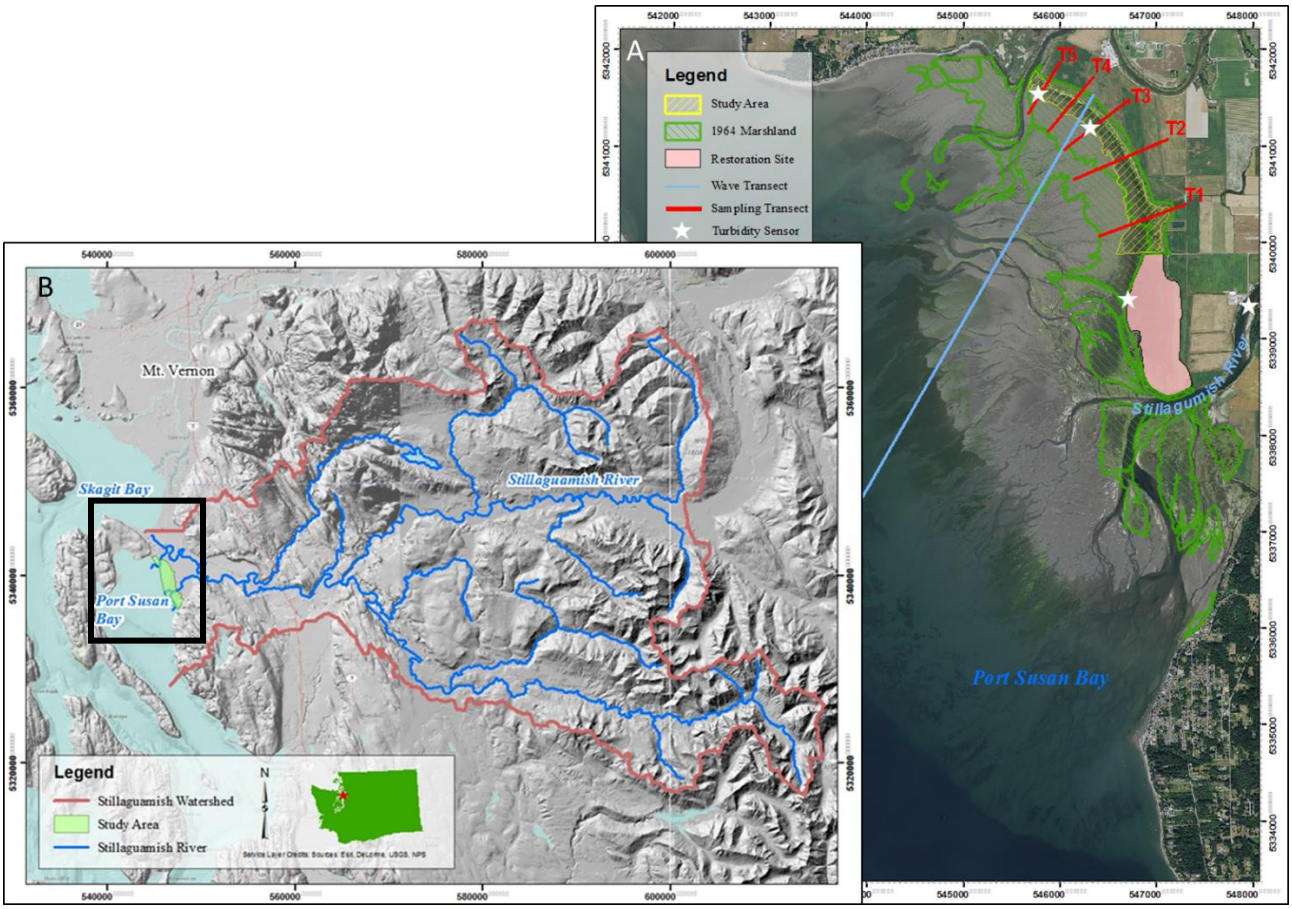

Figure 22. Map showing study area of Port Susan Bay. A) Historical wetland extent (green, 1964; yellow,2011) reconstructed from aerial photography and indicating up to 1km of marsh (shoreline) retreat since 1964 (Grossman and Curran, in review). Representative cross-shore transect (blue) of predominant wave approach). Yellow area is study area and northern 2014 marsh extent; Red lines are sediment sampling transects; White Stars are turbidity sensors with the YSI sensors within the study area, DTS at the channel into restoration site (pink) and the Stillaguamish River Sensor maintained by the USGS. B) Reference map detailing the extent and topography and the Stillaguamish River catchment.

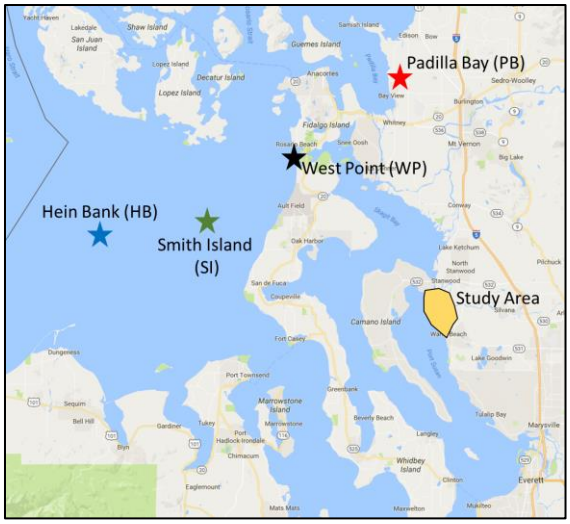

Figure 23. Locations for weather stations with continuous wind speed data near our study area; including Hien Bank (HB), Smith Island (SI), West Point (WP) and Padilla Bay (PB). Base map provided by google maps 2016.

Figure 24. Sediment Erosion Bar installation at tidal flat site (T3.5). Measurements are taken from the bar to the ground surface.

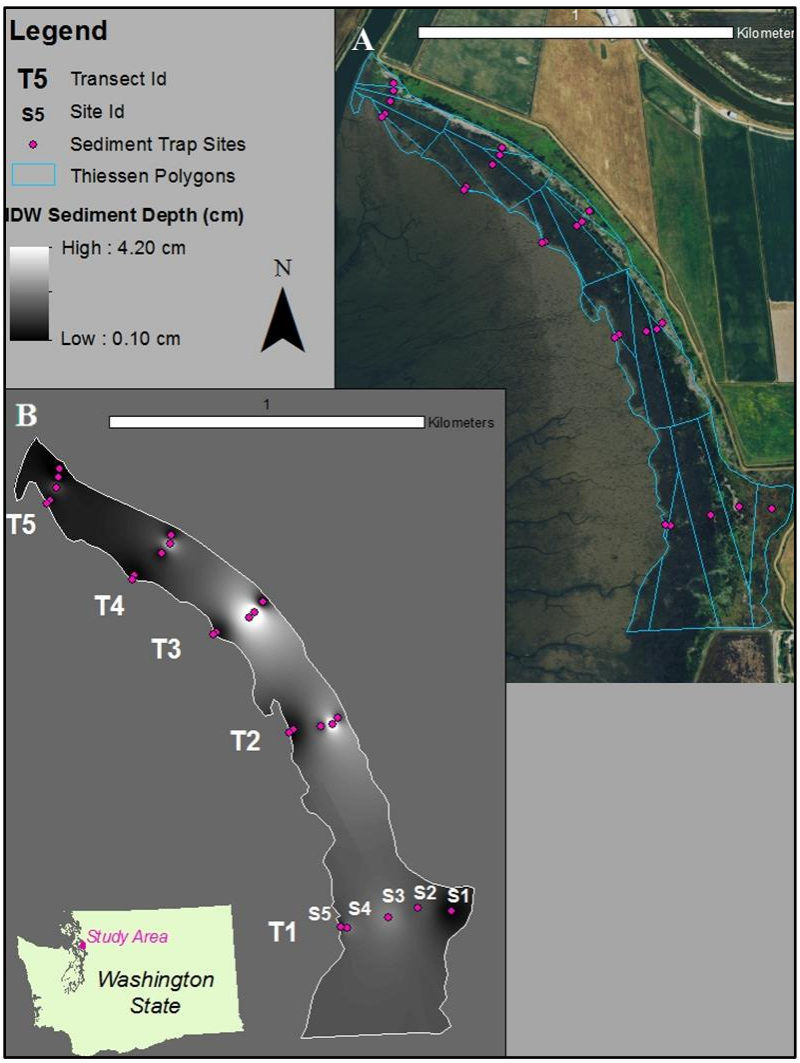

Figure 25.Map detailing tile trap and sampling sites along with Thiessen Polygon and Inverse Distance Weighted (IDW) analysis. A) Map of Thiessen Polygons within the study B) Map of IDW interpolated sediment thickness derived from tile trap data.

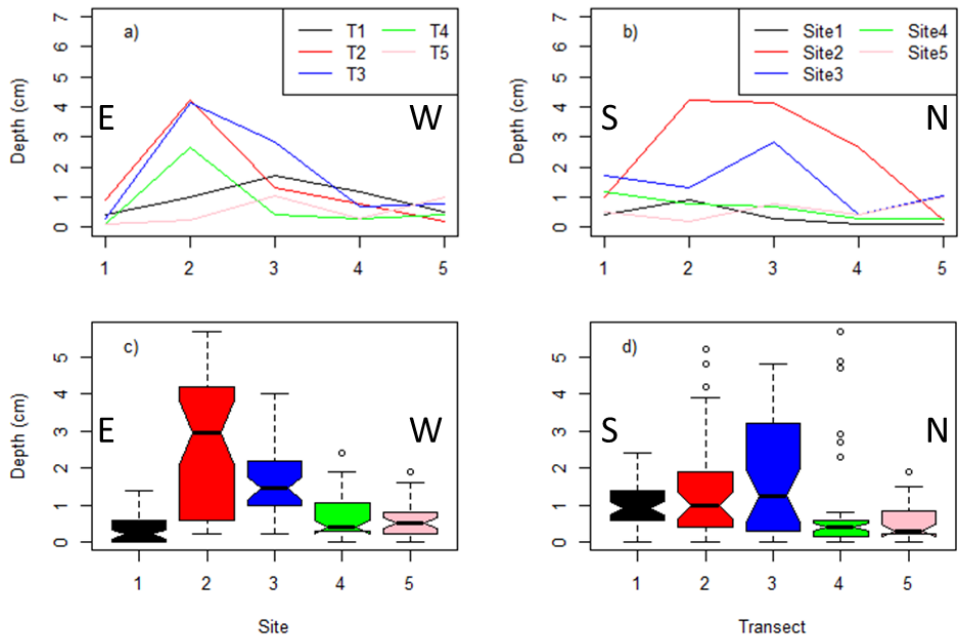

Figure 26. A) Line plot showing the average measured depth (cm) of sediment accumulated on tile traps cross shore (East to West). B) Line plot showing sediment thickness (cm) on tile traps alongshore, South to North. This plot shows that the majority deposition occurred at Sites 2 and 3 within the mid transects (Transect 2-4). C) Boxplots of measured sediment thickness by station. D) Boxplots of measured sediment thickness by transect.

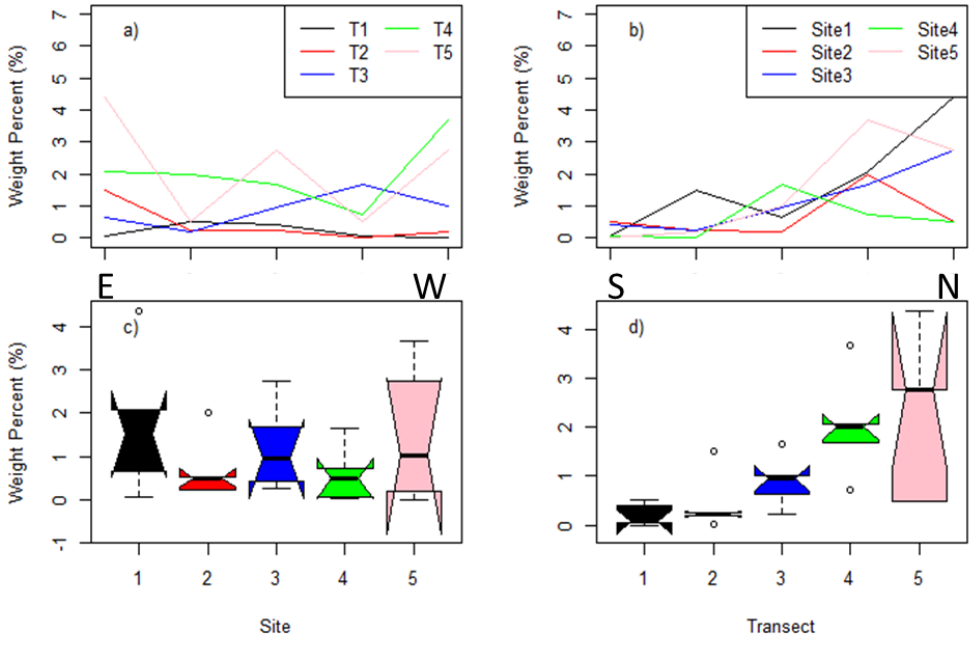

Figure 27. A) Line plot detailing the spatial patterns of sand deposits by weight percent across-shore. B) Line plot of sand deposits along-shore (south to north), showing a general increase toward the north. C-D) Box plots showing variation and average percent sand by station and transect respectively.

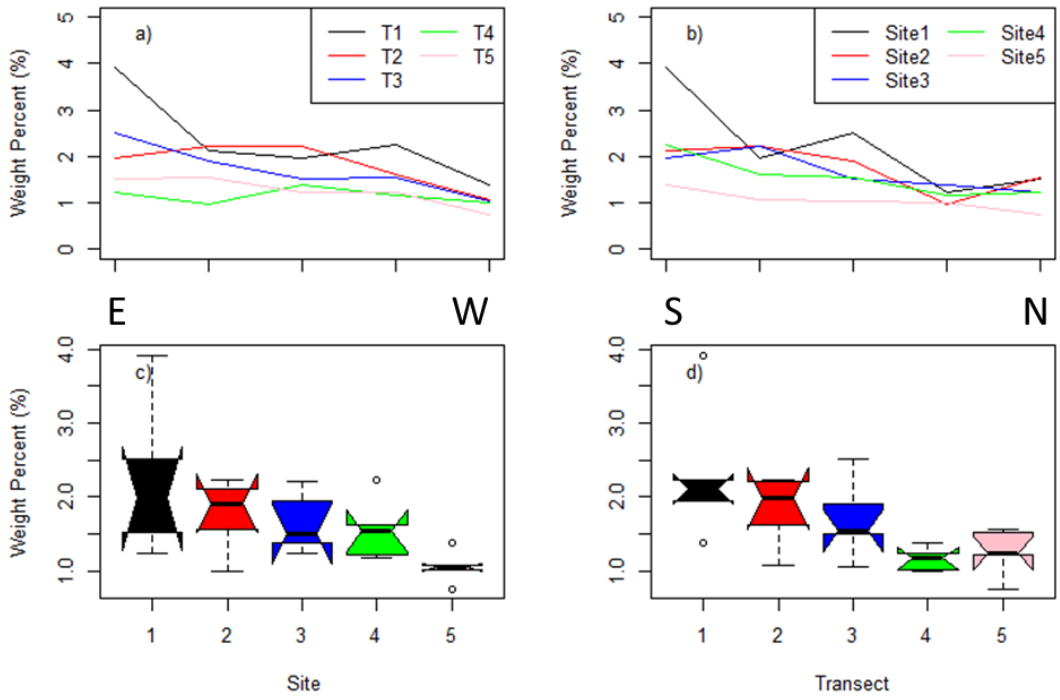

Figure 28. A) Line plot showing the cross-shore variation in weight percent of Total Organic Carbon (TOC), East to West. B) Line plot of weight percent of TOC by alongshore, North to South. C – D) Boxplots showing variation and average percent TOC by station and transect respectively.

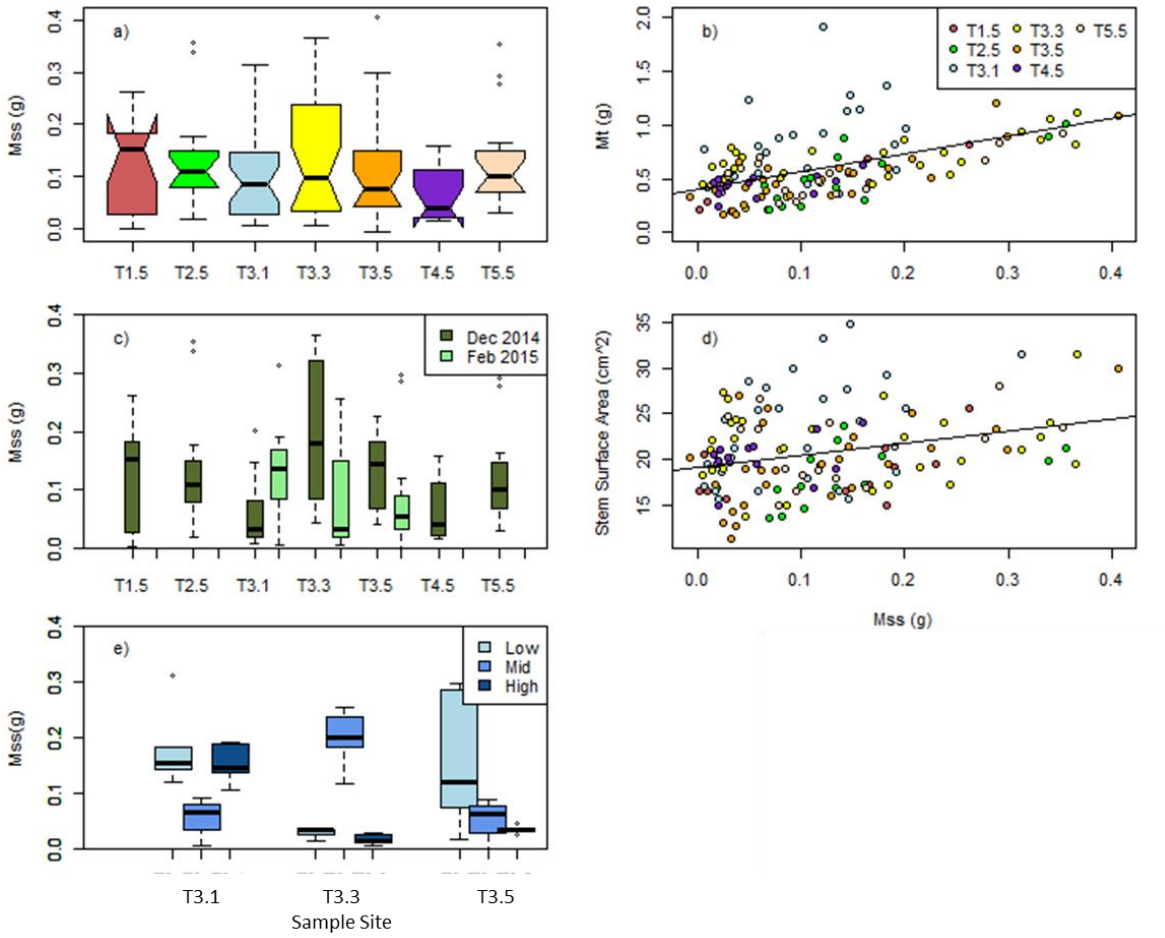

Figure 29. A) Boxplots of mass after skinning and burning through Loss on Ignition (Mss) by sediment sampling site. B) Scatter plot comparing Mss values to the total mass of stem segment (10 cm long segment) (Mt). Mss shows a significant linear relationship with Mt (p-value = $2.49x10^{-10}$; Kendalls Tau =0.38). C) Boxplot comparing Mss values to sampling period, December 2014 and February 2015. D) Scatter plot of estimated stem surface area compared to Mss. Mss shows a significant linear relationship with surface area (p-value = $2.72x10^{-3}$; Kendalls Tau =0.17). E) Boxplot comparing Mss values the height of the sample in the vegetation canopy; Low (marsh floor to 10 cm), Mid (20 cm to 30 cm), High (40 cm to 50 cm). Vertical assessment use samples from February sampling period.

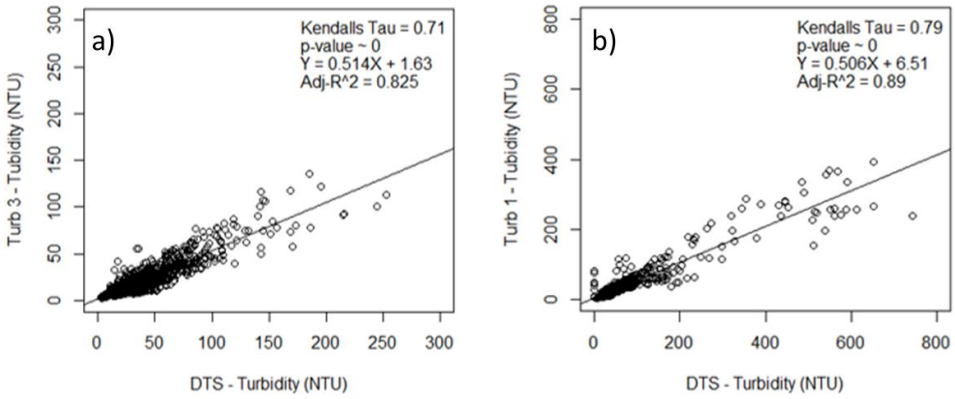

Figure 30. Scatter plots comparing turbidity measured by FTS DTS-12 sensor (DTS) and YSI 6136 turbidity sensors; a) Turb 3 and b) Turb1, within the restoration channel (PSB1).

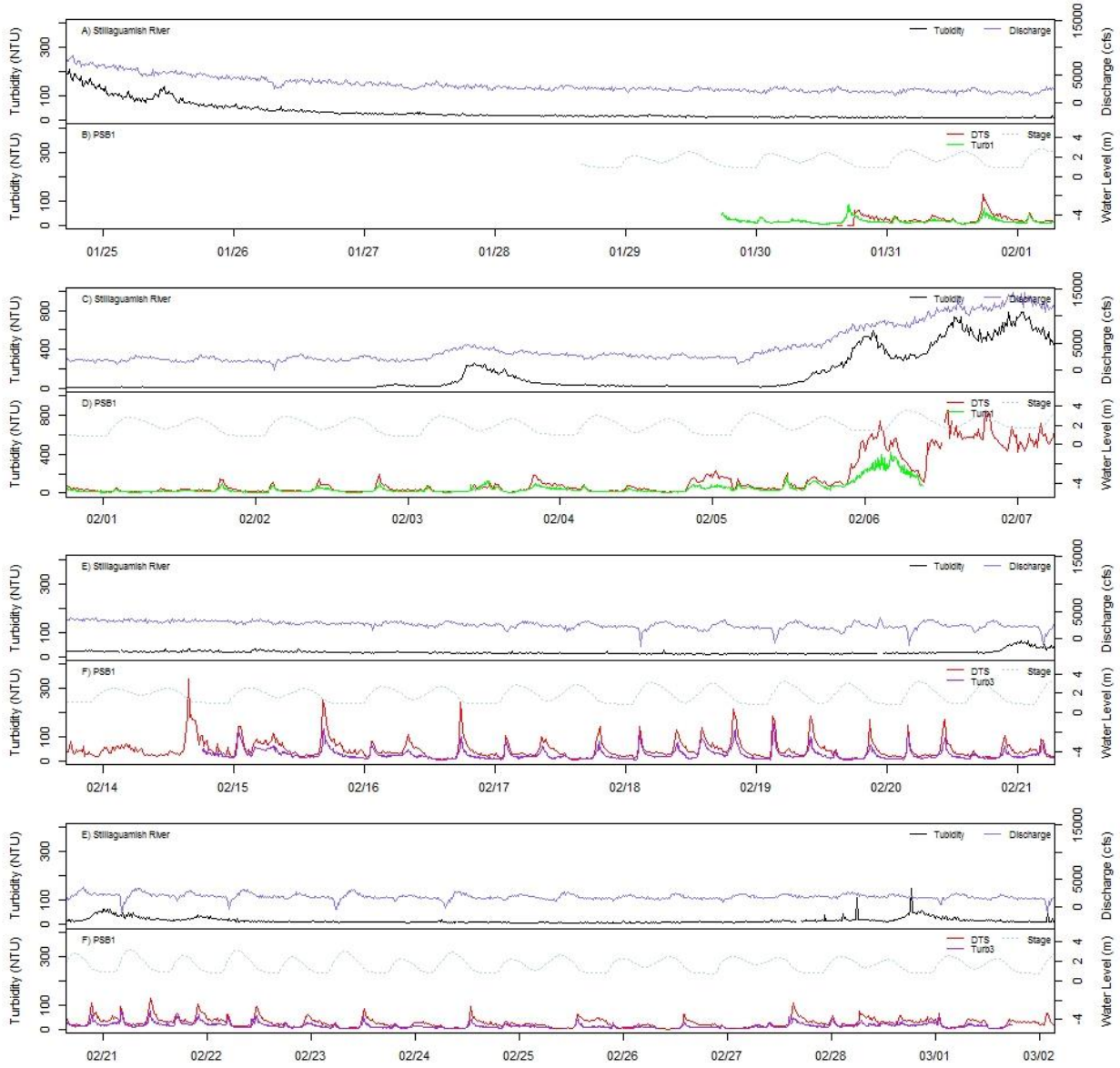

Figure 31. Time-series plots of turbidity and discharge of the Stillaguamish River(A,C,E,G) and within the restoration area tidal channel (B,D,F,H). Blue lines represent Stillaguamish River discharge (cfs); black represents turbidity (NTU) within the river; red lines represent turbidity (NTU) within the restoration channel. Green and purple lines represent YSI turbidity sensors (NTU) deployed along the marsh edge at stations T3.4 and T5.4, respectively. Continuous plots range from 1/25/2013 to 3/2/2014.

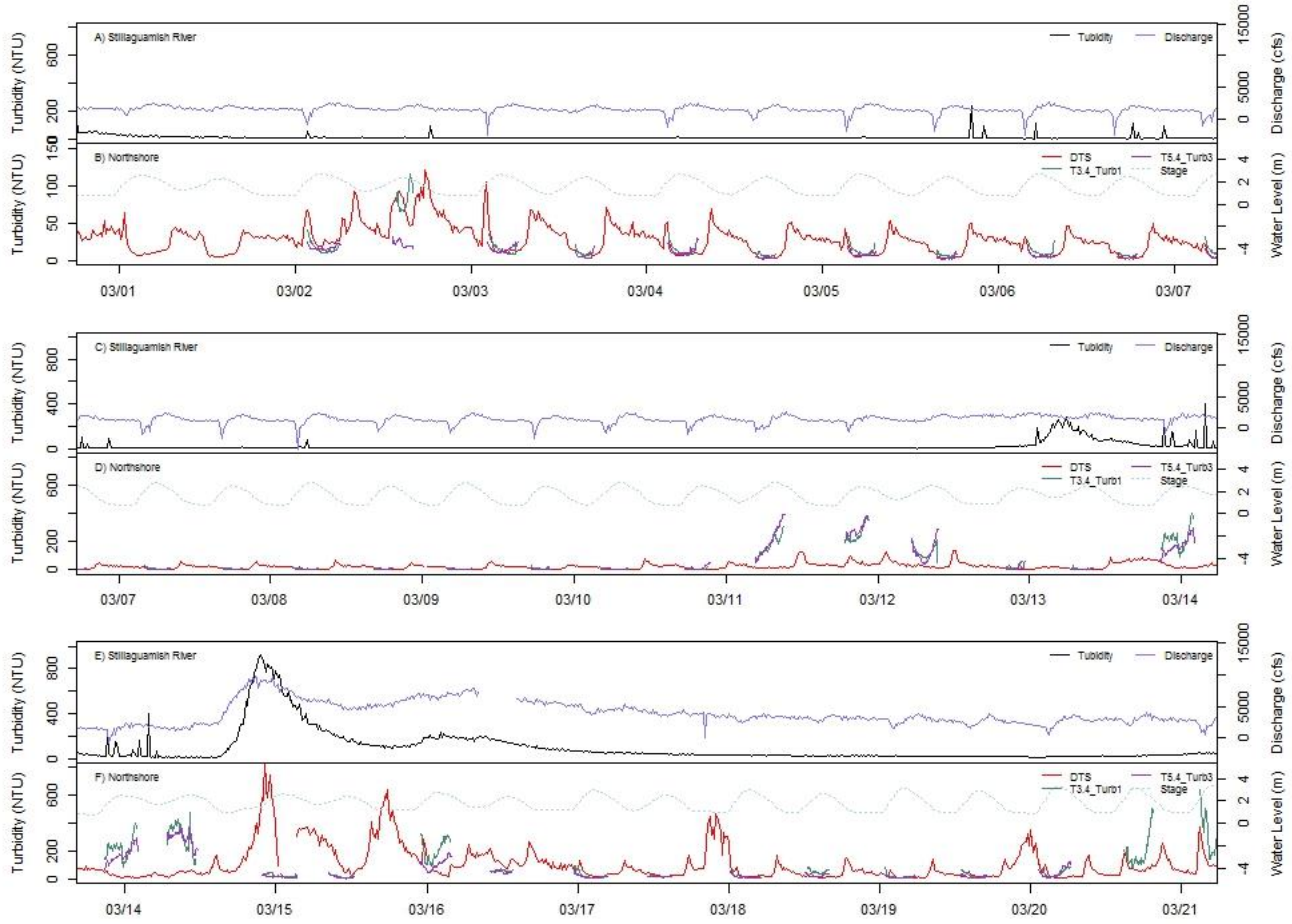

Figure 32. Time-series plots of turbidity and discharge of the Stillaguamish River(A,C,E,G) and along-shore turbidity and water level (B,D,F,H) at stations T3.4, T5.4. Blue lines represent Stillaguamish River discharge (cfs); black represents turbidity (NTU) within the river; red lines represent turbidity (NTU) within the restoration channel. Green and purple lines represent YSI turbidity sensors (NTU) deployed along the marsh edge at stations T3.4 and T5.4, respectively. Continuous plots range from 3/1 to 3/21/2014.

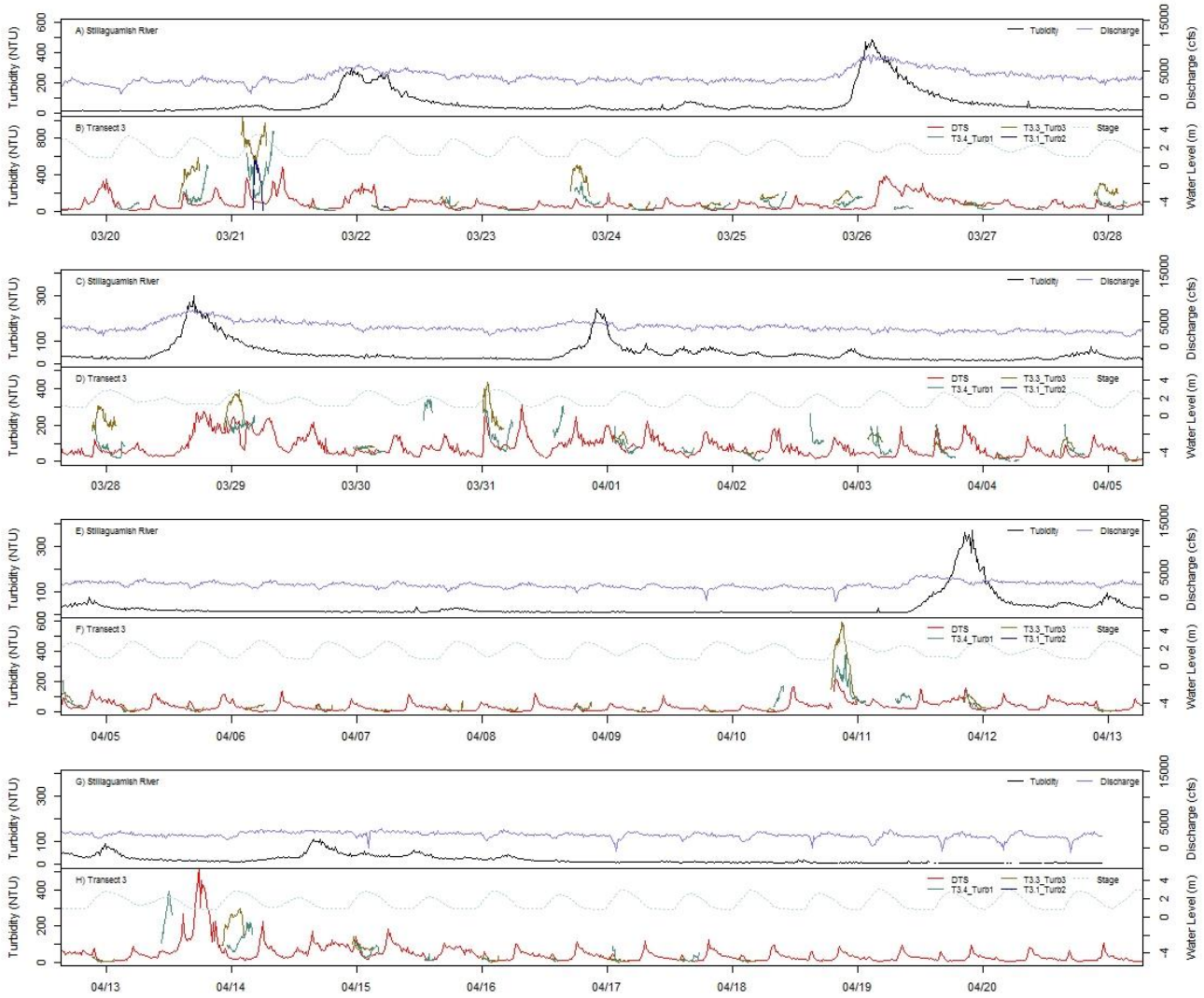

Figure 33. Time-series plots of turbidity and discharge (A,C,E,G) of the Stillaguamish River and cross-shore turbidity and water level (B,D,F,H) along Transect 3 (stations T3.1, T3.3, T3.4). Blue lines represent Stillaguamish River discharge (cfs); black represents turbidity (NTU) within the river; red lines represent turbidity (NTU) within the restoration channel. Dark blue, gold and green lines represent YSI turbidity sensors deployed at stations T3.1, T3.3 and, T3.4, respectively. Continuous plots range from 3/20 to 4/20/2014. There were no notable storm events during this timeframe.

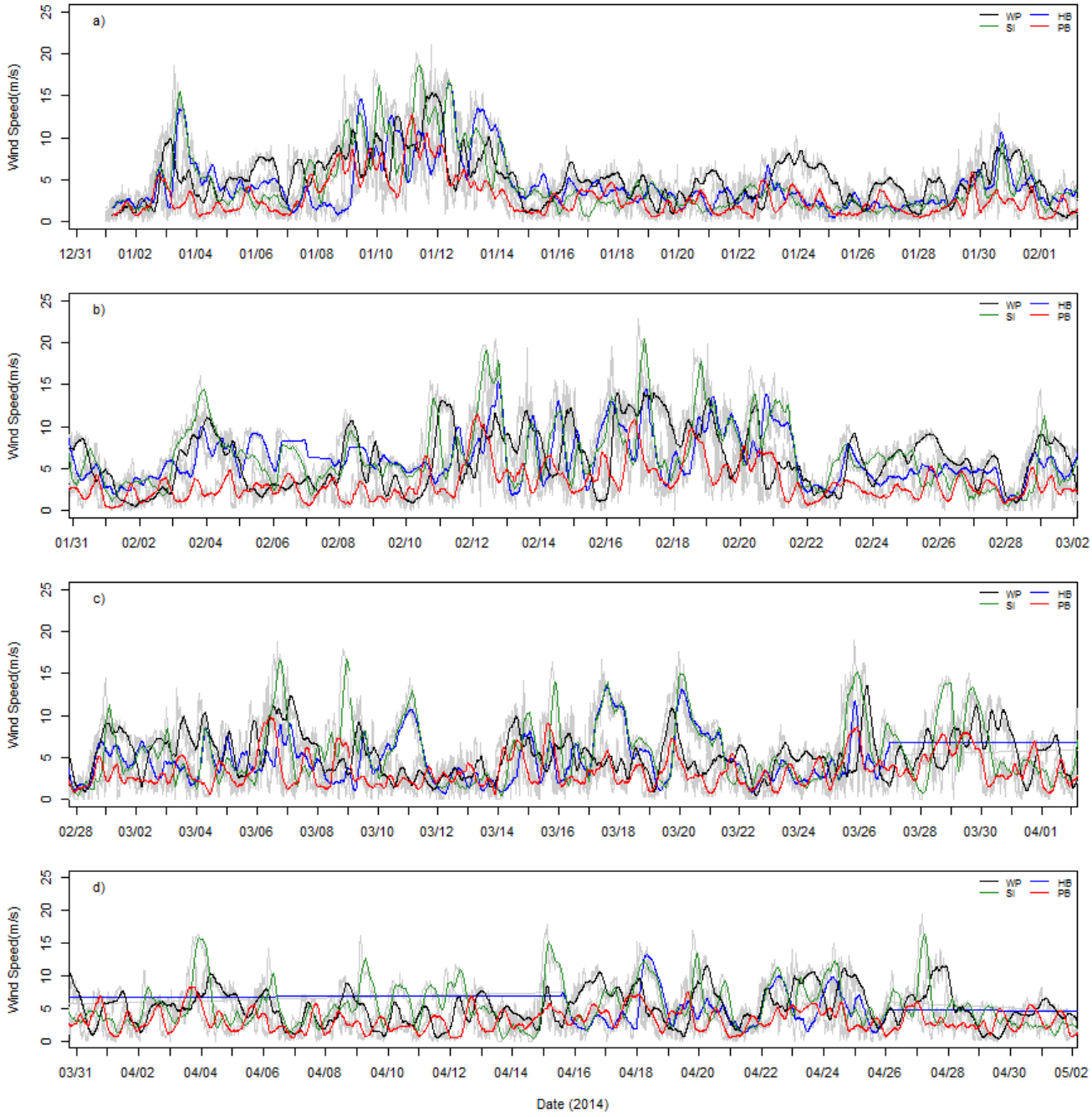

Figure 34. Line plots detailing wind speed data from local weather stations for January through April 2014. Weather station location is detailed within Figure 23. Grey lines show the raw wind speed data (measurements taken every 10 min to 1 hour), Colored lines show the running 6 hr average wind speed data at local weather stations: black lines represent West Point (WP), Blue lines represent Hien Bank (HB), green lines represent Smith Island (SI), red lines represent Padilla Bay (PB) weather station.

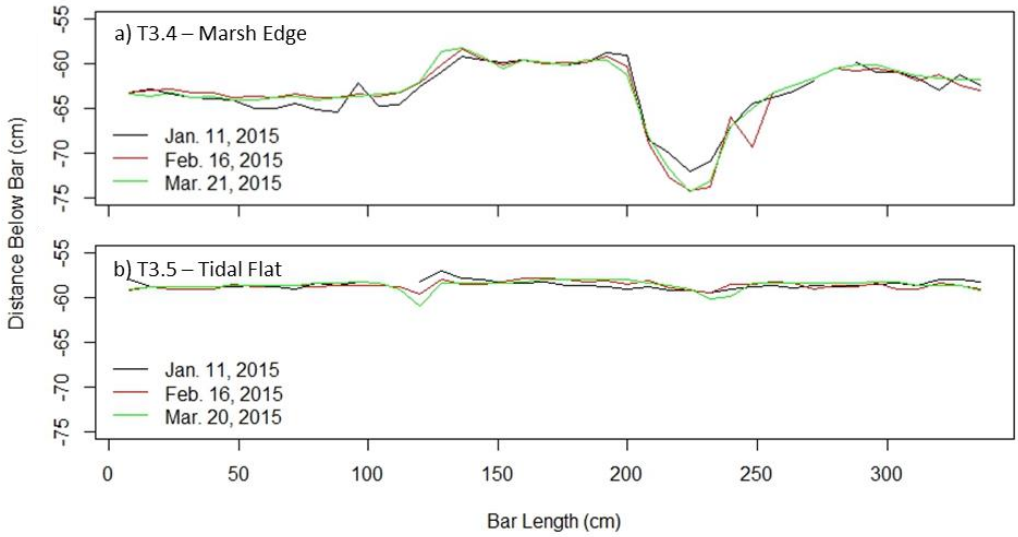

Figure 35. Results from Sediment Erosion Bar (SEB) analysis. A) Ground surface from site T3.4, approximately 15 m landward of the marsh edge. Data is displayed as distance below the bar as a function of bar length. Black, red and green lines represent 1/11, 2,16, and 3/20/2016 samplings, respectively. SEB support bars were located at bar lengths 0, 115 and 230 cm, respectively.

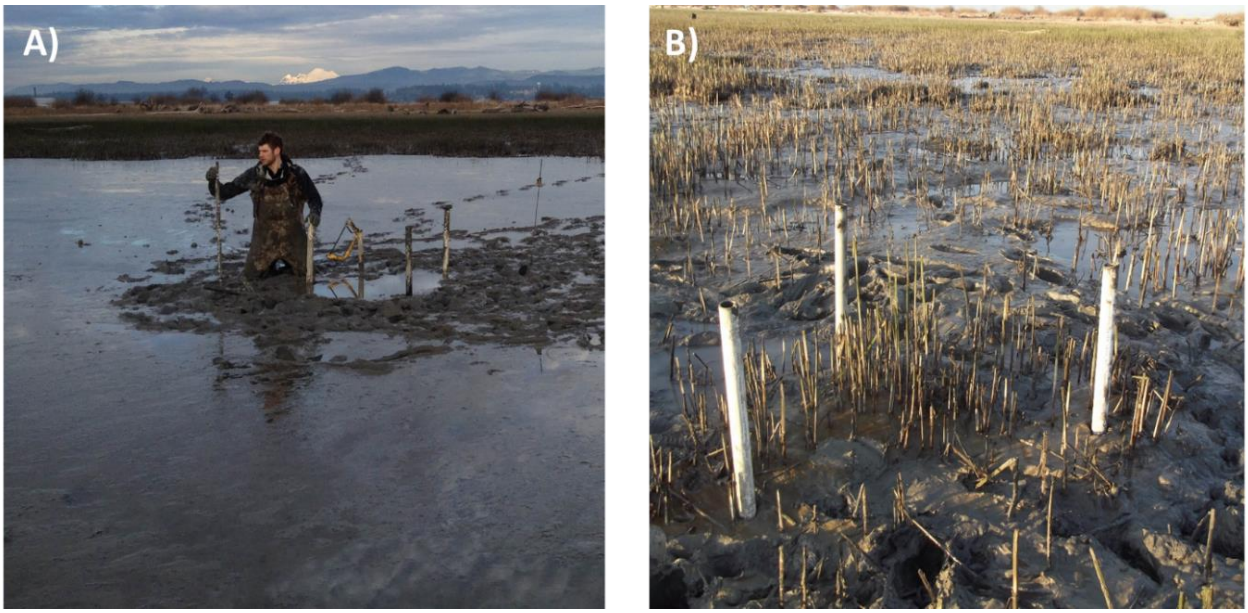

Figure 36. Sediment Erosion Bar installation showing site differences in vegetation and bed roughness. A) Tidal flat SEB site (T3.5). B) Marsh SEB site (T3.4).

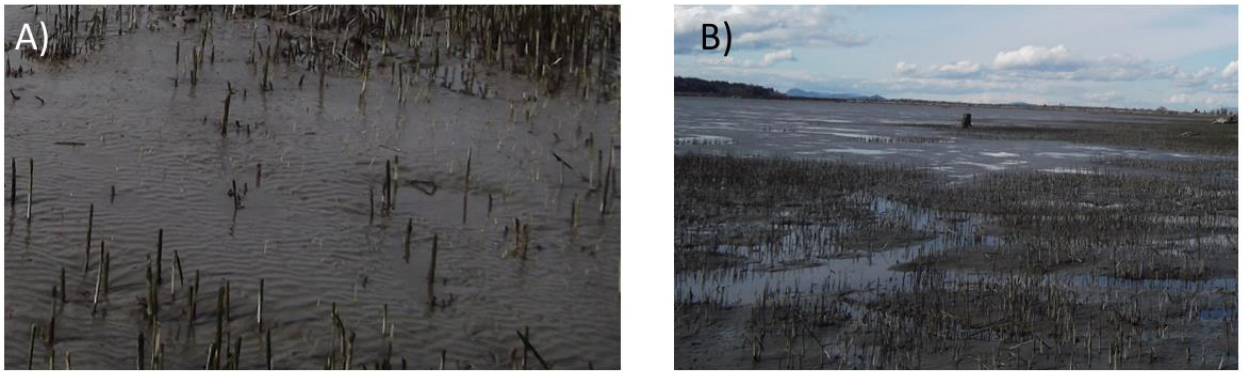

Figure 37. Images detailing field notes on sediment dynamics and bed roughness. A) Site T4.2 with notable ripple marks (1 cm in height, 6" crest to crest). B) Site T3.4 showing marsh edge microtopography including developing pedestals and rivulets.

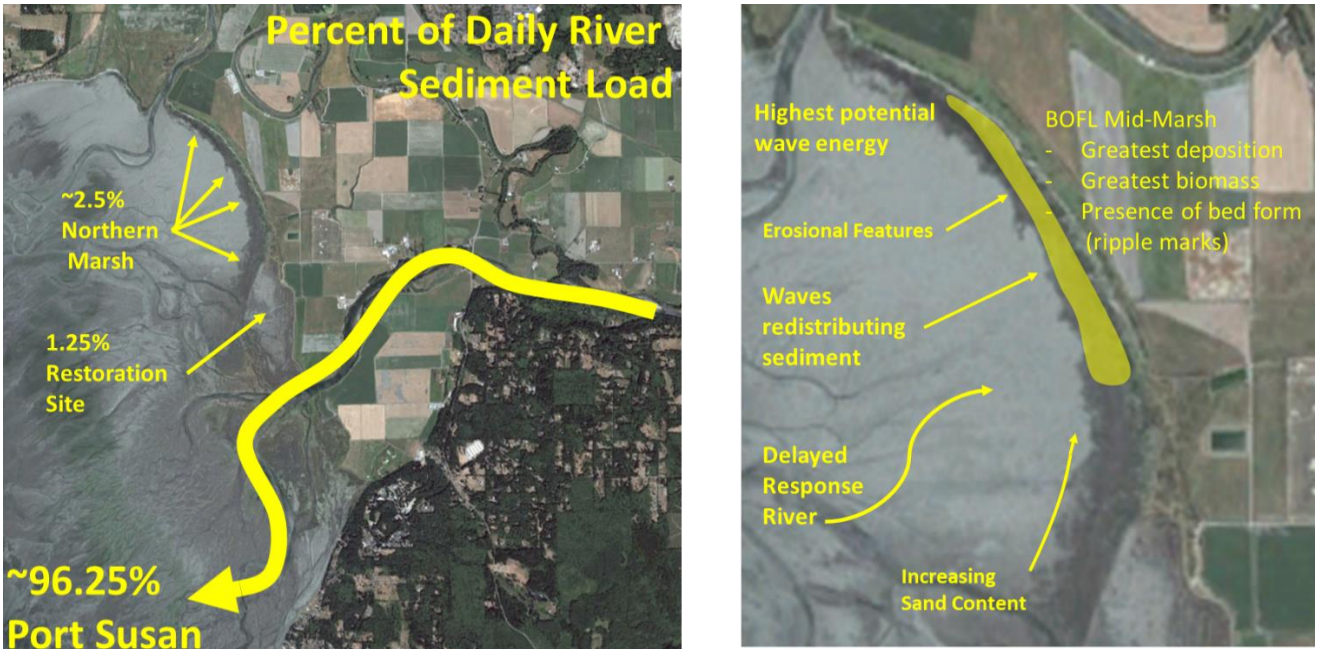

Figure 38. Overall summary and conclusions for sediment budget and dynamics analyses.

Overall Conclusions:

The purpose of these studies is to: 1) estimate vegetation canopy structures (elasticity, biomass, height, stem density, stem diameter) using image analysis and in-situ measurements, 2) accurately map vegetation assemblages using remote sensing and field surveys, 3) extrapolate vegetation characteristics across the delta, 4) estimate an overall sediment budget for the delta's most vulnerable marsh, 5) evaluate ecologic, hydrologic and climatic influences on sediment dynamics, within a temperate estuary within the Pacific Northwest, Port Susan Bay.

We found that our image analysis of strips of vegetation (Side-On Photos) was useful for estimating biomass, and vegetation height; however, our methods did not yield significant relationships between images and stem density due the potential interference of bladed leaves. Temporal analysis indicate that dominant Mid-Marsh bulrush maintain biomass through the winter months and beginning to degrade in February; though, leaves and associated surface area tend to decrease consistently with time.

We measured elasticity on two dominant bulrush species within the Mid-Marsh, *Bulboschoenus maritimus (BOMA)* and *Bulboschoenus fluviatilis (BOFL),* and found that resistance was a function of canopy height. Elastic resistance did not appear to vary with time because measured bulrush tended to become brittle and break as a main mechanism for decay.

Our remote sensing efforts, Maximum Likelihood Classification (MTC) and Decision Tree Classification (DTC) reasonably mapped vegetation assemblages and land cover with an overall accuracy of 77%.

Biomass was extrapolated using the relationship of field samples biomass data to the Red-Edge NDI and LiDAR Bare-Earth elevation and validated using percent cover data from Fuller (2015). We estimate overall biomass to be 4640 mT undifferentiated between marsh types. Our biomass analysis indicates relatively high biomass within the first 50 m, which likely contributes to high wave attenuation rates.

Our sediment budget analysis determined that the highest rate of deposition occurred within the Mid-Marsh near the High-Marsh boundary, where elevation and plant biomass increase. From field observations and Sediment Erosion Bar (SEB) data, we hypothesize that the marsh edge was experiencing enough hydraulic energy to cause erosion and bed load transport forming ripple marks within Mid-Marsh. Overall sediment deposition is likely abnormally high from increased sediment yield of the Stillaguamish River from the recent Oso (SR 530) Landslide.

Sediment dynamics showed a strong turbidity relationship between the Stillaguamish River and the tidal channel into the restoration site. The relationship between the northern marsh and the river turbidity shows a weak and delayed relationship. There does appear to be a relationship between marsh turbidity and regional wind data. These patterns lead to the conclusion that wind events are producing wave energy high enough to mobilize tidal flat sediment and transporting into the marsh. Alongshore turbidity data indicate that the suspended sediment is entering the marsh uniformly across the northern marsh. Cross-shore patterns show consistently higher turbidity readings in the central Mid-Marsh than the marsh edge coinciding with the study area's highest deposition rates. We speculate that during the study period the marsh edge was generally being eroded and the material being transported into the Mid-Marsh.

Appendix 1: RTKGPS Ground-Truth Analysis

This appendix describes our elevation ground-truth analysis for Port Susan Bay. LiDAR, a powerful remote sensing tool, is often used to measure elevation and is insensitive to vegetated land-cover. However, the dense vegetation of marshlands is often impenetrable to LiDAR leading to an over prediction in marshland elevation. Here we assess the accuracy of the 2014 Bare Earth LiDAR DEM (BE DEM) using RTKGPS data collected by Fuller (in review) in 2015.

To assess the accuracy of the LiDAR BE DEM, we populated Fuller's (in review) 2015 RTKGPS data with z-values from the 2014 BE DEM and land-cover assemblages' data from our decision tree classification (DTC). We used these data to produce elevation statistics, BE LiDAR and RTKGPS z values, with respect to vegetation assemblages (Table 10 -11). We subtracted RTKGPS z-values from BE LiDAR z-values to assess relative difference (Table 12).

We found that the LiDAR BE DEM over predicts elevation values by an average of 0.40 m for all marsh species (Figures 39 – 43, Table 10). BOFL dominated marsh was the least accurate (0.49 m), followed by BOMA (0.43 m), SCAM (0.38), and High-Marsh (0.35 m). All marsh species showed an over prediction of elevation by the LiDAR BE DEM (Figures 39 – 43, Table 12).

Bare sediment land-cover should have very little difference between the two z-values because of minimal interference from vegetation. We estimate the BE LiDAR dataset to be off by 0.15 m +/- 0.06 m on average (Table 12). This difference is within the precision of the LiDAR instruments; however, the fact that there is an average over prediction may indicate an increase in elevation from 2014 to 2015.

Table 10. Elevation (2014 LiDAR Bare Earth DEM) statistics in meters with respect to vegetation assemblages. All values are in NAVD88.

Lidar Elevation Analysis					
Cover Type	**Min**	**Max**	**Mean**	**STD**	**n**
All Marsh Types	**1.270**	**3.340**	**2.376**	**0.467**	**409**
High Marsh	**2.160**	**3.340**	**2.874**	**0.241**	**77**
Mid Marsh	**1.650**	**3.210**	**2.400**	**0.368**	**184**
BOFL	1.870	3.210	2.591	0.223	62
BOMA/SCAM	1.650	2.810	2.313	0.391	122
Low Marsh	**1.270**	**2.840**	**2.081**	**0.429**	**149**
Bare -undifferentiated	**1.125**	**1.902**	**1.609**	**0.185**	**89**

Table 11. Fuller's (2015) RTKGPS statistics with respect to vegetation assemblages. All Elevation values are in meters and NAVD88.

RTKGPS Elevation Analysis					
Cover Type	**Min**	**Max**	**Mean**	**STD**	**n**
All Marsh Types	**0.258**	**3.945**	**1.972**	**0.419**	**409**
High Marsh	**0.258**	**3.945**	**2.521**	**0.360**	**77**
Mid Marsh	**1.369**	**2.738**	**1.963**	**0.283**	**182**
BOFL	1.734	2.738	2.106	0.275	62
BOMA/SCAM	1.369	2.467	1.887	0.256	122
Low Marsh	**1.118**	**2.234**	**1.701**	**0.295**	**150**
Bare -undifferentiated	**1.077**	**1.838**	**1.460**	**0.195**	**89**

Table 12. Statistics of the difference between the 2015 Fuller's (in review) data with the 2014 LiDAR Bare Earth DEM (LiDAR – RTKGPS) with respect to vegetation assemblage. Positive values represent an over prediction of elevation by the LiDAR dataset. All values are in meters and NAVD88.

Differnce Analysis					
Cover Type	**Min**	**Max**	**Mean**	**STD**	**n**
All Marsh Types	**-0.925**	**3.017**	**0.404**	**0.271**	**409**
High Marsh	-0.925	3.017	0.354	0.363	**77**
Mid Marsh	**-0.055**	**1.061**	**0.448**	**0.239**	**184**
BOFL	0.087	0.789	0.492	0.174	62
BOMA/SCAM	-0.055	1.061	0.426	0.263	122
Low Marsh	**0.005**	**0.949**	**0.376**	**0.242**	**149**
Bare -undifferentiated	**-0.011**	**0.276**	**0.150**	**0.062**	**89**

.

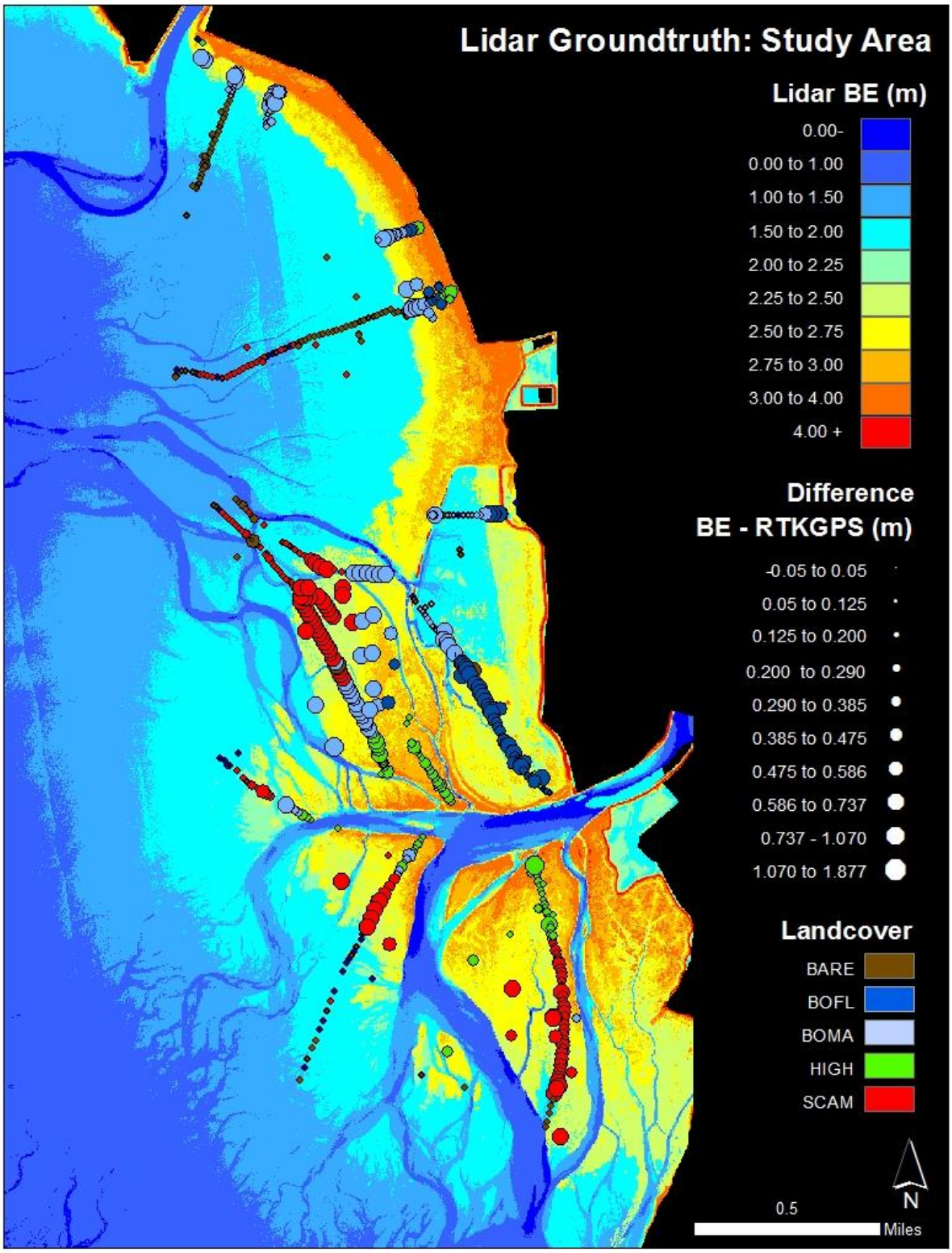

Figure 39. Map detailing the difference between the RTKGPS and Bare Earth LiDAR for full study area. All elevation values are in meters and NAVD88.

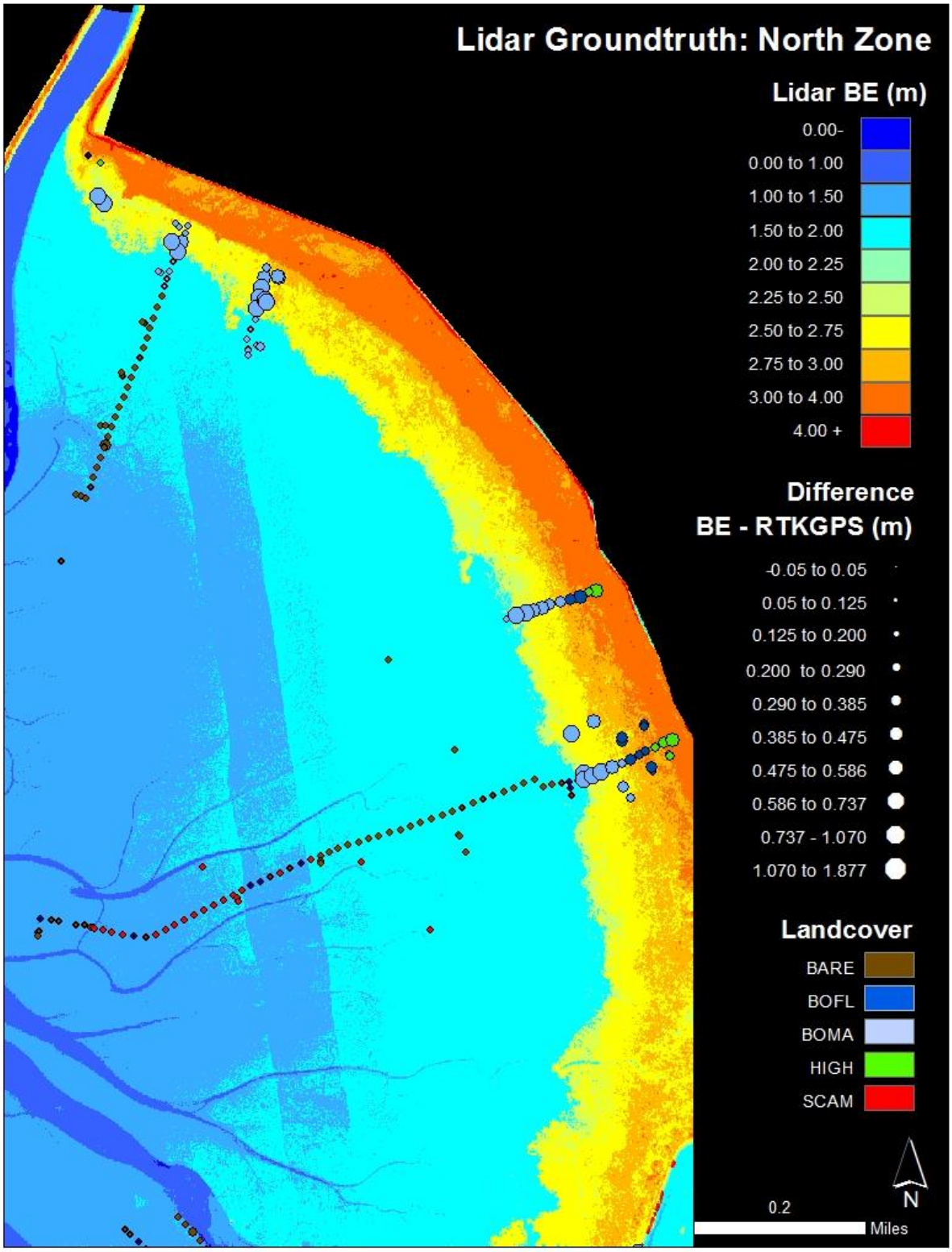

Figure 40. Map detailing the difference between the RTKGPS and Bare Earth LiDAR for North Zone of the study area. All elevation values are in meters and NAVD88.

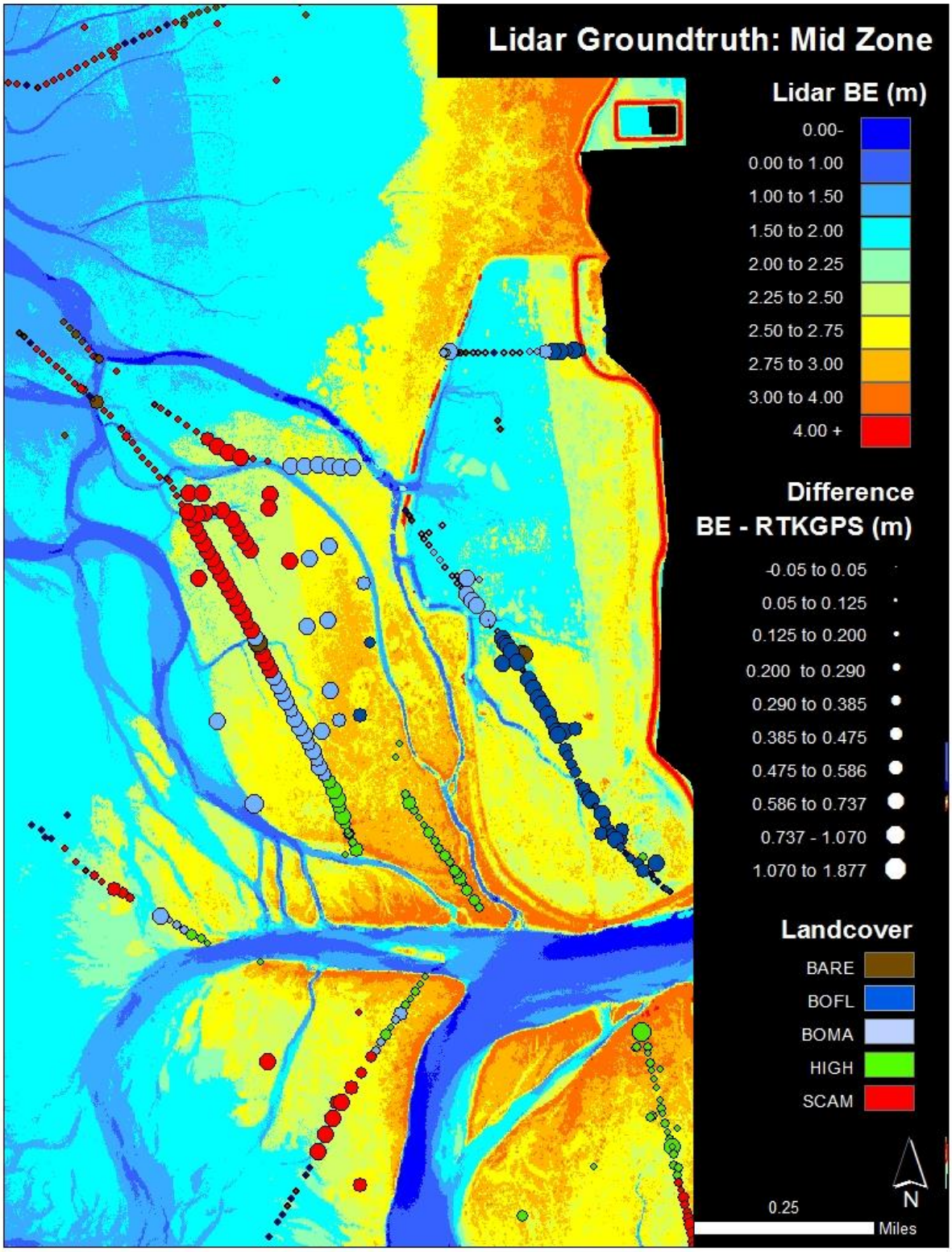

Figure 41. Map detailing the difference between the RTKGPS and Bare Earth LiDAR for Restoration site and Mid Zone of the study area. All elevation values are in meters and NAVD88.

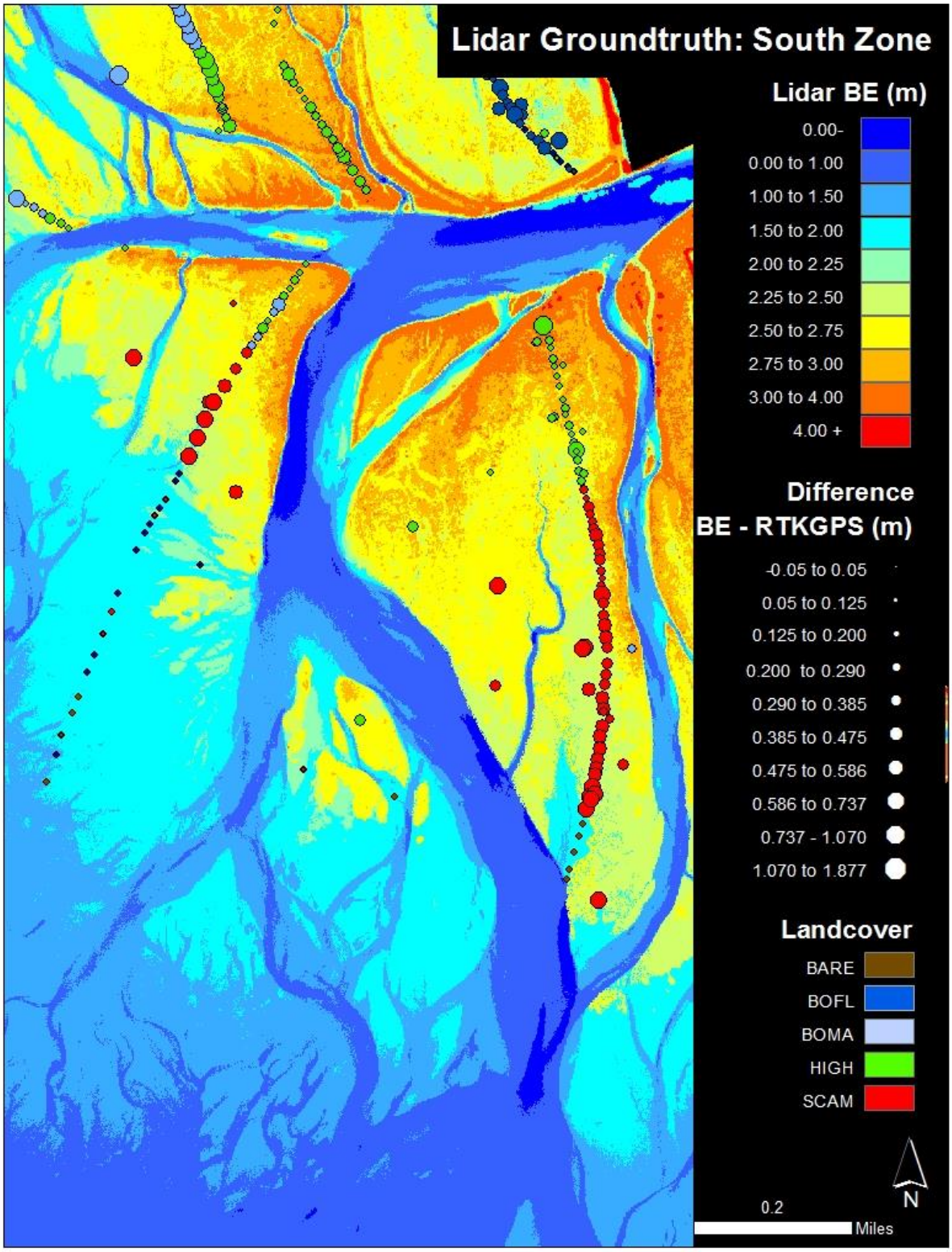

Figure 42. Map detailing the difference between the RTKGPS and Bare Earth LiDAR for South Zone of the study area. All elevation values are in meters and NAVD88.

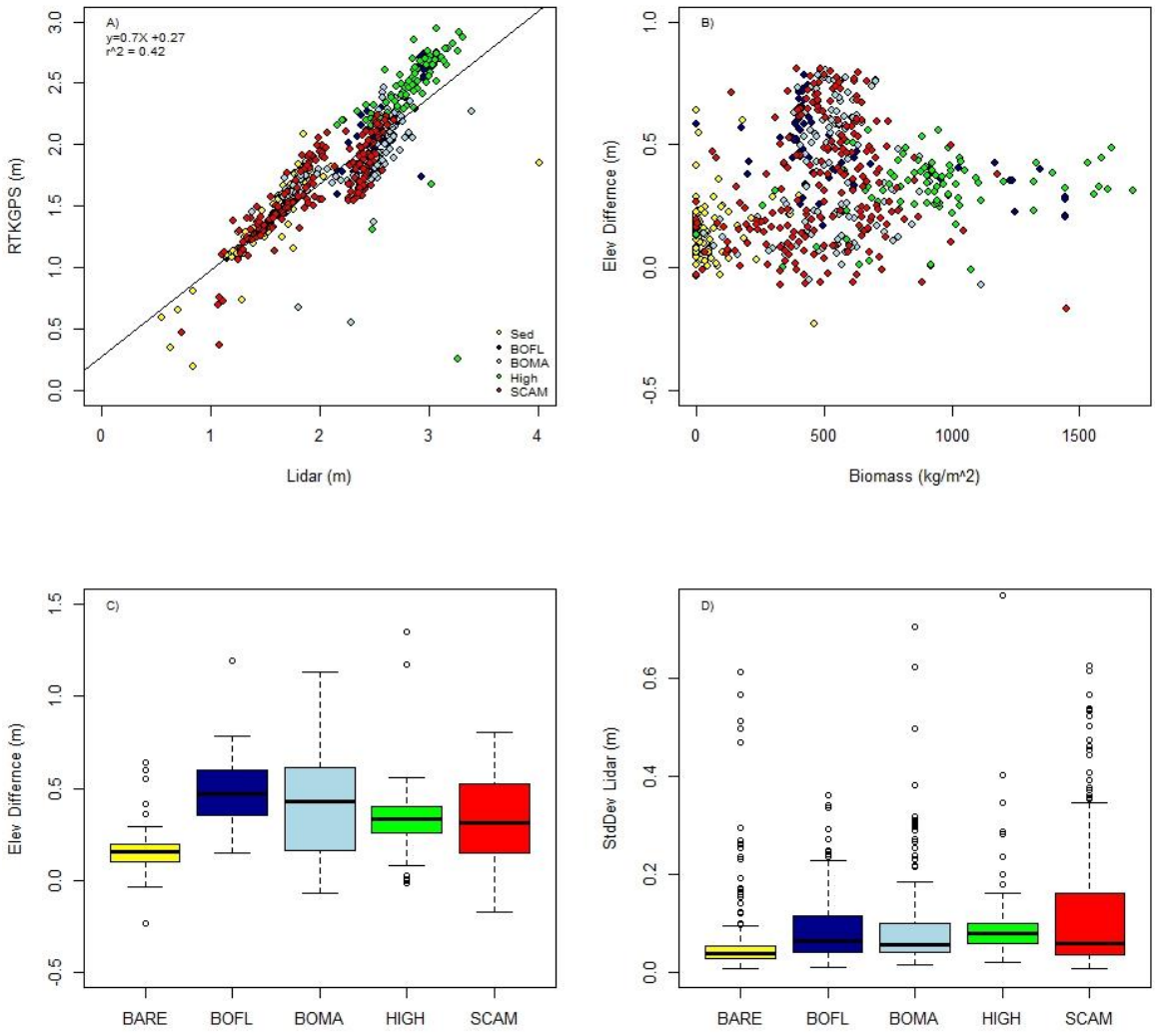

Figure 43. Exploratory plots of the RTKGPS and difference (LiDAR BE minus RTKGPS z values) data compared to LiDAR BE and Biomass. Box plots of difference values and Standard deviation of LiDAR BE values within the 5 m radius polygons around RTKGPS points.

Appendix 2: Cover Classes and Spectral Signatures

This appendix details the spectral signatures for all cover types (Figures 44 – 49). Spectral signatures were assessed in two ways: 1) remotely using hyperspectral data taken on September 10th 2014; 2) in-situ measurements using an ASD FieldSpec® HandHeld 2.

Hyperspectral imagery was taken by the Joint Airborne LiDAR Bathymetry Technical Center of Expertise (JALBTCX) within the US Army Corps of Engineers and funded by the USGS's Coastal Habitat in Puget Sound (CHIPS) project. Hyperspectral imagery data were taken with a Compact Airborne Spectrographic Imager (CASI) on September 10th at a 2000 m elevation at during low tide and (approximately 1500 hours). CASI imagery contains 48 spectral bands that are evenly spaced (14.0625nm bandwidths) to provide continuous spectral coverage from 375nm to 1050nm at 1 m pixel resolution. Spectral signatures were derived by using a 10 m diameter buffer around GPS land cover ground truth points.

In-situ spectral signatures were taken using the ASD FieldSpec® Handheld 2 on September 11th and 12th 2014 within Port Susan Bay. These data are shared here for comparison only; these field spectral signatures were not applied to the remote sensing classification scheme of the CASI dataset. At each ground truth site we took spectral signatures within a roughly homogenous patch of vegetation or sediment at least 10 m in diameter. We took 9 spectral signatures within a ¼ m^2 quadrat: 3 spectral signatures were taken 6in above land cover at nadir; 3 were taken 6 in above land-cover off nadir (~45 degrees); 3 signatures were taken at chest height (1.5 m) (Table 13). Note: additional in-situ spectral data were taken at Padilla bay and Skagit Bay estuaries. In general, these data are not shown here except for the native eelgrass data taken from Padilla Bay while floating at the water surface. We made an exception for these data because native eelgrass data were not taken in Port Susan Bay.

Table 13. Details of the number of spectral signatures and ground truth sites for both the ASD and CASI datasets. CASI spectral signatures are the average of all the pixels within a 5 m radius of a GPS ground truth point.

Land-cover	***ASD*** *Spectral Signature Count*	***ASD*** *Site Count*	***CASI*** *Site Count*
Beachwood	-	-	5
Blackberries	-	-	2
BOFL	-	-	14
BOMA	27	3	27
Carrex	18	2	5
Cattails	18	2	2
Native Eelgrass	18	2	11
Grass	9	1	10
Japanese Eelgrass	18	2	7
Juncus	18	2	2
Bare (Mud)	14	2	28
POPA	9	1	1
Sand	27	3	6
SCAM	54	6	30
SCTA	9	1	4
Trees	-	-	3

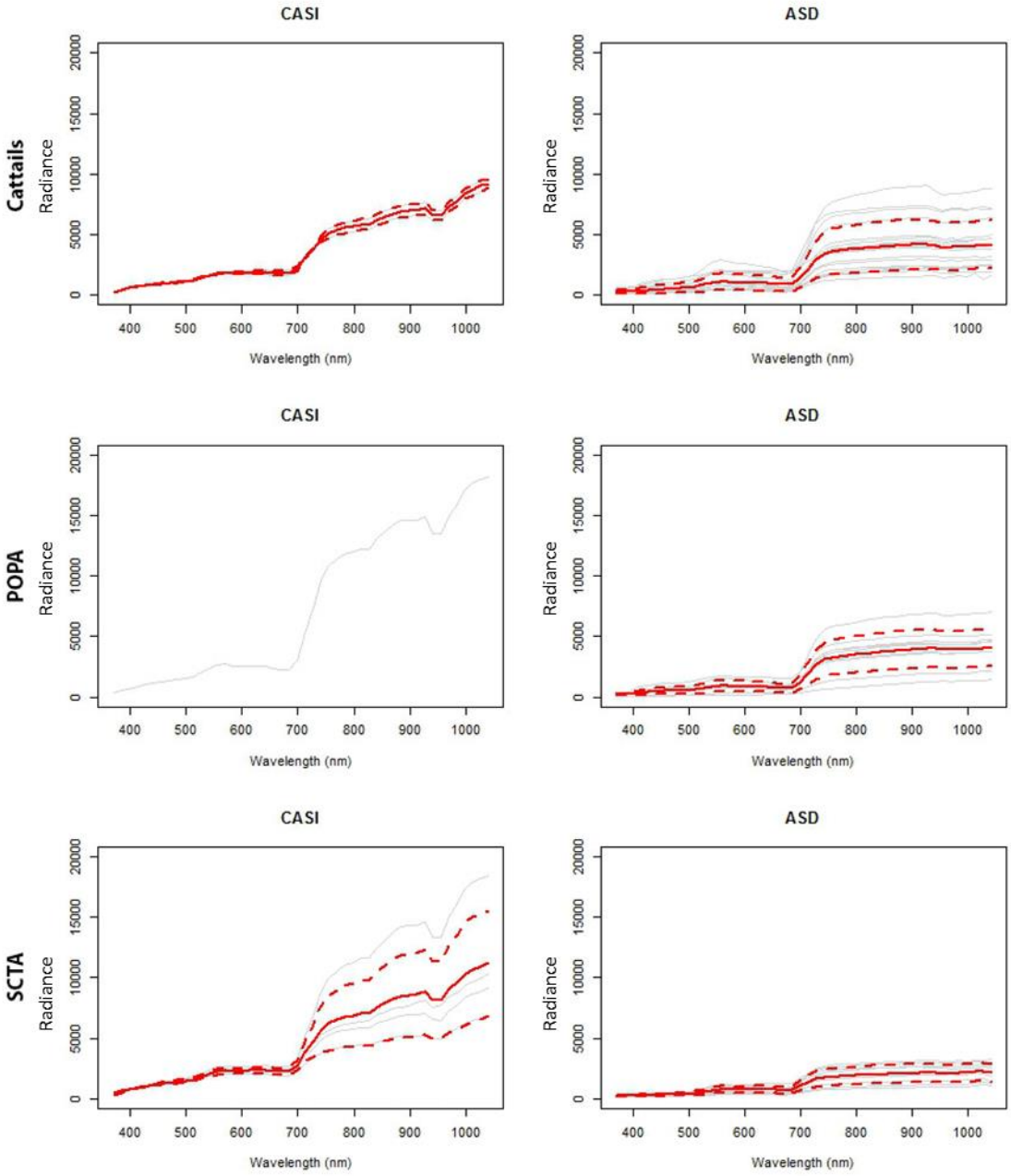

Figure 44. Spectral signatures for High-Marsh vegetation species including Cattails (Typha latifolia and angustifolia), POPA (Potentilla Pacifica) and SCTA (Schoenoplectis tabernaemontani). Solid red line is the mean spectral signature; dashed redlines are one standard deviation; solid light gray lines are individual spectral signatures. Note: CASI spectral signatures are the average for a defined region of interest (5 m radius around a GPS point). See Table 13 for spectral signature count and site count.

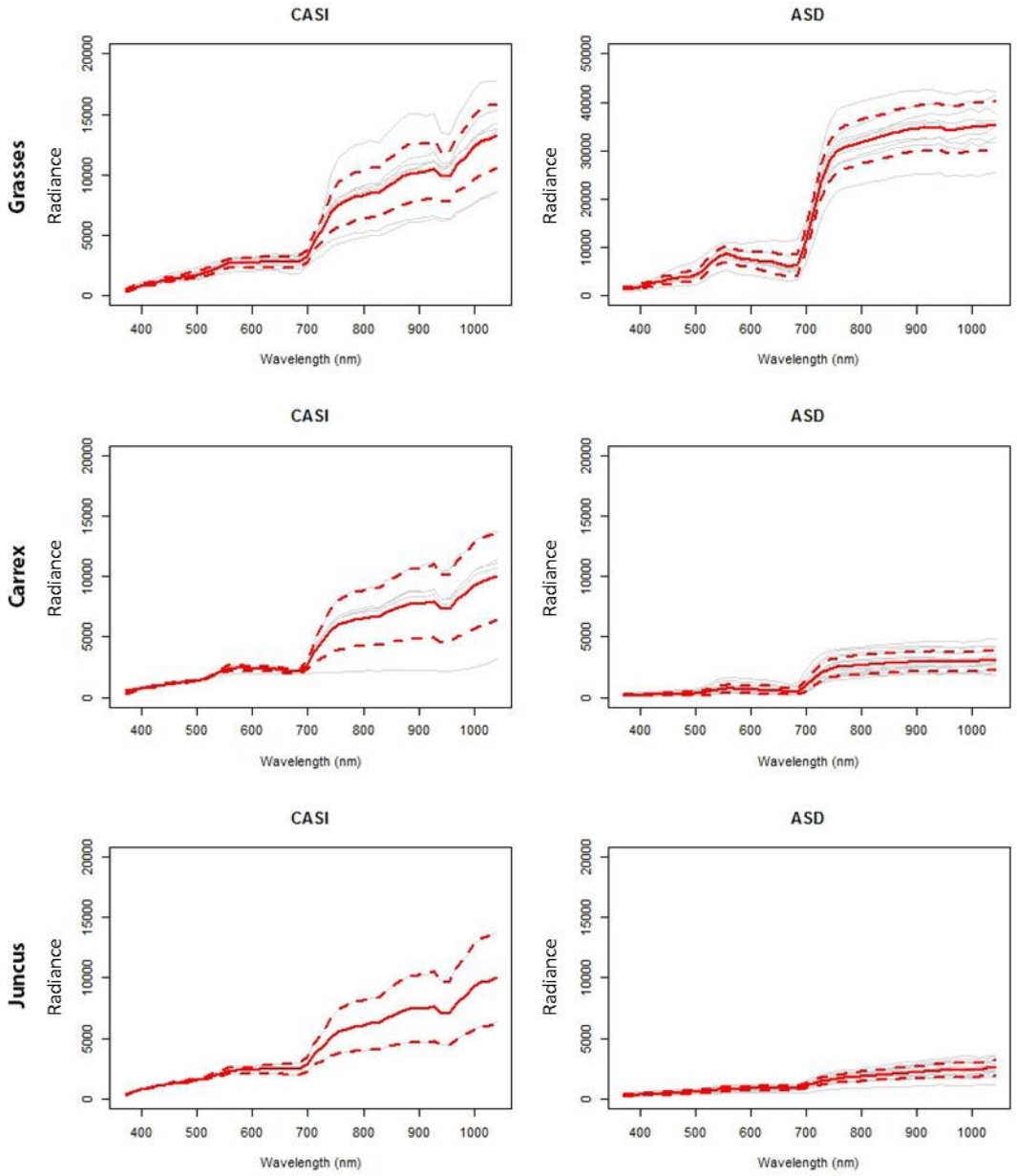

Figure 45. Spectral signatures for High-Marsh vegetation species including undifferentiated Grasses, Carex (Carex lyngbyei) and Juncus (Juncus Balticus)). Solid red line is the mean spectral signature; dashed redlines are one standard deviation; solid light gray lines are individual spectral signatures. Note: CASI spectral signatures are the average for a defined region of interest. Note: the change in scale for ASD signatures for Grasses land-cover.

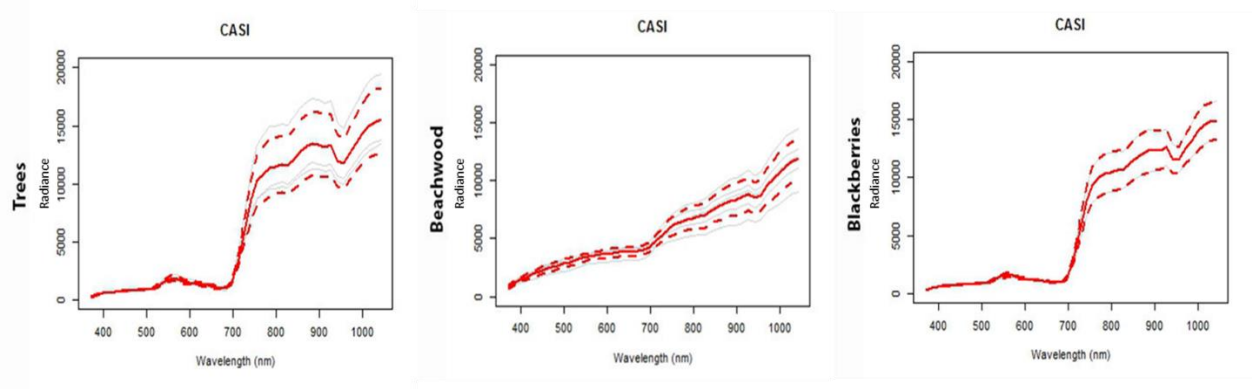

Figure 46. Spectral signatures for other High-Marsh land-cover classes defined during the aerial imagery classification: Himalayan blackberries (Rubis discolor); Beachwood, and undifferentiated trees. Solid red line is the mean spectral signature; dashed redlines are one standard deviation; solid light gray lines are individual spectral signatures. Note: CASI spectral signatures are the average for a defined region of interest. The ground truth areas for these cover types were digitized from aerial imagery because these were not priority cover types.

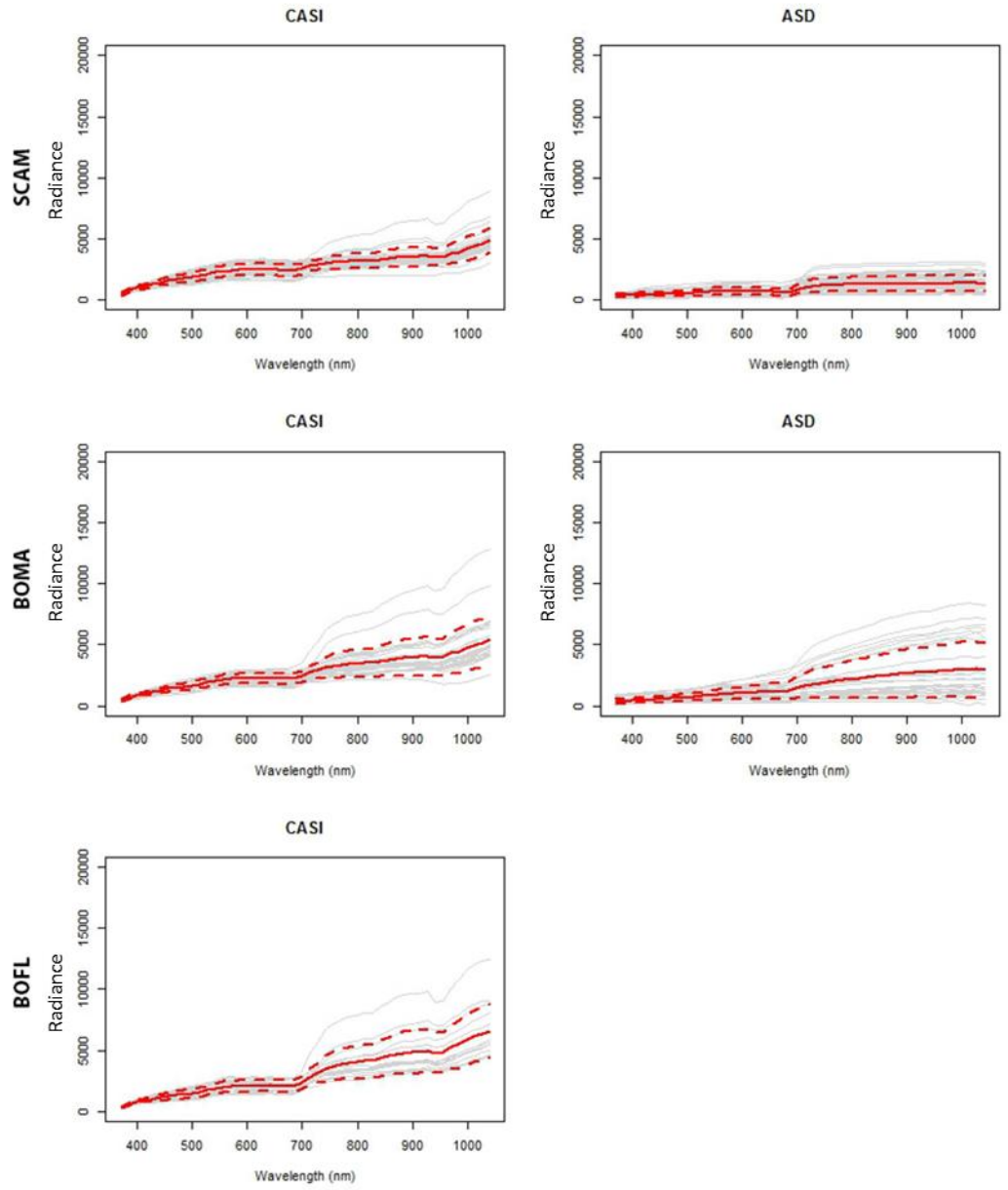

Figure 47. Spectral signatures for emergent Mid-Marsh vegetation species: SCAM (Schoenoplectis americanus); BOMA (Bolboschienus maitimus); BOFL (Bolboschoenus fluviatilis). Solid red line is the mean spectral signature; dashed redlines are one standard deviation; solid light gray lines are individual spectral signatures. Note: CASI spectral signatures are the average for a defined region of interest. There may be some misclassified BOFL spectral signatures as BOMA. At the beginning of this study, BOFL and BOMA were considered the same species.

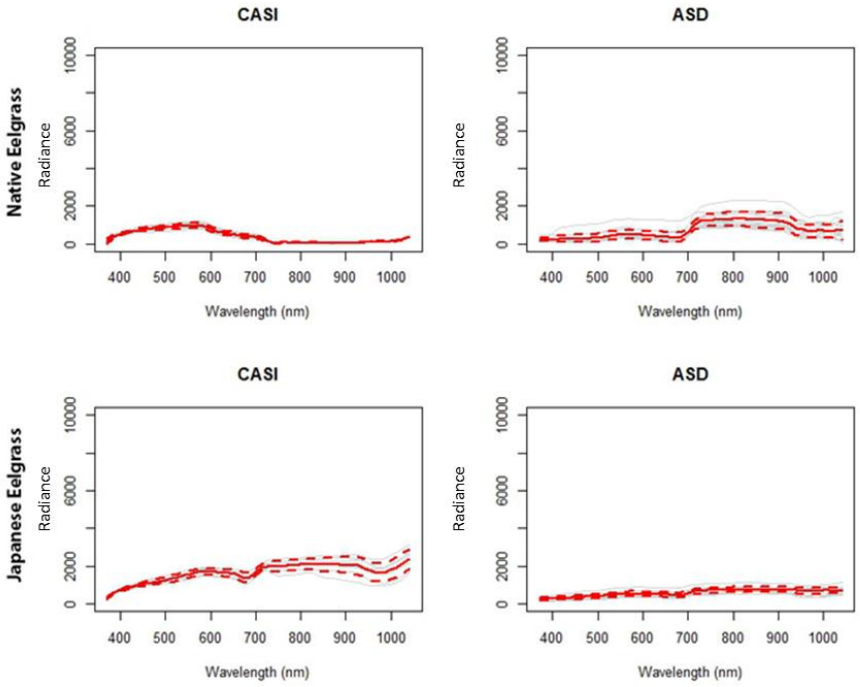

Figure 48. Spectral signatures for submergent vegetation species: Japanese Eelgrass (Zostera Japonica) and Native Eelgrass (Zostera marina) floating on water surface. Solid red line is the mean spectral signature; dashed redlines are one standard deviation; solid light gray lines are individual spectral signatures. Note: CASI spectral signatures are the average for a defined region of interest.

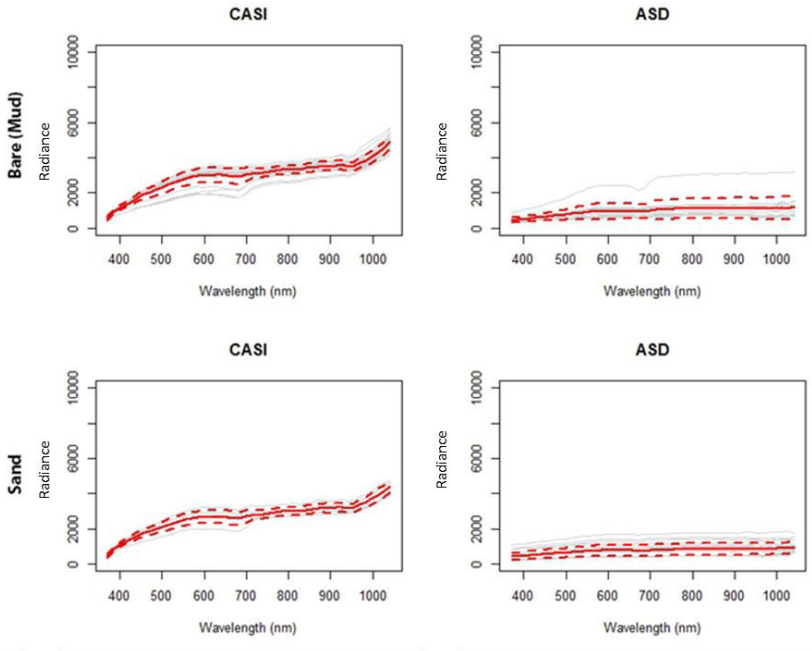

Figure 49. Spectral signatures for bare sediment: undefined bare defaults to Bare (Mud) and Sand. Solid red line is the mean spectral signature; dashed redlines are one standard deviation; solid light gray lines are individual spectral signatures. Note: CASI spectral signatures are the average for a defined region of interest.

Appendix 3: Decision Tree Classification (DTC)

This appendix details the criteria used for the decision tree classification. This appendix first outlines the step-by-step thought process we used to develop these decision trees. Second, we detail the statistics and regions used to complete our decision tree classification. Our decision trees were created using the ENVI remote sensing software program.

We decided on the appropriate land-cover classes; these were slightly different than the land-cover classes used in the Maximum-Likelihood Classification (MLC). The MLC utilized the dominant plant species, assemblage or land-cover. During the DTC, we grouped the marsh assemblages into four categories: High, Mid-BOFL, Mid-BOMA and Low-Marsh. The MLC began with 6 cover types for High-Marsh (SCTA, POPA, Carex, Juncus, Grasses, and Cattails) and 3 cover types for each of the Mid (BOMA and BOFL) and Low-Marsh (SCAM) assemblages based on plant density (low density; moderate density; high density). The MLC was not able to capture plant densities accurately; therefore, these sub-classes were combined.

Next, we generated the statistics for the NDVI and elevation data for our ground truth areas (Tables 15 – 16). These data come from the average value of a 5 m radius buffer around GPS ground truth points. Elevation data is from the LiDAR bare earth dataset, which represents elevation and an unknown portion of the marsh canopy (~0.6 m from marsh surface) (Appendix 1).

Through experimental analysis, we discovered that the elevation ranges for assemblages differ spatially; this was confirmed by Fuller (2015, Written comm.). We divided the delta in to three zones: North; South; and Restoration Zone (Figure 50). We defined these zones by areas north of the main stem of the Stillaguamish River (North zone), south of the Stillaguamish River (South Zone) and, within the restoration area. The south zone typically has the highest elevation for assemblages, suggestion higher sediment delivery and retention. The restoration site has the lowest elevation for Mid-Marsh

assemblages because of subsidence before the farmland was reclaimed. We assume that NDVI values do not differ spatially.

We separated cover type statistics by zone and addressed the zones with separate decision trees. For every marsh cover type, we created three decision trees, one for each zone (Figures 51-53). Note: the restoration site only contained Mid-Marsh species (BOFL and BOMA).

The decision trees are a series of conditional statements that we applied to the MLC classification to minimize misclassified pixels within the mid and Low-Marsh. We focused primarily on the Mid and Low-Marsh because they did not separate well from each other during the MLC and their importance to wave attenuation. Each decision tree is formatted to separate a cover type from its most likely neighbors. The general format is for a pixel to be reclassified it must fail the minimum NDVI to be considered plants or fall outside one standard deviation in both elevation and NDVI. However, we occasionally deviated from this format depending on the how similar the cover class was to its neighbors. Below is the detailed thought process for each decision tree.

The restoration site is rather unique in that region dominated by BOMA and/or BOFL. Using the training data, we estimated the cutoff as 2.3 m elevation. Biophysically speaking, BOFL and BOMA and non-distinct; we separate the two according to height in this study. However, if the BOFL is stressed then it is likely to be shorter and indistinguishable from BOMA without lab testing (Fuller, 2015, written comm.). This 2.3 m cutoff may seem arbitrary but is more to distinguish plant height rather than species.

BOMA North-Zone

1) Is the pixel classified as BOMA in the MLC and within the North Zone?
    a. Yes – Continue to Step 2
    b. No - Not considered in the decision tree.
2) Is the NDVI value high enough to be plant material (NDVI > 0.06)?
    a. Yes – Continue to step 3
    b. No – Reclassify pixel as Bare
3) Is the elevation greater than one sigma **below** the mean elevation (Elev > 2.03)?
    a. Yes – continue to step 4
    b. No – continue to step
4) Is the elevation greater than one sigma **above** the mean elevation (Elev > 2.77)?
    a. Yes – continue to step 5
    b. No – within the average elevation range for BOMA. Remains classified as BOMA.
5) Is the NDVI greater than the mean + 0.5 sigma NDVI value for BOMA (NDVI >0.25)?
    a. Yes – pixel failed two assumptions –reclassify to BOFL
    b. No – pixel did not fail two assumptions – retain as BOMA
        i. Note: BOFL and BOMA had overlapping NDVI values. We decide that ½ sigma above the mean NDVI values for BOMA would be a more appropriate separate than a whole standard deviation.
6) Is the elevation greater than 2 sigma **below** the mean elevation (Elev > 1.68)?
    a. Yes – continue to step 7
    b. No – continue to step 8
7) Is the NDVI greater the mean NDVI value for BOMA (NDVI >0.2)?
    a. Yes – Retain pixel as BOMA
    b. No – pixel failled two assumptions – reclassify as SCAM
        i. Note: We decided that the mean NDVI value would be more appropriate value through experimentation. When we used one sigma below the NDVI mean value, there was large portions of the SCAM-dominated Low-Marsh that remained misclassified.
8) Is the pixel below 1.2 m elevation?
    a. Yes – reclassify as bare
    b. No – reclassify as SCAM
        i. Note: this conditional statement is a reclassify outliers. These pixels have already failed 2 sigma below the BOMA mean elevation and therefore needs to

be reclassified. SCAM minimum elevation is 1.2 m. Any pixel below that threshold is assumed to be bare sediment.

BOMA South-Zone

1) Is the pixel classified as BOMA in the MLC and within the South-Zone?
    a. Yes – continue to step 2
    b. No – not considered in this decision tree

2) Is the NDVI value high enough to be plant material (NDVI > 0.06)?
    a. Yes – Continue to step 3
    b. No – Reclassify pixel as Bare

3) Is the Elevation value less than 2.6 m?
    a. Yes – Reclassify as SCAM
    b. No- continue to step 4
        i. The southern zone is particularly dominated by SCAM and has very little BOMA or BOFL. Therefore, we decided that we would use an elevation cutoff above the mean value for BOMA. We chose 2.6 m elevation as the cut-off because it was 2 sigma greater than the mean elevation for SCAM.
4) Is the NDVI value greater than 0.2?
    a. Yes – retain as BOMA
    b. No – reclassify as SCAM

We chose 0.2 as the NDVI cut-off because the south zone NDVI statistics only take into account 27 ground truth points containing 3 BOMA and 1 BOFL site. We assume that NDVI values do not vary spatially. We used all training ground truth points for the NDVI statics and decision tree cut-offs.

BOMA – Restoration Site

1) Is the pixel classified as BOMA in the MLC and within the restoration site?
    a. Yes – continue to step 2
    b. No – not considered in this classification
2) Is the NDVI value high enough to be plant material (NDVI > 0.06)?
    a. Yes – Continue to step 3
    b. No – Reclassify pixel as Bare
3) Is the elevation above 2.3 m elevation?
    a. Yes – reclassify as BOFL
    b. No – retain as BOMA
    c. The restoration site is rather unique in that region dominated by BOMA and/or BOFL. Using the training data, we estimated the cutoff as 2.3 m elevation. Biophysically speaking, BOFL and BOMA and non-distinct; we separate the two according to height in this study. However, if the BOFL is stressed then it is likely to be shorter and indistinguishable from BOMA without lab testing (Fuller, 2015, written comm.). This 2.3 m cutoff may seem arbitrary but is to distinguish plant height rather than species.

SCAM – North Zone

1) Is the pixel classified as SCAM in the MLC and within the North Zone?
    a. Yes – Continue to Step 2
    b. No - Not considered in the decision tree.

2) Is the NDVI value high enough to be plant material (NDVI > 0.06)?
    a. Yes – Continue to step 3
    b. No – Reclassify pixel as Bare
3) Is the DEM value below 1.2?
    a. Yes –Continue to step 4
    b. No – reclassifiy as Bare
        i. Recall that 1.2 m elevation is the lowest occurrence of SCAM
4) Is the DEM value above 2.75 m?
    a. Yes – reclassifiy as BOFL
    b. No – continue to step 5.
        i. Max elevation for SCAM is 2.5 m. 2.75 m is one sigma above the mean elevation values for BOMA
5) Is the NDVI value less than 0.22?
    a. Yes - continue to step 7
    b. No – continue to step 6
6) This is to generally separate BOMA from SCAM based on NDVI values. If the NDVI values are lower, more similar than SCAM, then to be reclassified the pixel would need to be outside the DEM range of SCAM (2.5 m – step7). If the pixel has a higher NDVI value, more similar to BOMA, then it only needs to be outside one sigma of SCAM's elevation range (elev >1.9; Step 6).
7) Is the elevation value greator than 1.9 m?

a. Yes – reclassify as BOMA
b. No – retain as SCAM

8) Is the elevation value outside the range of SCAM (Elev > 2.5)?
    a. Yes – reclassify as BOMA
    b. No – retain as SCAM

SCAM – South Zone

1) Is the pixel classified as SCAM in the MLC and within the South Zone?
    a. Yes – Continue to Step 2
    b. No - Not considered in the decision tree.
2) Is the NDVI value high enough to be plant material (NDVI > 0.06)?
    a. Yes – Continue to step 3
    b. No – Reclassify pixel as Bare
3) Is the elevation value below 1.2?
    a. Yes –Continue to step 4
    b. No – reclassify as Bare
        i. Recall that 1.2 m elevation is the lowest occurrence of SCAM
4) Is the Elevation value greater than 2.6 m?
    a. Yes – continue to step 5
    b. No- retain pixel as SCAM
        i. The southern zone is dominated by SCAM. we decided that we would use an elevation cutoff above the mean value for BOMA. We chose 2.6 m elevation as the cut-off because it was 2 sigma greater than the mean elevation for SCAM.
5) Is the NDVI value greater than 0.22
    a. Yes - Reclassify as BOMA
    b. No – Retain as SCAM

SCAM – Restoration Site

1) Is the pixel classified as SCAM in the MLC and within the restoration site?
    a. Yes – continue to step 2
    b. No – not considered in this classification
2) Is the NDVI value high enough to be plant material (NDVI > 0.06)?
    a. Yes – Continue to step 3
    b. No – Reclassify pixel as Bare
3) Is the elevation above 2.3 m elevation?
    a. Yes – reclassify as BOFL
    b. No – retain as BOMA
        i. Recall that there was no notable SCAM patches with in restoration site in 2014.

BOFL North-Zone

1) Is the pixel classified as BOFL in the MLC and within the North Zone?
    c. Yes – Continue to Step 2
    d. No - Not considered in the decision tree.
2) Is the NDVI value high enough to be plant material (NDVI > 0.06)?
    a. Yes – Continue to step 3
    b. No – Reclassify pixel as Bare
3) Is the elevation greater than one sigma **below** the mean elevation (Elev > 2.48)?

    a. Yes – continue to step 4
    b. No – continue to step 6
4) Is the NDVI greater than one sigma **above** the mean NDVI value (NDVI >0.13)?
    a. Yes – retain as BOFL
    b. No – Reclassify as BOMA
5) Is the elevation less than 2 sigma **below** mean elevation value for BOFL (Elev <2.0)?
    a. Yes – pixel failed two assumptions –continue to Step 7
    b. No – continue to step 6
6) Is the NDVI greater than 1 sigma **below** the mean NDVI value for BOFL (NDVI >0.29)?
    a. Yes – maintain as BOFL
    b. No – pixel failed to assumptions – reclassify to BOMA
7) Is the pixel below 1.2 m elevation?
    a. Yes – reclassify as bare
    b. No – reclassify as SCAM
        i. Note: this conditional statement is a reclassify outliers. These pixels have already failed 2 sigma below the BOMA mean elevation and therefore needs to be reclassified. SCAM minimum elevation is 1.2 m. Any pixel below that threshold is assumed to be bare sediment.
8) Is the NDVI greater the mean NDVI value for BOMA (NDVI >0.2)?
    a. Yes – reclassify pixel as BOMA
    b. No – reclassify as SCAM
        i. Note: We decided that the mean NDVI value would be more appropriate value through experimentation. When we used one sigma below the NDVI mean

value, there was large portions of the SCAM-dominated Low-Marsh that remained misclassified.

BOFL South-Zone

1) Is the pixel classified as BOFL in the MLC and within the South-Zone?
    c. Yes – continue to step 2
    d. No – not considered in this decision tree
2) Is the NDVI value high enough to be plant material (NDVI > 0.06)?
    a. Yes – Continue to step 3
    b. No – Reclassify pixel as Bare
3) Is the Elevation value greater than 2.75 m?
    a. Yes – Retain as BOFL
    b. No- continue to step 4
4) Is the Elevation value greater than 2.5 m?
    a. Yes – Reclassify as BOMA
    b. No – Continue to Step 5
5) Is the NDVI value greater than 0.3?
    a. Yes – retain as BOMA
    b. No – reclassify as SCAM

BOFL – Restoration Site

1) Is the pixel classified as BOMA in the MLC and within the restoration site?
    d. Yes – continue to step 2
    e. No – not considered in this classification
4) Is the NDVI value high enough to be plant material (NDVI > 0.06)?
    a. Yes – Continue to step 3
    b. No – Reclassify pixel as Bare
5) Is the elevation above 2.3 m elevation?
    a. Yes – reclassify as BOFL
    b. No – retain as BOMA

Table 15. Elevation Statistics for all cover classes for the South, North and All Zones.

			NDVI All				NDVI South Zone					NDVI North Zone				
Landcover	Pixel Count	Min	Max	Mean	StdDev	Pixel Count	Min	Max	Mean	StdDev	Pixel Count	Min	Max	Mean	StdDev
Blackberries	873	0.655	0.896	0.837	0.039	653	0.690	0.896	0.849	0.029	220	0.655	0.870	0.803	0.044
Beachwood	1781	0.070	0.804	0.209	0.129						1781	0.070	0.804	0.209	0.129
Juncus	195	0.265	0.581	0.406	0.081	195	0.265	0.581	0.406	0.081					
Trees	394	0.272	0.904	0.826	0.096	394	0.272	0.904	0.826	0.096					
Carrex	472	-0.185	0.749	0.442	0.222	284	0.330	0.629	0.530	0.051	188	-0.185	0.749	0.309	0.300
Grasses	940	0.165	0.800	0.485	0.124	285	0.404	0.800	0.595	0.119	655	0.165	0.668	0.438	0.092
SCTA	285	0.318	0.760	0.484	0.112	285	0.318	0.760	0.484	0.112					
POPA	98	0.594	0.793	0.684	0.037	98	0.594	0.793	0.684	0.037					
Cattails	192	0.300	0.624	0.510	0.083	192	0.300	0.624	0.510	0.083					
JapEel	95	-0.278	0.297	-0.063	0.119						95	-0.278	0.297	-0.063	0.119
Sand	382	-0.066	0.352	0.078	0.096	95	-0.066	0.352	0.207	0.118	287	-0.027	0.124	0.035	0.020
Mud	2092	-0.034	0.397	0.050	0.048						2092	-0.034	0.397	0.050	0.048
BOFL	1222	0.037	0.711	0.329	0.174	96	0.225	0.588	0.498	0.074	1126	0.037	0.711	0.314	0.172
BOMA	3330	-0.003	0.675	0.217	0.117	288	0.256	0.494	0.339	0.039	3042	-0.003	0.675	0.205	0.115
SCAM	2383	-0.358	0.438	0.106	0.092	479	0.124	0.438	0.227	0.044	1904	-0.358	0.365	0.075	0.074

Table 14. NDVI statistics for all cover classes for the South, North and All Zones. Note: we assumed that the NDVI values did not vary spatially and used the combined All zones for the development of the decision trees. However, all data is included here.

			Elevation				South Zone ELelvation					North Zone Elevation				
Landcover	Pixel Count	Min	Max	Mean	StdDev	Pixel Count	Min	Max	Mean	StdDev	Pixel Count	Min	Max	Mean	StdDev
Blackberries	1277	2.950	3.760	3.230	0.139	974	2.950	3.760	3.183	0.116	303	3.130	3.570	3.379	0.092
Beachwood	2463	2.440	3.760	3.029	0.296						2463	2.440	3.760	3.029	0.296
Juncus	263	2.350	3.080	2.774	0.213	263	2.350	3.080	2.774	0.213					
Trees	591	2.310	3.940	3.363	0.232	591	2.310	3.940	3.363	0.232					
Carrex	675	0.590	3.140	2.525	0.641	407	2.470	2.990	2.773	0.101	268	0.590	3.140	2.147	0.885
Grasses	1339	2.550	3.550	2.995	0.174	400	2.780	3.230	3.006	0.086	939	2.550	3.550	2.991	0.201
SCTA	401	2.310	3.080	2.678	0.234	401	2.310	3.080	2.678	0.234					
POPA	137	2.940	3.360	3.050	0.084	137	2.940	3.360	3.050	0.084					
Cattails	265	2.480	3.050	2.735	0.103	265	2.480	3.050	2.735	0.103					
JapEel	133	0.360	0.930	0.549	0.112						133	0.360	0.930	0.549	0.112
Sand	532	0.620	2.550	1.307	0.453	131	0.830	2.550	1.803	0.608	401	0.620	1.530	1.145	0.212
Mud	2929	0.960	2.910	1.694	0.330						2929	0.960	2.910	1.694	0.330
BOFL	1742	2.310	3.470	2.765	0.262	131	2.640	3.040	2.786	0.092	1611	2.310	3.470	2.763	0.271
BOMA	4711	1.480	3.145	2.412	0.357	404	2.330	2.740	2.500	0.071	4307	1.480	3.145	2.404	0.371
SCAM	3342	0.480	2.760	1.738	0.459	668	1.810	2.760	2.415	0.112	2674	0.480	2.520	1.569	0.343

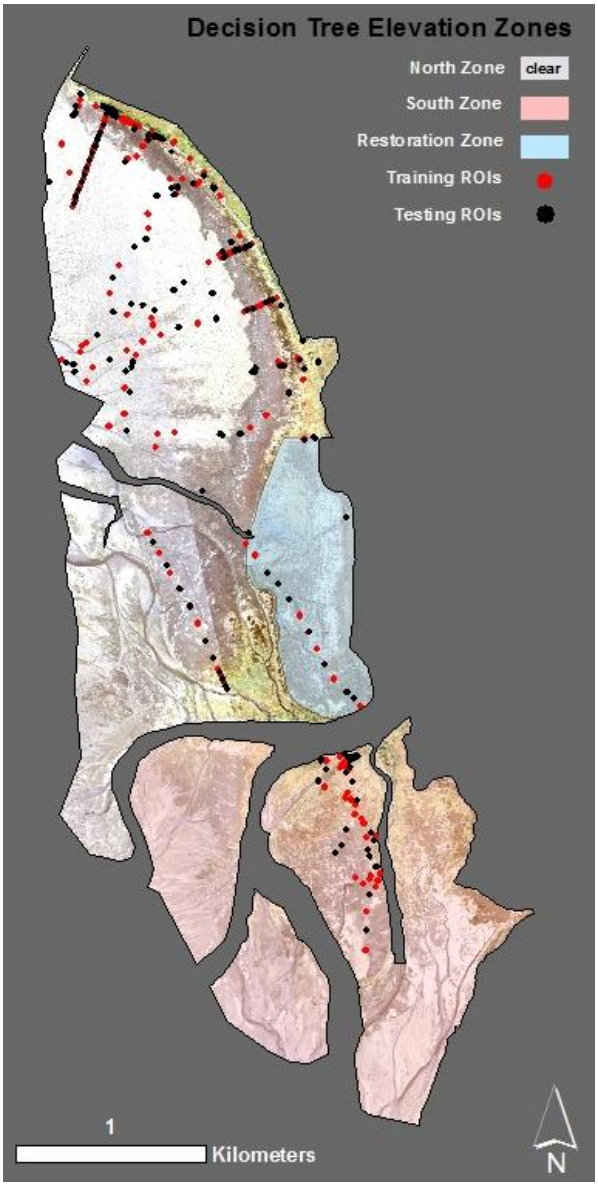

Figure 50. Map detailing the zones for the decision tree classifications. Training ROIs were used to generate the statistics in Table 12 and 13. Testing ROIs were used to create the confusion matrices.

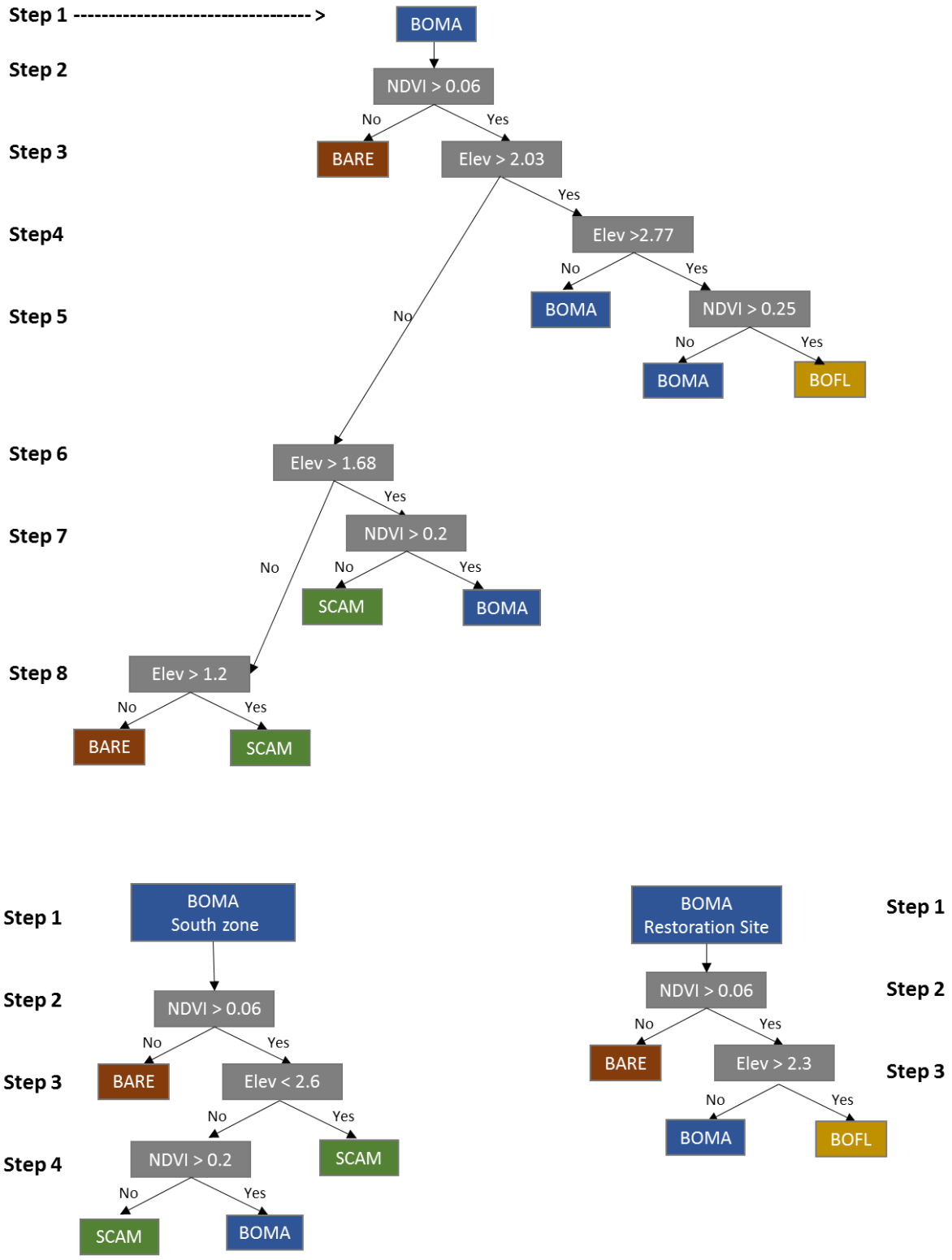

Figure 51. Decision Tree diagrams to isolate BOMA. Decision trees were initially created using data in Tables 12-13, where a pixel would only be reclassified if it fell out of the standard deviation of two or more classes. Decision trees were altered to account for spatially dependent elevation (South Zone and Restoration Site).

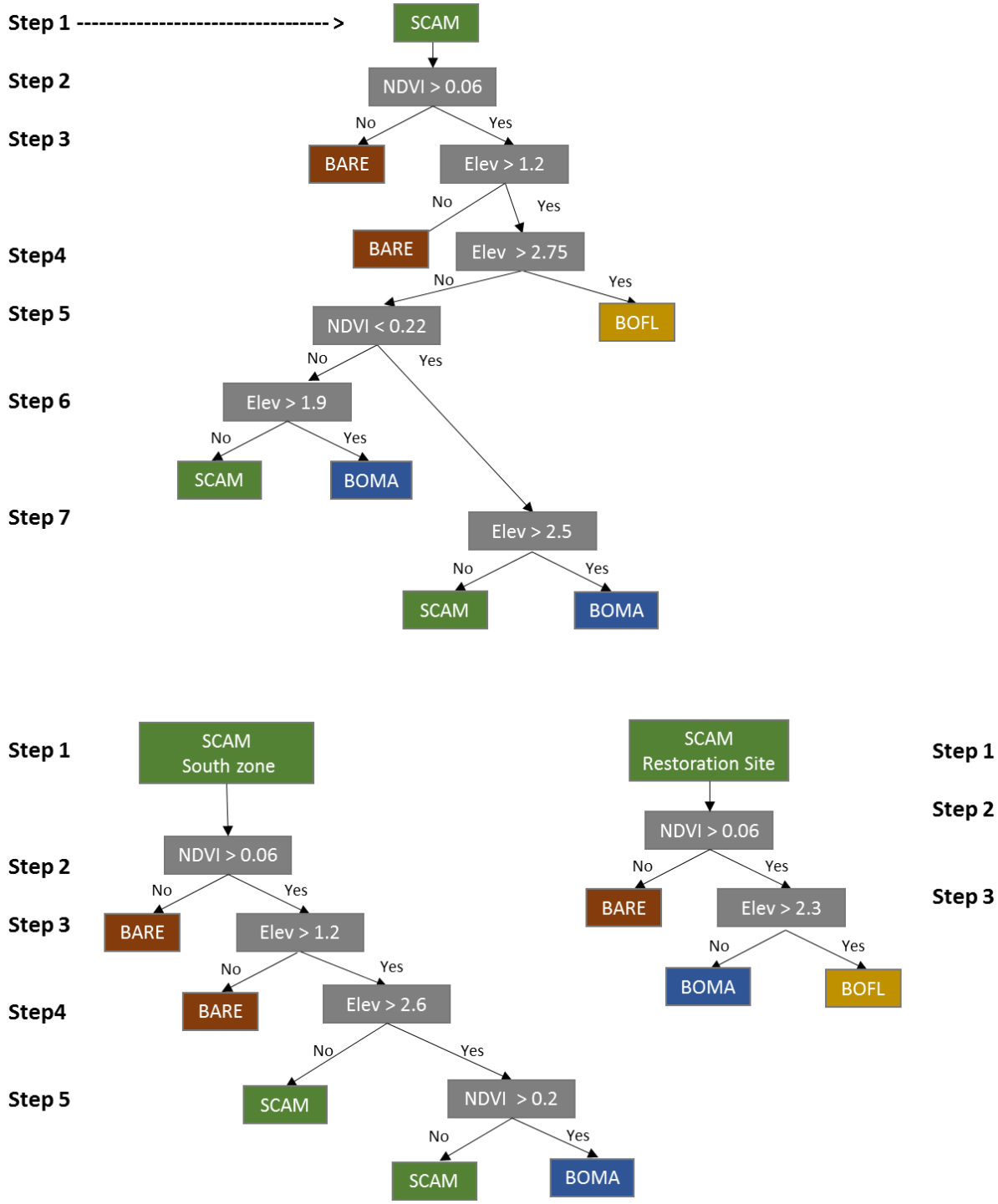

Figure 52. Decision Tree diagrams to isolate SCAM. Decision trees were initially created using data in Tables 12-13, where a pixel would only be reclassified if it fell out of the standard deviation of two or more classes. Decision trees were altered to account for spatially dependent elevation (South Zone and Restoration Site).

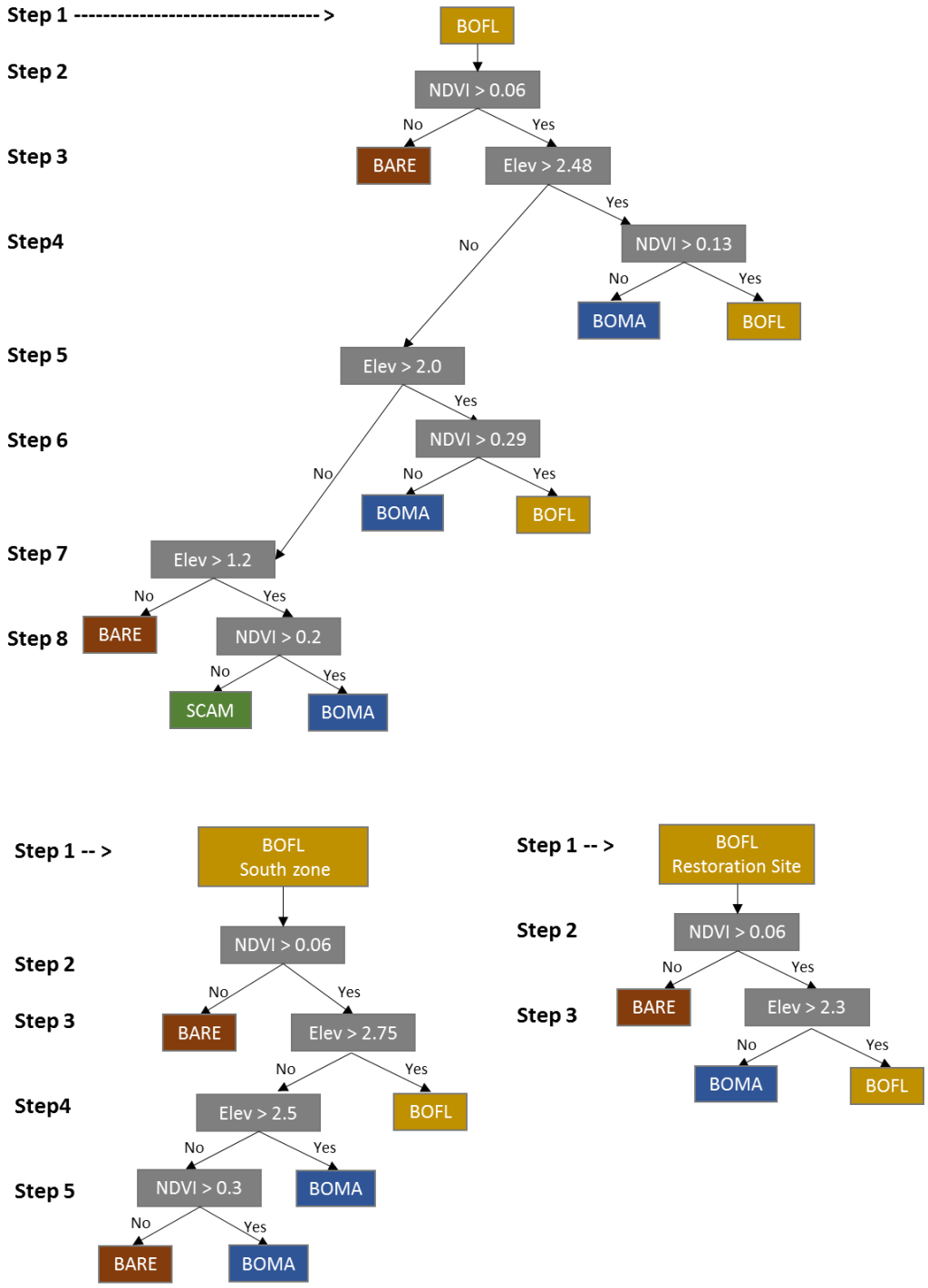

Figure 53. Decision Tree diagrams to isolate BOFL. Decision trees were initially created using data in Table 12, where a pixel would only be reclassified if it fell out of the standard deviation of two or more classes. Decision trees were altered to account for spatially dependent elevation (South Zone and Restoration Site).

Appendix 4: Biomass Model Derivation

This appendix is to detail our exploratory analysis in order to be able to extrapolate biomass and stem density across our study area. We compared our physical lab measurements (Biomass, stem count) from the Side-on Photo (SOP) sampling sites with LiDAR BareEarth DEM (Figure 54) and 8 vegetation indices derived from CASI hyperspectral imagery (Figure 55 – 56). We used the 8 vegetation indices compared in Delegido (2013) (Table 16). Note: aerial LiDAR is unable to penetrate the dense emergent marshlands and according to our analysis of RTKGPS data the BE LiDAR DEM is off by approximately 0.5 m within the dense marsh (Appendix 1).

Through this exploratory analysis, we found that a combination of elevation and the Red- Edge Normalized Difference Index (RE-NDI) yielded the best Kendall's correlation values when compared to biomass (Figure 56, Table 17-18). This relationship was used to create an exponential model to predict and extrapolate biomass across the delta (Figure 54 -56). Stem density did not correlate well with any of the vegetation indices and was not used in extrapolation (Table 17). We chose to use the RE-NDI for our biomass extrapolation because it had the most accurate linear model.

Table 16. Vegetation indices from Table 1 in Delegido et al. (2013), where R_λ is the reflectance values at wavelength λ. Note: equations were altered from Delegido et al (2013) to show median wavelength of bandwidths from the CASI dataset used in this study.

Vegetation Indices	*Equation*	*Reference*
NDVI	$(R_{804}-R_{669})/(R_{804}+R_{669})$	*Rouse et al. (1973)*
RE - NDI	$(R_{719}-R_{669})/(R_{719}+R_{669})$	*Delegido et al. (2013)*
MCARI	$[(R_{705}-R_{669}) -0.2(R_{705}-R_{550})R_{705}/R_{669}]$	*Daughtry et al. (2000)*
MTCI	$(R_{747}-R_{710})/(R_{710}+R_{680})$	*Dash and Curran (2004)*
TCI	$1.2(R_{705}-R_{550}) - 1.5(R_{669}-R_{550})(R_{705}/R_{669})^{0.5}$	*Haboudane et al. (2008*
RM	$R_{747}/R_{719} - 1$	*Gitelson et al. (2005)*
OSAVI	$(R_{804}-R_{669})/(R_{804}+R_{669}+0.16)$	*Rondeaux et al. (1996)*
SR	R_{804}/R_{669}	*Jordan (1969)*

Table 17. Statistics for vegetation indices and BE LiDAR DEM with respect to stem count.

	Stem Count				
	Kendall's Tau		*Linear model*		
Vegetation Indices	*Tau*	*p-value*	*Equation*	*adj. r^2*	*p-value*
NDVI	0.158	0.319	Y = 95.28 x + 67.59	-0.022	0.461
RE - NDI	0.196	0.216	Y = 230 x + 61.29	-0.006	0.36
MCARI	0.158	0.319	Y = 0.06 x + 78.9	-0.039	0.618
MTCI	0.033	0.833	Y = -2.91 x + 94.2	-0.052	0.943
TCI	0.167	0.29	Y = 0.04x + 79.67	-0.041	0.647
RM	0.081	0.608	Y = 7.81 x + 89.6	-0.052	0.918
OSAVI	0.158	0.319	Y = 95.3 x + 67.6	-0.022	0.461
SR	0.138	0.381	Y = 6.97 x + 81.0	-0.05	0.849
BE LiDAR DEM	0.148	0.349	Y = 36.1 x + 4.0	-0.02	0.45

Table 18. Statistics for vegetation indices and BE LiDAR DEM with respect to lab measured biomass in grams.

	Lab Measured Biomass (g)				
	Kendall's Tau		*Linear model*		
Vegetation Indices	*Tau*	*p-value*	*Equation*	*adj. r^2*	*p-value*
NDVI	0.396	0.015	Y = 279 x + 101.9	0.271	0.011
RE - NDI	0.417	0.01	Y = 577 x + 96.2	0.31	0.006
MCARI	0.449	0.006	Y = 0.23 x + 120.3	0.24	0.016
MTCI	0.269	0.098	Y = 60.5 x + 117.5	0.101	0.094
TCI	0.48	0.003	Y = 0.179 x + 119	0.238	0.017
RM	0.417	0.01	Y = 135 x + 137	0.168	0.041
OSAVI	0.396	0.015	Y = 279 x + 102	0.271	0.011
SR	0.396	0.015	Y = 66.6 x + 70.44	0.179	0.036
BE LiDAR DEM	0.406	0.012	Y = 116x -109	0.356	0.003

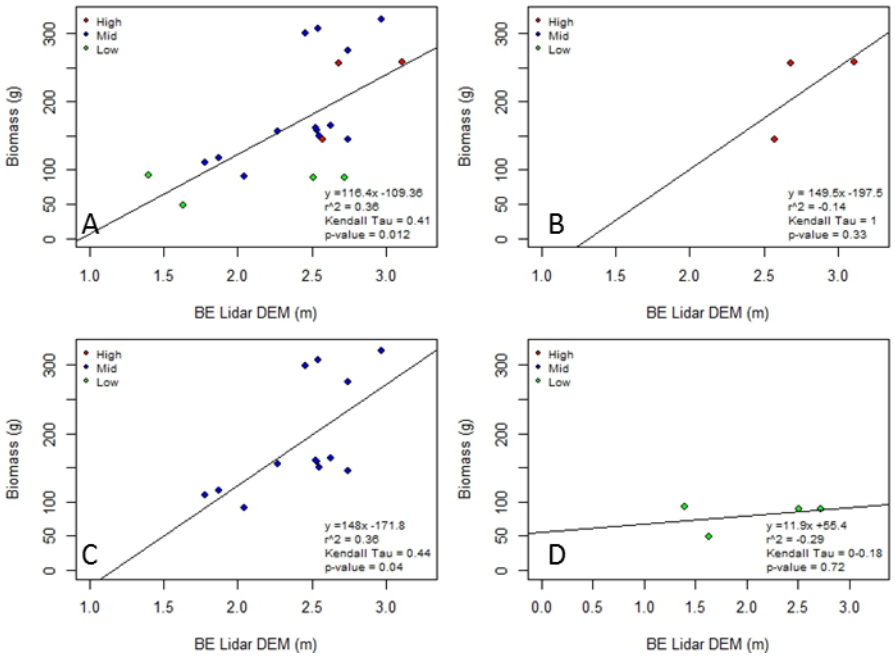

Figure 54. Scatter plots detailing the relationship of biomass to the BE LiDAR DEM. A) all marsh assemblages; B) High-Marsh; C) Mid – marsh, BOFL and BOMA assemblages undifferentiated; D) Low-Marsh

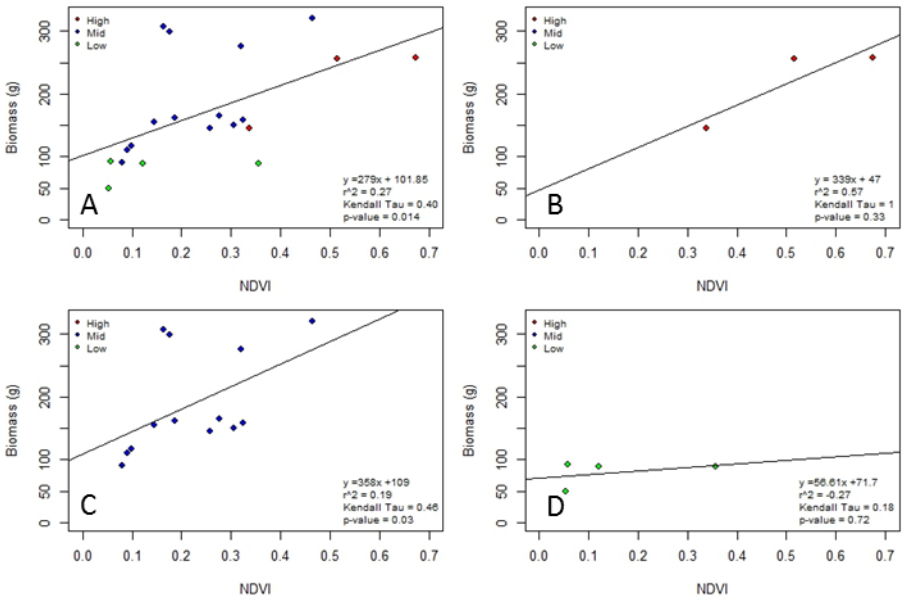

Figure 55. Scatter plots detailing the relationship of biomass to the NDVI from the CASI dataset. A) all marsh assemblages; B) High-Marsh; C) Mid – marsh, BOFL and BOMA assemblages undifferentiated; D) Low-Marsh

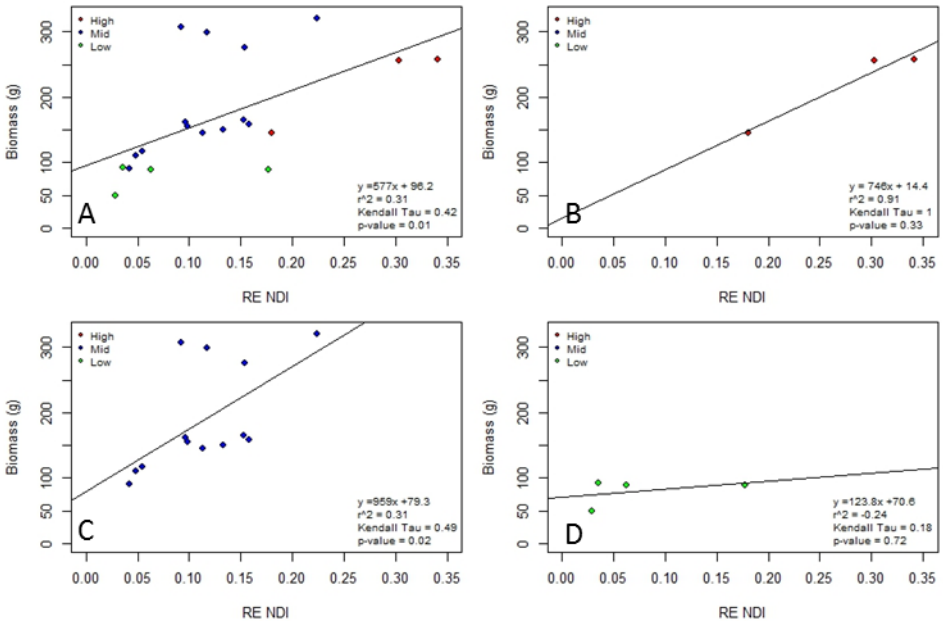

Figure 56. Scatter plots detailing the relationship of biomass to the RE – NDI. A) all marsh assemblages; B) High-Marsh; C) Mid – marsh, BOFL and BOMA assemblages undifferentiated; D) Low-Marsh

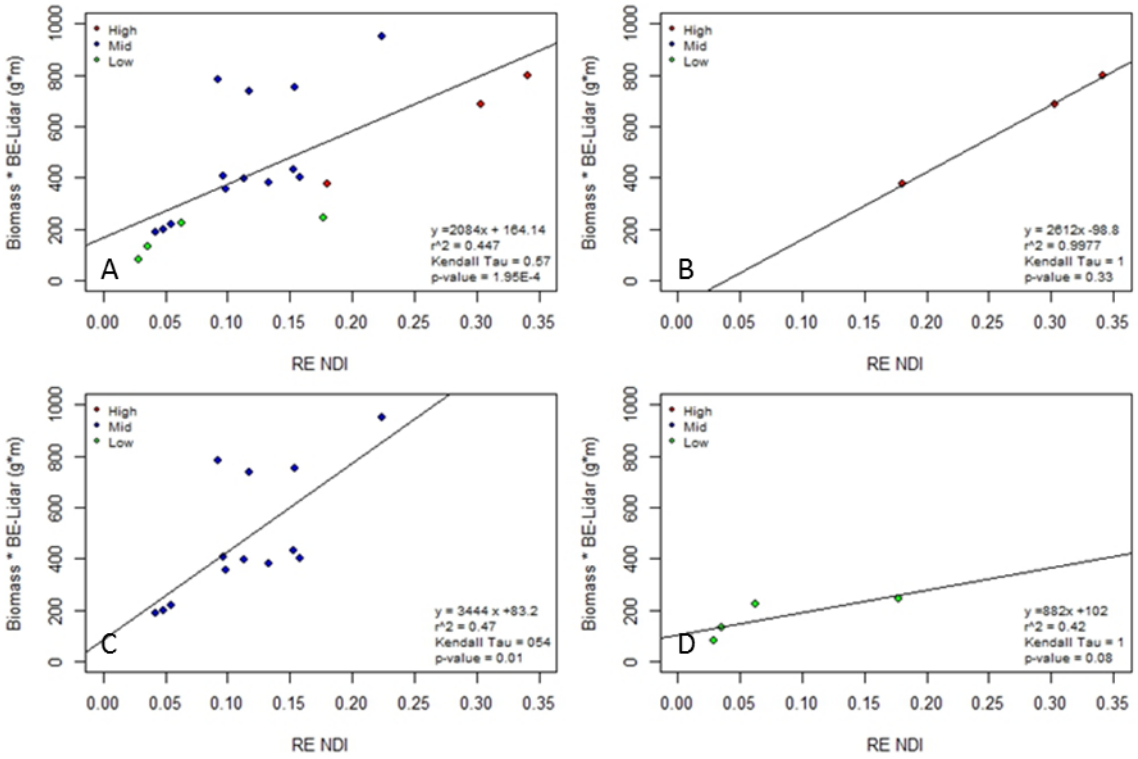

Figure 57. Scatter plots detailing the relationship of biomass to the BE LiDAR DEM. A) all marsh assemblages; B) High-Marsh; C) Mid – marsh, BOFL and BOMA assemblages undifferentiated; D) Low-Marsh

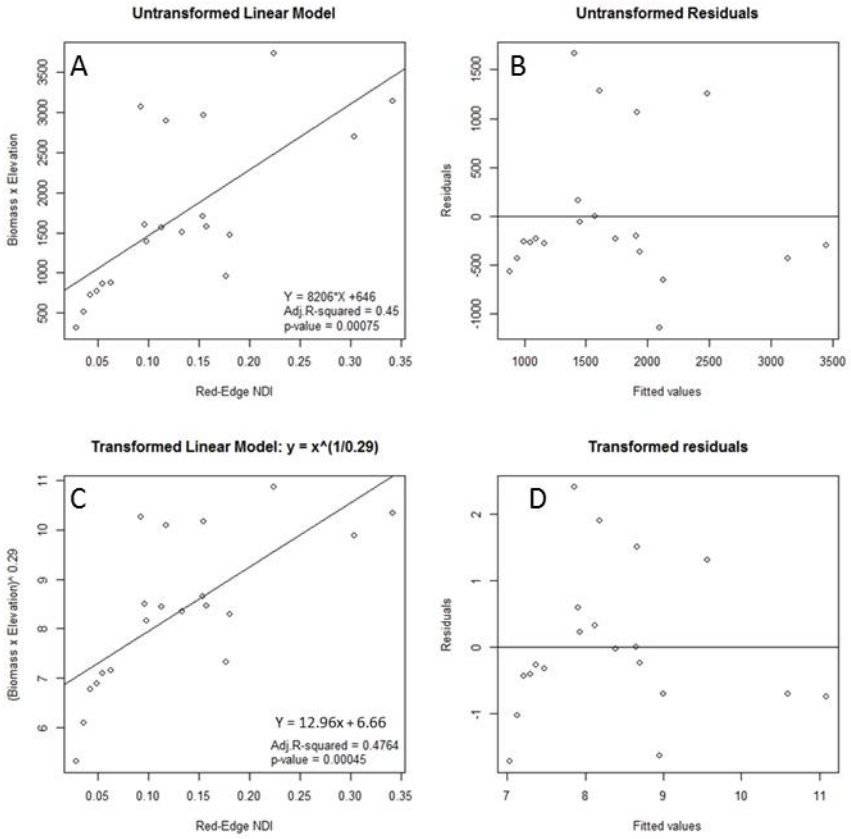

Figure 58. Derivation of exponential model for Biomass with respect to LiDAR BE (Elevation) and Red-Edge NDI.

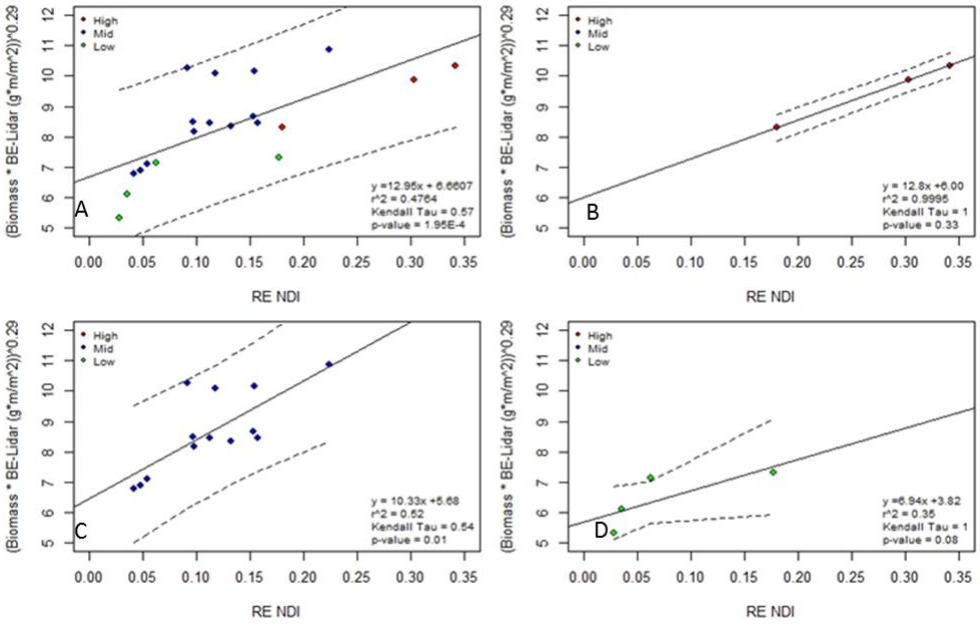

Figure 59. Final exponential model with 95% confidence lines for considering RE-NDI and BE LiDAR DEM with respect to marsh assemblage. A) shows all marsh type assemblages; B) High-Marsh; C) Mid – marsh, BOFL and BOMA assemblages undifferentiated; D) Low-Marsh. Dashed lines are 95% confidence intervals to the linear model.

Appendix 5: Exploratory Analysis of Side-On Photography Data

This appendix details the exploratory analysis of the Side-On Photography (SOP) data. Here we compare all relevant SOP data with its lab measured equivalent for all sites and separated by marsh assemblage. Through this analysis, we found that our SOP analysis could be used to predict biomass, and plant height (Figures 60 and 61). Our analysis did not yield an acceptable relationship with between our lab measured stem count and stem diameter with their assumed equivalents.

Biomass was found to correlate to the number of vegetated pixels within our digital images when considering all marsh assemblages (Figure 60a). Mid-Marsh assemblage also showed a correlation between biomass and vegetated pixels (Figure 60c). High and Low-Marsh did not show a correlation (Figure 60b and 60d); this lack of correlation in High and Low-Marsh could factor of low sample size. 3-4 data points are not likely to capture the variance within each cover type.

Height showed a similar pattern as biomass; where all cover types and the Mid-Marsh showed a strong correlation between the image processing measured height and lab measured height (Figure 61a and c). Mid and Low-Marsh assemblages did not show a valuable relationship, perhaps due to low sample size.

Stem density is common plant metric used in hydrodynamic wave models; unfortunately, our analysis did not show a valuable relationship between stem count and row-hole count in the image processing. Row-hole count is the number of contiguous non-vegetated pixels that is measured per row of a defined thickness (Zehm et al., 2003). For this study, we looked at row-hole counts for 1 cm tall rows at 25 cm, 50 cm, and 75 cm above the marsh floor (Figure 62, 63 and 64 respectfully). Row-hole count at 25 cm did show a week Kendall's tau correlation with stem count (Figure 61a and c); however, row-hole count at the other heights and individual assemblages did not yield a correlation with stem count (Figures 62 – 64). Moreover, within the higher (50 and 75 cm) row-hole count measurements there were less data

points particularly for Low and High-Marsh, where the majority of plants were below the 50 cm and 75 cm measurement height.

The Sidelook software used in this study does not have a direct equivalent measurement for stem diameter. In Figure 65 we look at four variable combinations to assess if stem diameters are able to be predicted through our digital image processing methods. Figure 65a compares average row-hole size, length of contiguous non-vegetated pixels, to stem diameter; this comparison did not yield a correlation. Figure 65b compares stem diameter to the ration between vegetated pixels and row-hole count at 25 cm above the marsh floor; this yielded a very weak correlation and an insensitive linear model. Figure 64c compares stem diameter to the ration of count of vegetated pixels within the 25 cm row over average row-hole size; this analysis did not produce a correlation. Figure 65d compares stem diameter with the ration of total vegetated pixels within a digital image over the vegetated pixels within the 25 cm row; this analysis yielded a weak correlation but this ration is insensitive to changes in stem diameter.

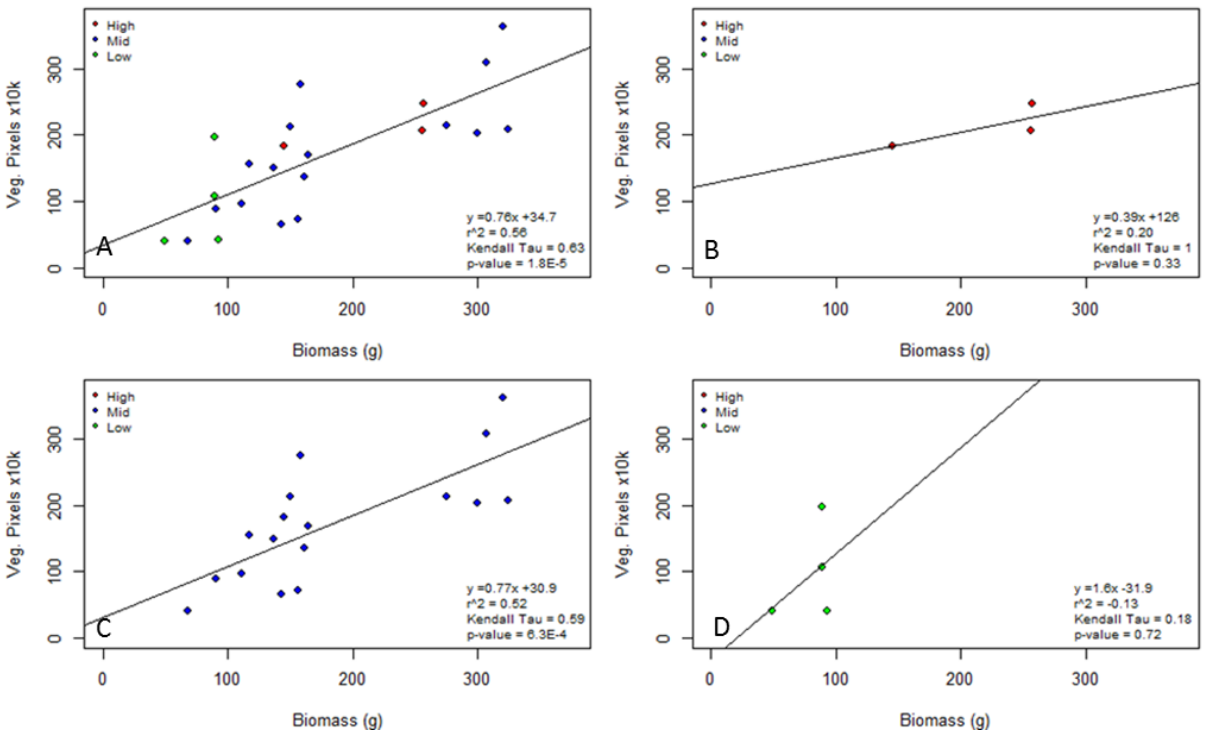

Figure 60. Vegetated pixels from SOP analysis compared to lab measured biomass with respect to marsh type. A) all marsh assemblages; B) High-Marsh; C) Mid-Marsh assemblages (BOFL and BOMA undifferentiated); D) Low-Marsh.

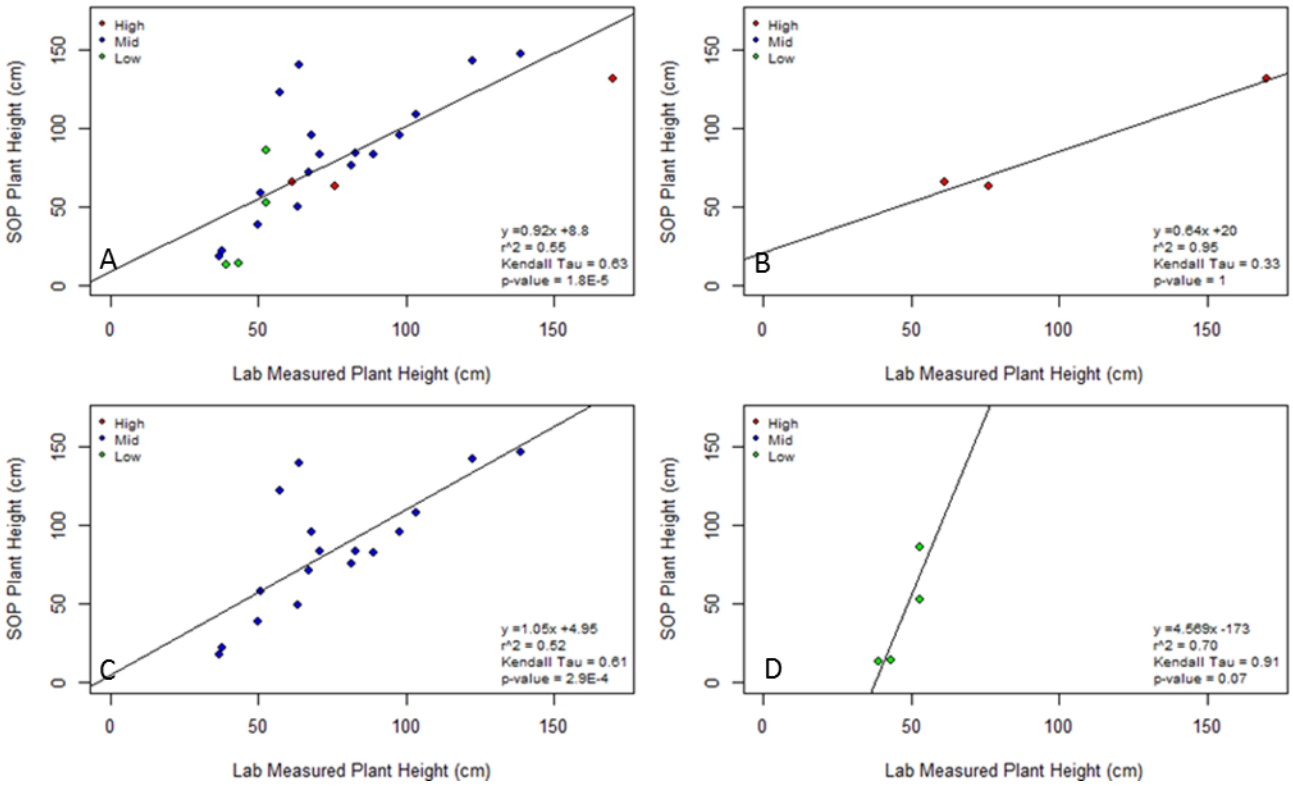

Figure 61. Average maximum vegetated pixel height by 1 cm wide column from SOP analysis compared to the mean lab measured plant height with respect to marsh type. A) all marsh assemblages; B) High-Marsh; C) Mid-Marsh assemblages (BOFL and BOMA undifferentiated); D) Low-Marsh.

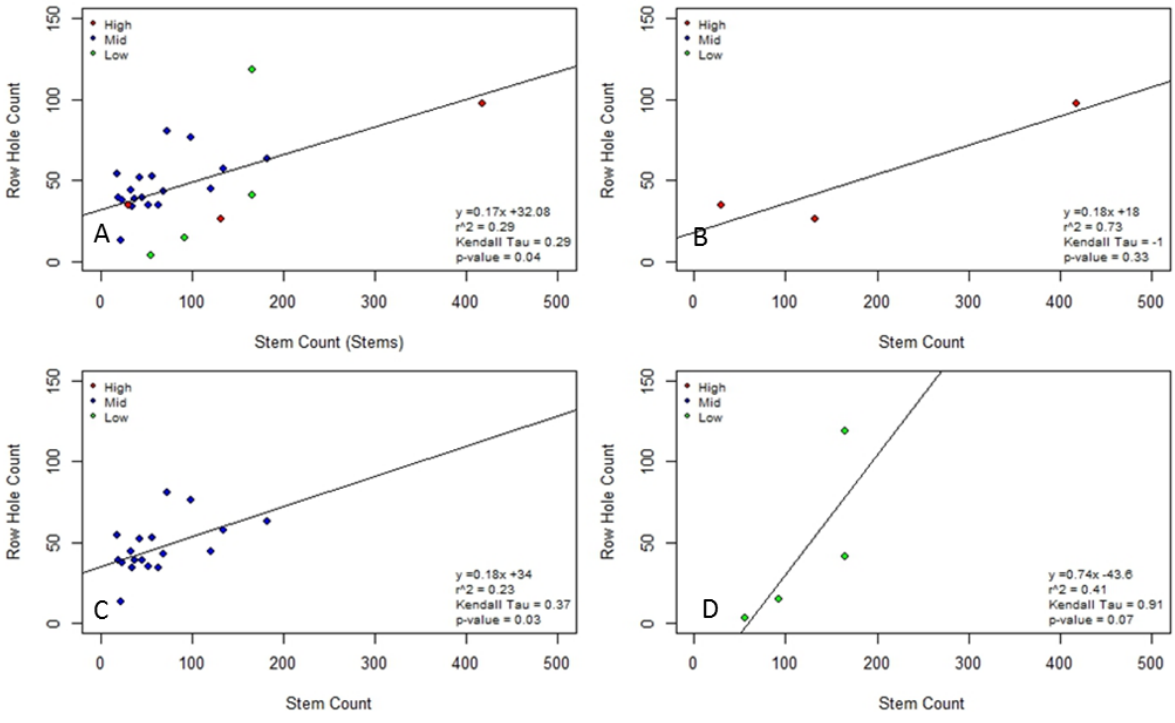

Figure 62. Row-hole count (contiguous non-vegetated pixels) of a 1 cm tall row at 25 cm height above the marsh floor compared to the lab measure stem count. A) all marsh assemblages; B) High-Marsh; C) Mid-Marsh assemblages (BOFL and BOMA undifferentiated); D) Low-Marsh.

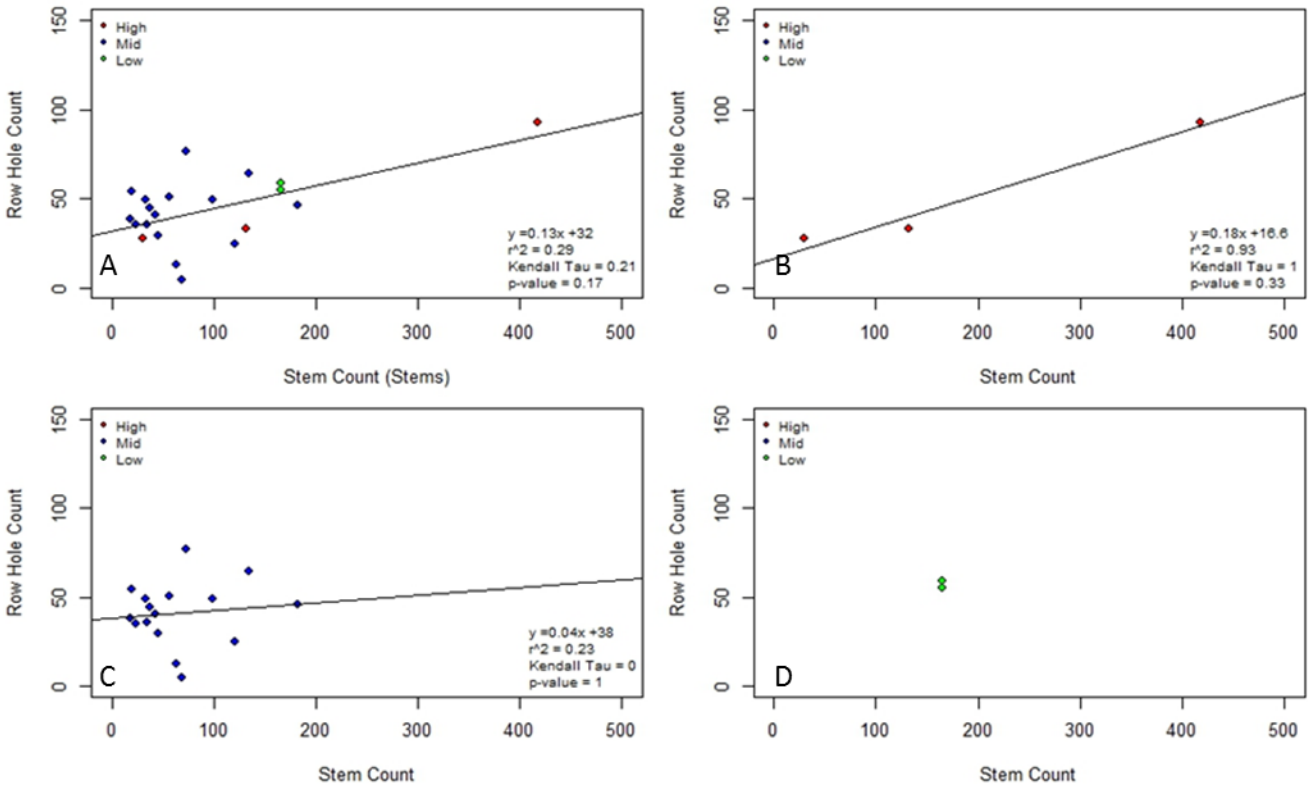

Figure 63. Row-hole count (contiguous non-vegetated pixels) of a 1 cm tall row at 50 cm height above the marsh floor compared to the lab measure stem count. A) all marsh assemblages; B) High-Marsh; C) Mid-Marsh assemblages (BOFL and BOMA undifferentiated); D) Low-Marsh.

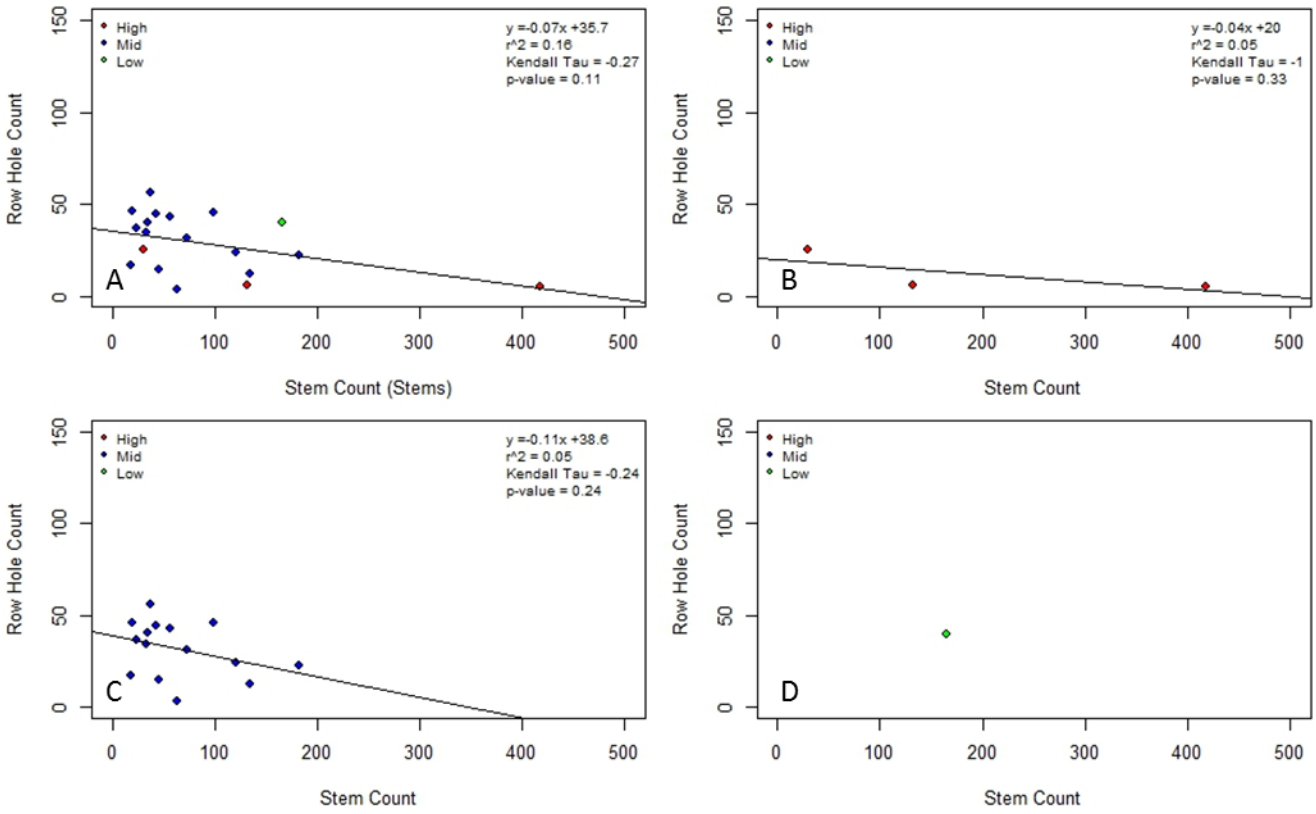

Figure 64. Row-hole count (contiguous non-vegetated pixels) of a 1 cm tall row at 75 cm height above the marsh floor compared to the lab measure stem count. A) all marsh assemblages; B) High-Marsh; C) Mid-Marsh assemblages (BOFL and BOMA undifferentiated); D) Low-Marsh.

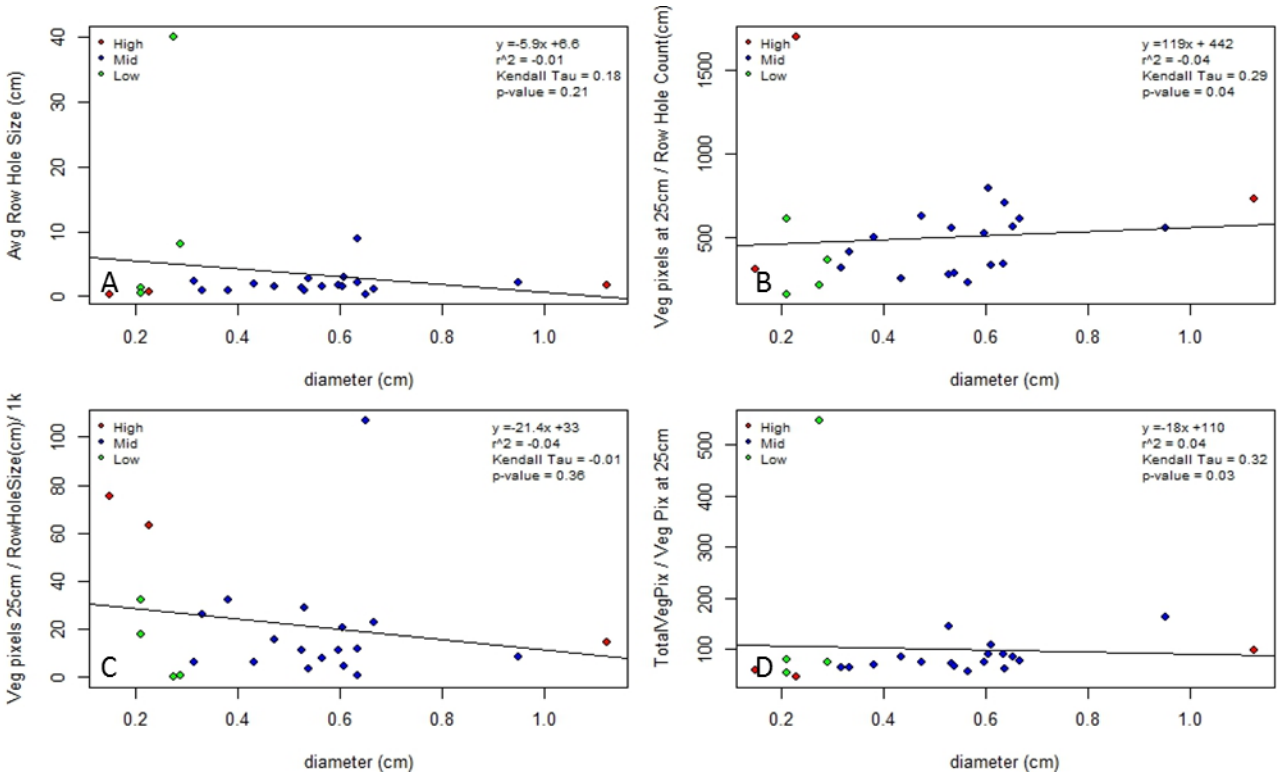

Figure 65. Exploratory analysis to derive a model to predict stem diameter. A) Comparison between average row-hole size at 25 cm height and lab measured stem diameter. B) Ration of vegetated pixels within the 1 cm tall row at 25 cm over row-hole count compared to lab-measured stem diameter. C) Ration of vegetated pixels within the 1 cm tall row at 25 cm over mean row-hole size compared to lab-measured stem diameter. D) Ration of total vegetated pixels over vegetated pixels within the 1 cm tall row at 25 cm compared to stem diameter.

Appendix 6: Exploratory Analysis of Elasticity Data

This appendix details the exploratory analysis of our elasticity data set. Here we compare our 9 elasticity measurements to plant height, stem diameter and measurement height with respect to seasonality and plant type. As a reminder, we took 9 elasticity measurements per stem. We measured the force required to bend a stem to 3 angles (15, 30, 45 from vertical) at 3 heights (25 cm, half height, full plant height) using a handheld scale. Elasticity was measured biweekly from September through November and then monthly through March. In the majority of stems, elasticity measurements taken at full plant height or to 15degrees from vertical were below the measurability of our hand-held digital scale. These zero values were not included in this study.

We found that our elasticity measurements correlated well with stem diameter, particularly measurements lower on the stem (half height and 25 cm) and higher angles (30 and 45 degrees from vertical) (Figure 66 and 67). These relationships appear to be insensitive to seasonality. These strong correlations are present in both BOMA and BOFL species (Table 19-20; Figure 66 - 67).

Overall, the elasticity measurements have inconsistent and/or weak relationships with total plant height but may show some clustering with respect to seasonality (Figure 67 and 68). Similar to diameter, the weakest relationships are with force measurements taken at plant height and to 15 degrees from vertical. BOFL measurements tend to have a logarithmic relationship, random, and parabolic with measurements taken at plant height, half height, and 25 cm respectfully (Figure 68). BOMA measurements tend to have weak negative or random relationships with plant height (Figure 69).

BOMA and BOFL elasticity measurements both show strong logarithmic relationships to measurement height (Figure 70 and 71; Table 18-19). This is intuitively a function of torque and lever arm length. There does not appear to have a linear relationship with seasonality in either BOFL or BOMA (Figure 70 and 71).

BOFL			
45 degrees			
	Equation	**Adj-r^2**	**P-value**
All	ln(Y) = -1.36*ln(X) + 9.64	0.66	2.20E-16
Oct	ln(Y) = -1.47*ln(X) + 10.22	0.73	2.20E-16
Nov	ln(Y) = -1.20*ln(X) + 8.65	0.6	2.20E-16
Dec	ln(Y) = -1.45*ln(X) + 10.06	0.8	2.20E-16
Jan	ln(Y) = -1.37*ln(X) + 9.91	0.63	2.20E-16
Feb	ln(Y) = -1.51*ln(X) + 10.39	0.63	1.12E-10
Mar	ln(Y) = -1.25*ln(X) + 9.06	0.58	4.32E-12
30 degrees			
	Equation	**Adj-r^2**	**P-value**
All	ln(Y) = -1.48*ln(X) + 9.57	0.64	2.20E-16
Oct	ln(Y) = -1.60*ln(X) + 10.29	0.75	2.20E-16
Nov	ln(Y) = -1.08*ln(X) + 7.35	0.52	2.20E-16
Dec	ln(Y) = -1.63*ln(X) + 10.25	0.76	3.41E-16
Jan	ln(Y) = -1.53*ln(X) + 10.11	0.66	2.20E-16
Feb	ln(Y) = -1.53*ln(X) + 9.97	0.66	8.61E-14
Mar	ln(Y) = -1.39*ln(X) + 9.10	0.63	3.02E-16
15 degrees			
	Equation	**Adj-r^2**	**P-value**
All	ln(Y) = -1.43*ln(X) + 8.82	0.58	2.20E-16
Oct	ln(Y) = -1.35*ln(X) + 8.58	0.56	2.20E-16
Nov	ln(Y) = -1.30*ln(X) + 8.18	0.63	2.20E-16
Dec	ln(Y) = -1.63*ln(X) + 9.43	0.66	4.67E-10
Jan	ln(Y) = -1.46*ln(X) +9.11	0.59	2.20E-16
Feb	ln(Y) = -1.52*ln(X) + 9.22	0.52	1.14E-09
Mar	ln(Y) = -1.10*ln(X) + 7.40	0.37	5.51E-08

Table 19. Logarithmic regression equations and statistics for BOFL force measurements as a function of measurement height with respect to bending angle and seasonality.

BOMA			
45 degrees			
Data	**Equation**	**Adj-r^2**	**P-value**
All	ln(Y) = -1.43*ln(X) + 9.07	0.52	2.20E-16
Oct	ln(Y) = -0.82*ln(X) + 6.95	0.09	1.25E-01
Nov	ln(Y) = -1.41*ln(X) + 8.88	0.6	2.20E-16
Dec	ln(Y) = -1.46*ln(X) + 9.17	0.54	6.87E-15
Jan	ln(Y) = -1.14*ln(X) + 7.68	0.47	2.95E-10
Feb	ln(Y) = -0.98*ln(X) + 7.79	0.22	2.78E-04
Mar	ln(Y) = -1.43*ln(X) + 9.37	0.47	6.36E-11
30 degrees			
	Equation	**Adj-r^2**	**P-value**
All	ln(Y) = -1.44*ln(X) + 8.46	0.46	2.20E-16
Oct	ln(Y) = -1.17*ln(X) + 7.28	0.19	4.37E-02
Nov	ln(Y) = -1.37*ln(X) + 8.11	0.57	2.20E-16
Dec	ln(Y) = -1.37*ln(X) + 8.23	0.47	3.96E-12
Jan	ln(Y) = -1.48*ln(X) + 7.83	0.47	1.53E-09
Feb	ln(Y) = -1.27*ln(X) + 8.15	0.26	3.36E-05
Mar	ln(Y) = -1.48*ln(X) + 8.91	0.42	9.11E-10
15 degrees			
	Equation	**Adj-r^2**	**P-value**
All	ln(Y) = -0.99*ln(X) + 6.06	0.2	2.20E-16
Oct	ln(Y) = -1.60*ln(X) + 8.04	0.48	3.27E-03
Nov	ln(Y) = -0.80*ln(X) + 5.09	0.16	1.04E-05
Dec	ln(Y) = -1.21*ln(X) + 6.84	0.35	2.56E-07
Jan	ln(Y) = -0.71*ln(X) + 4.84	0.11	1.53E-02
Feb	ln(Y) = -0.94*ln(X) + 6.19	0.13	5.65E-03
Mar	ln(Y) = -0.87*ln(X) + 6.03	0.21	1.33E-04

Table 20. Logarithmic regression equations and statistics for BOMA force measurements as a function of measurement height with respect to bending angle and seasonality.

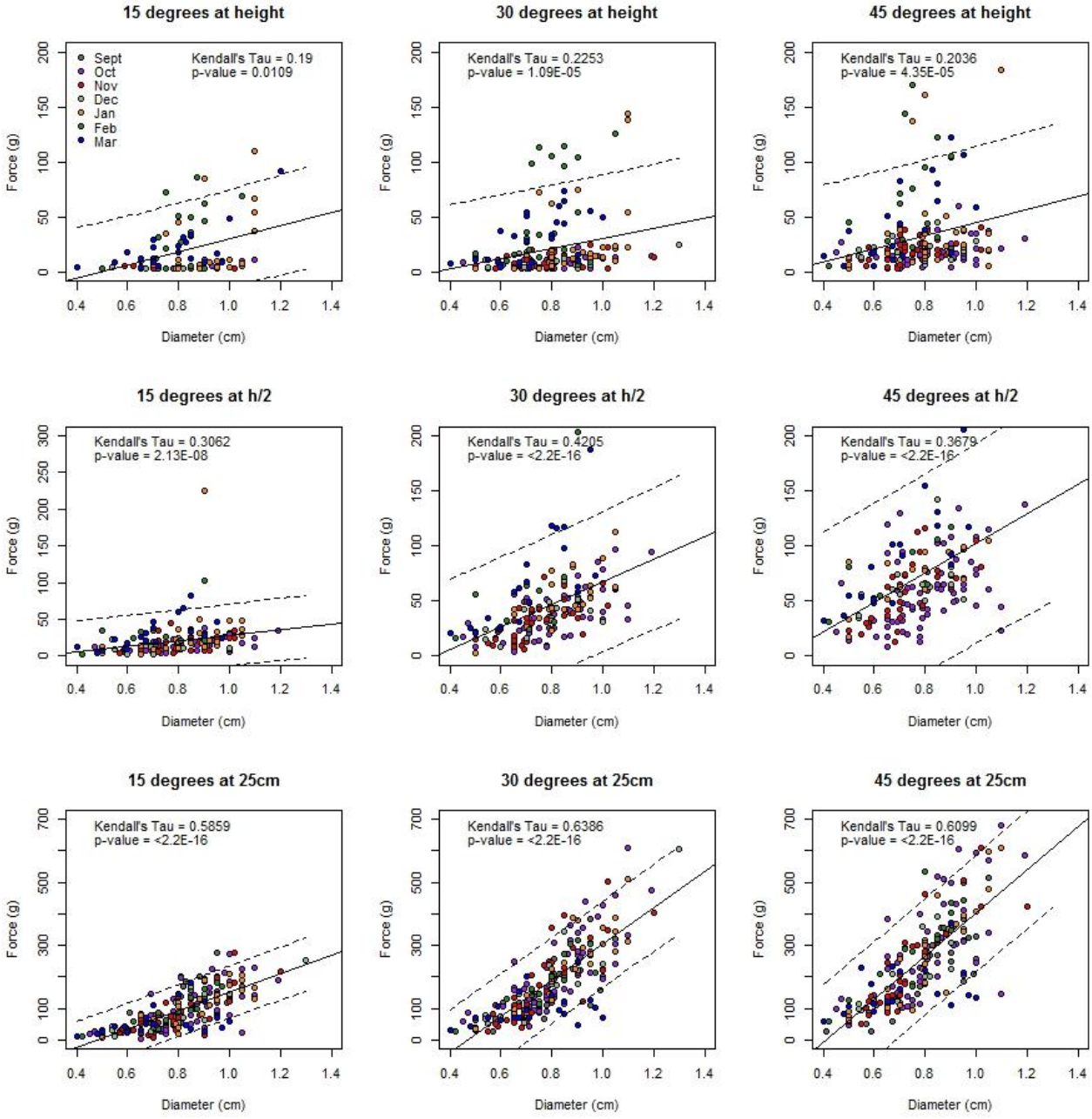

Figure 66. Scatter plot diagrams between stem diameter at 25 cm above marsh surface and 9 separate force measurements for BOFL. Note: many force measurements equal to zero were not considered in this analysis. Force measurements at plant height were often too low to register on hand held digital scale.

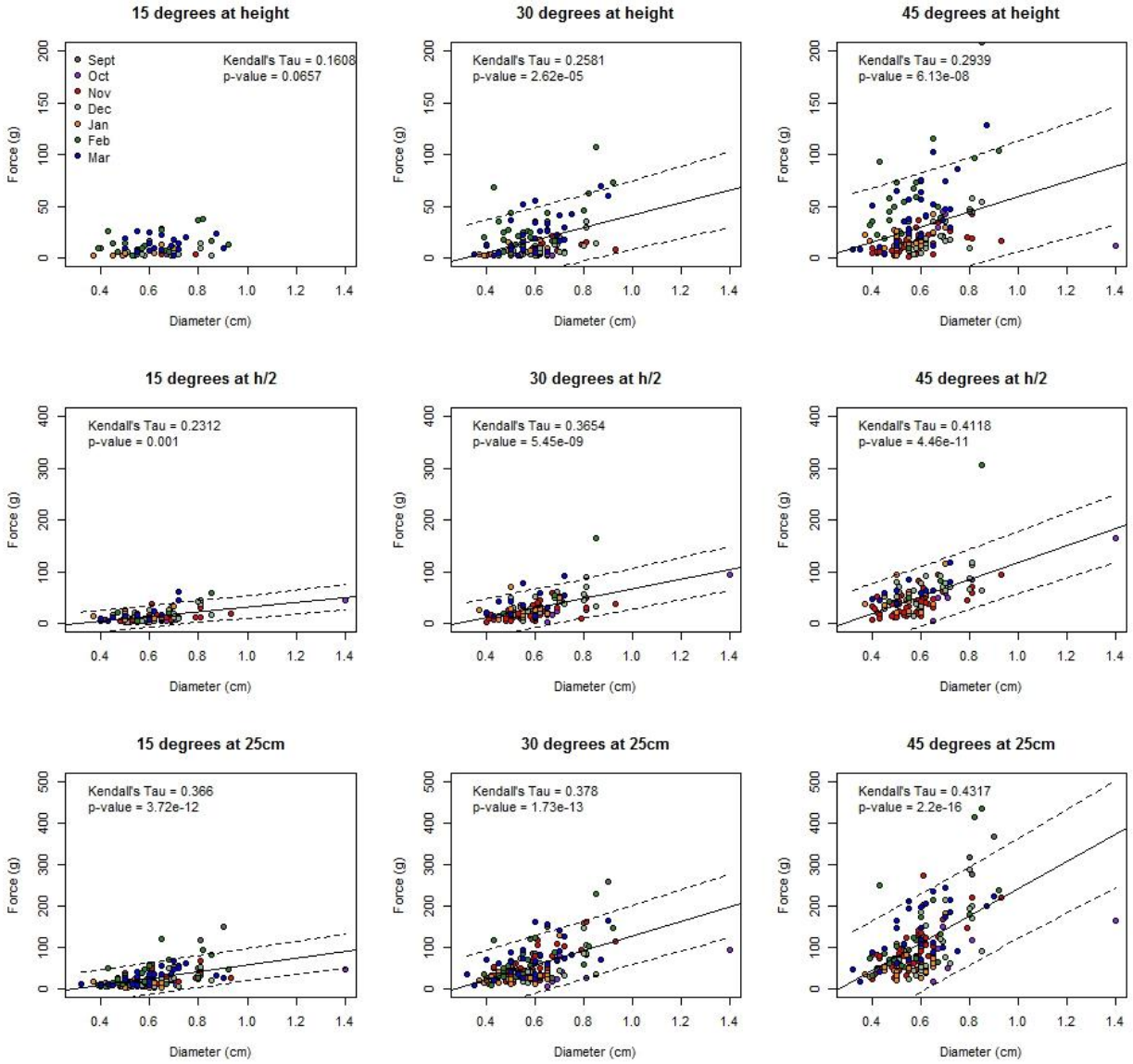

Figure 67. Scatter plot diagrams between stem diameter at 25 cm above marsh surface and 9 separate force measurements for BOMA. Note: many force measurements equal to zero were not considered in this analysis. Force measurements at plant height were often too low to register on hand held digital scale.

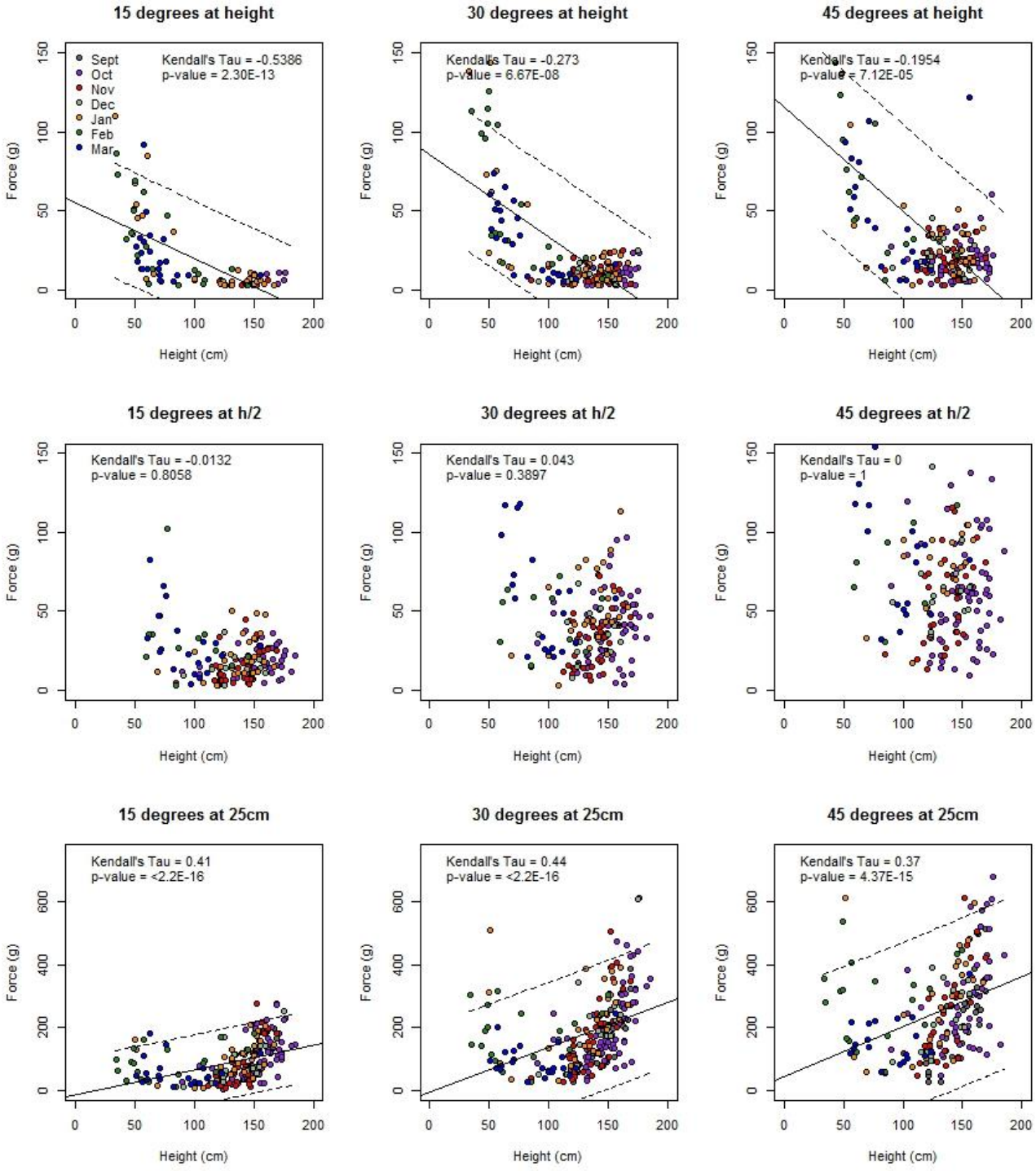

Figure 68. Scatter plot diagrams between plant height and the 9 separate force measurements for BOFL. Note: many force measurements equal to zero were not considered in this analysis. Force measurements at plant height were often too low to register on hand held digital scale.

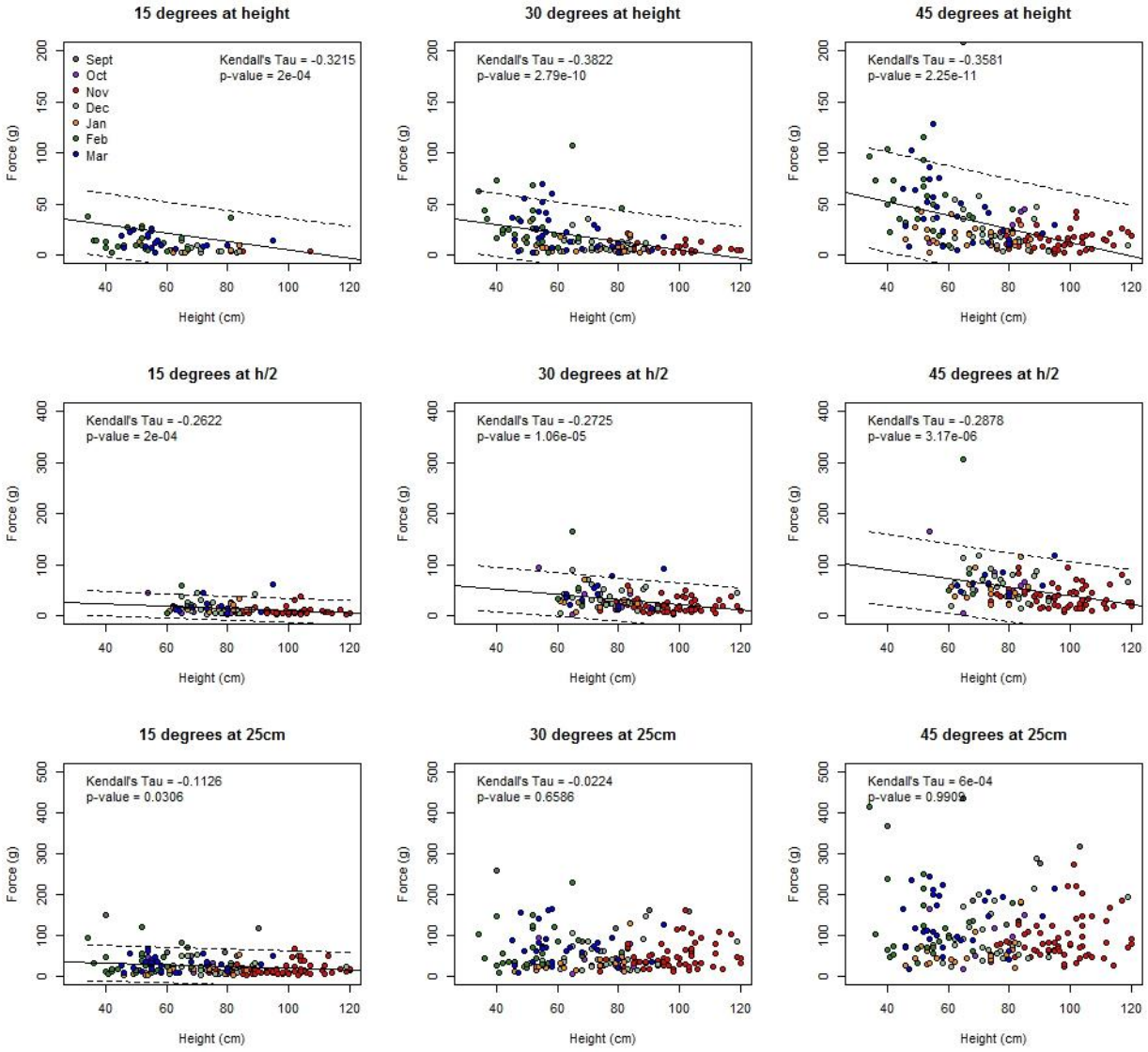

Figure 69. Scatter plot diagrams between plant height and the 9 separate force measurements for BOMA. Note: many force measurements equal to zero were not considered in this analysis. Force measurements at plant height were often too low to register on hand held digital scale. For stems, less than 60 cm in height, half height force measurements were not taken because it is thought to be a redundant measurement with the 25 cm force measurements.

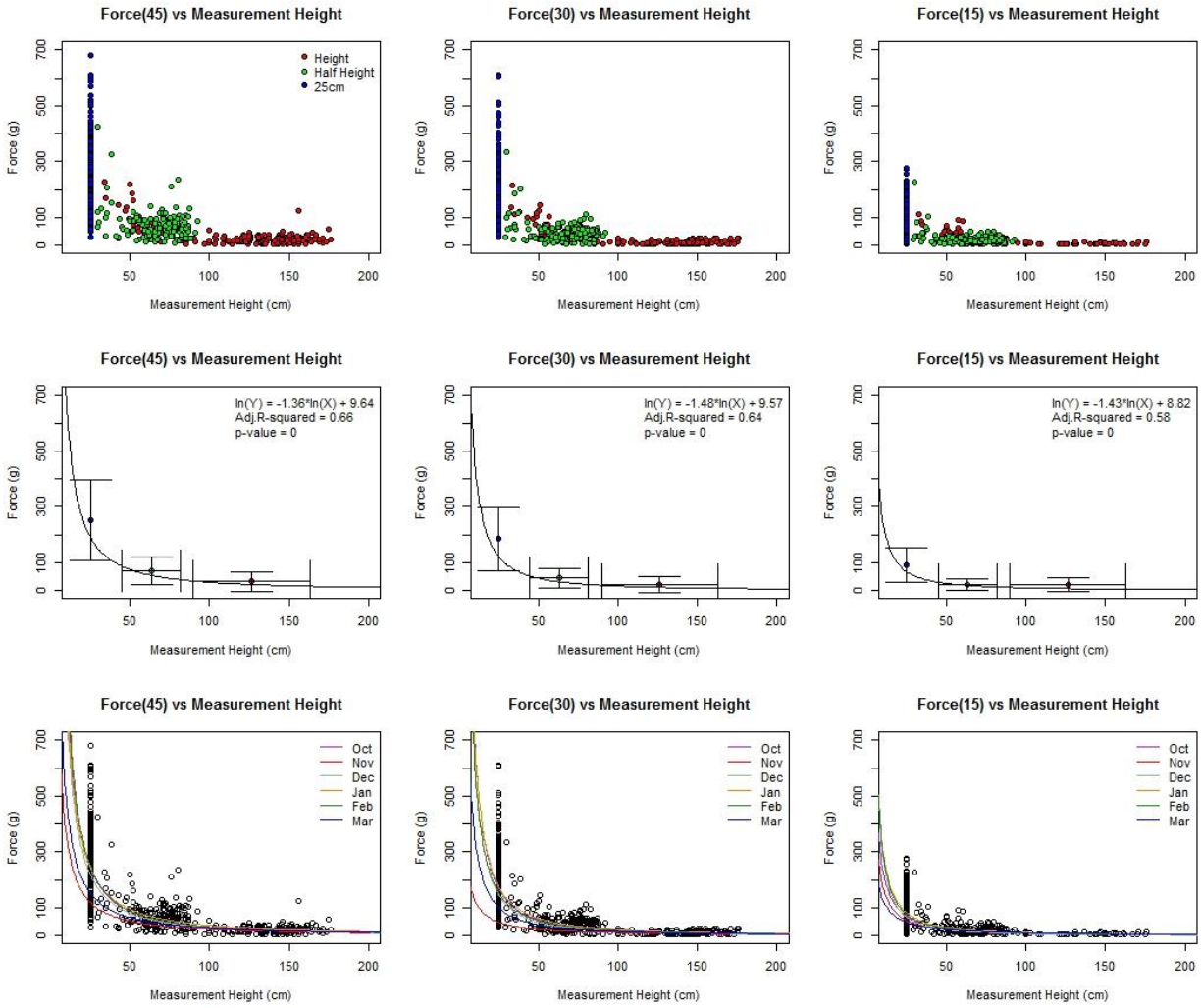

Figure 70. Force vs Measurement Height analysis for BOFL. These series of plots show the relationship between Force and measurement height detailing the measurement height type (Height, Half height, 25 cm); the overall logarithmic regression where error bars represent plus/minus one standard deviation; and the temporal differences of force regressions by month. Note: we were unable to calculate an accurate regression for the September data because stems were only measured at 25 cm not at height or half height.

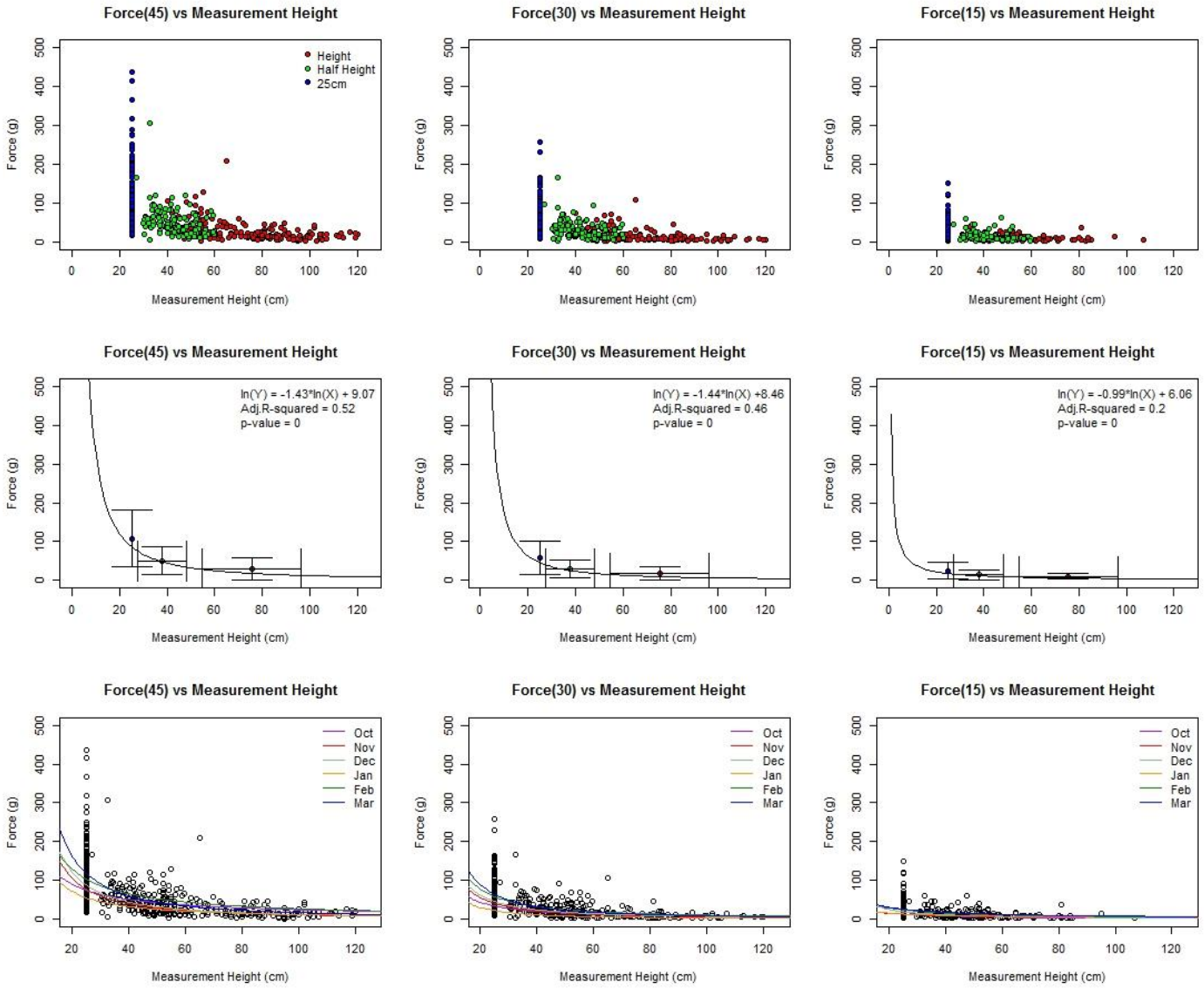

Figure 71. Force vs Measurement Height analysis for BOMA. These series of plots show the relationship between Force and measurement height detailing the measurement height type (Height, Half height, 25 cm); the overall logarithmic regression where error bars represent one standard deviation; and the temporal differences of force regressions by month. Note: we were unable to calculate an accurate regression for the September data because stems were only measured at 25 cm not at height or half height.

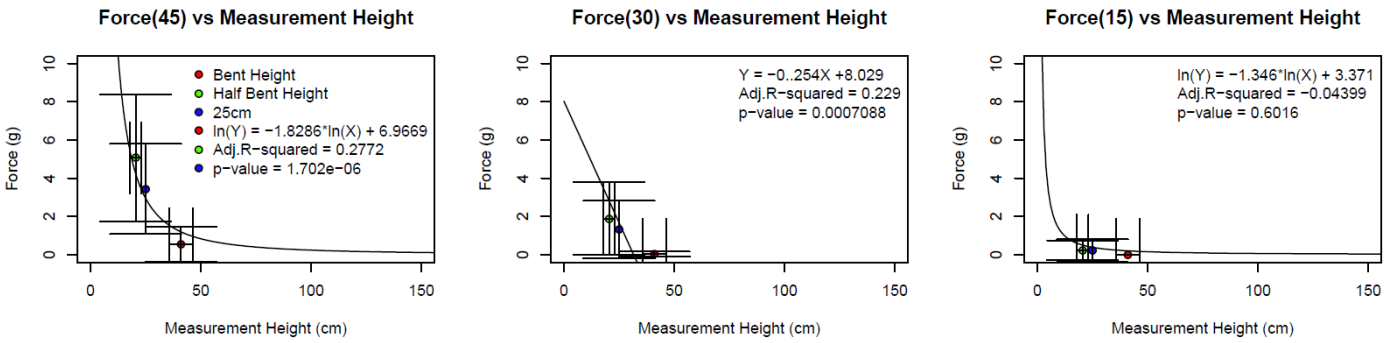

Figure 72. Force vs Measurement Height analysis for SCAM. These series of plots show the relationship between Force and measurement height detailing the measurement height type (Height, Half height, 25 cm); the overall logarithmic regression where error bars represent one standard deviation; and the temporal differences of force regressions by month. Note: we were unable to calculate an accurate regression for the September data because stems were only measured at 25 cm not at height or half height.

Appendix 7: Eel Grass Analysis

This appendix details our methods and analysis to isolate Japanese (*Zostera Japonica*) and native *(Zostera marina)* using the combination of Maximum Likelihood Classification (MLC) and (DTC). We altered from our main analysis by 1) including the total areal extent of the deltaic shelf; 2) digitizing eelgrass ground truth polygons (Figure 73); 3) Decision tree developed using band ratios (Table 21), NDVI and elevation data (Figure 74). We found that the combination of MLC and DTC analyses applied to the CASI dataset was able to isolate eelgrass species to native (99) and Japanese (90) eelgrass species, respectively (Figure 75; Table 22-4) .

Methods:

Ground truth points were digitized using the real-color display of the CASI data (Figure 73). Native eelgrass polygons were separated by density. Over 50% coverage of assumed eelgrass was classified as dense; less than 50% was classified as sparse. Japanese Eelgrass covers a higher elevation range than the native eelgrass. The tideline bisected the Japanese eelgrass at the time the imagery was taken. To account for this, we defined 6 cover-types for Japanese eelgrass: submerged dense; submerged sparse; tideline dense; tideline sparse; exposed dense; exposed sparse.

Japanese Eelgrass cover-types were able to be separated using NDVI and LIDAR Bare Earth (LIDAR BE) datasets. We used the band ratios to classify native eelgrass cover-types. According to the native eelgrass spectral signatures for the CASI data set, there is a distinct rise in reflectance between 400 (Band 4) and 725 (Band 25) nm with its peak around 575 nm (Band 15) (Figure 49, Appendix 2). We found the ratio between the end points (B4 and B25) over the peak (B15) to be very useful in separating the eelgrass from the surrounding sediment.

Decision trees for eelgrass species were developed in the same manner as other cover types (Chapter 1). We separated ground truth points into testing (50%) and training (50%) polygons. We calculated the

statistics for the cover types from 6 random points within the training polygons (Table 21). We developed the if-then statements from these statistics (Figure 74). We used only band ratios for the native eelgrass because BE LiDAR data was incomplete and NDVI is not useful for submerged vegetation at that water depth. Bare sediment, submerged or exposed, was the most commonly confused for eelgrass and therefore decision trees were created to isolate the eelgrass cover types from only sediment.

The Japanese Eelgrass decision tree is based on the statistics from the training ROI for the LIDAR BE and NDVI datasets (Table 21). However, this decision tree was altered through experimental analysis to isolate the best cutoffs (Figure 73).

Results and Discussion:

We predict that in the summer of 2014, PSB had 4.5 and 2.4 km^2 of Japanese and Native Eelgrass, respectively (Table 22, Figure 74). The MLC classification was successful at separating the eelgrass cover types from each other and marsh cover types, 72 and 89 percent for native and Japanese eelgrass respectfully (Table 23). Bare sediment, submerged or exposed, was the most commonly confused for eelgrass. The decision tree classification was able to improve the accuracy to 99 and 90 percent for native and Japanese eelgrass (Table 24). We did not differentiate between sparse and dense or submerged and exposed eelgrass for this study because of the qualitative nature of the distinctions.

These results are likely to be biased towards higher than realistic producer's accuracy because of the limited number of digitized ground truth points within the lower deltaic shelf. The majority of the sediment ground truth points are near the marsh vegetation and are smaller in size than the eelgrass polygons.

Although we are satisfied with the accuracy of the DTC and MLC for the eelgrass species, a more thorough and comprehensive study could be conducted. We would recommend isolating the lower deltaic shelf separately and rerunning the classification schemes for future efforts.

Table 21 Areal data statistics for eelgrass cover types and bare sediment.

Landcover/ Band Ratio		Mean	Min	Max	STD	n (pixel count)
Native Eelgrass- Dense						
b4/b15		0.617	0.499	0.727	0.068	6
b25/15		0.315	0.248	0.422	0.054	6
Native Eelgrass- Sparse						
b4/b15		0.515	0.443	0.617	0.058	6
b25/15		0.297	0.223	0.352	0.048	6
Bare - Undifferentiated						
b4/b15		0.461	0.394	0.495	0.033	6
b25/15		0.253	0.192	0.293	0.032	6
Elevation - mud only		1.694	0.960	2.910	0.330	2929
NDVI		0.050	-0.034	0.397	0.048	2092
Japanese Eelgrass						
Elevation		0.549	0.360	0.930	0.112	133
NDVI		-0.063	-0.278	0.297	0.119	95

Table 22. Potential areal coverage of eelgrass cover types from the decision tree classification.

Eelgrass Analysis		
Cover Type	**Area (sq-m)**	**Percent of Study Area**
Japanese Eelgrass	**4.51E+06**	**11.8%**
Sparse	3.13E+06	8.2%
Dense	1.38E+06	3.6%
Native Eelgrass	**2.38E+06**	**6.2%**
Sparse	4.54E+05	1.2%
Dense	1.93E+06	5.0%
Bare	**2.45E+07**	**64.1%**
Mud	2.01E+07	52.5%
Sand	2.07E+06	5.4%
Deepwater	2.35E+06	6.1%
Macroalgae	**1.43E+06**	**3.7%**
Total Study Area	**3.83E+07**	**100.0%**

Table 23. Confusion Matrix of Decision Tree Classification using combined cover classes. High-Marsh species (Grasses, Cattails, Juncus, Carrex, and POPA) and sediment types (Bare and Sand) have been combined into HiMarsh and Sed classes respectively. Overall accuracy is heightened because the large ground truth ROIs for the Deepwater class. Values are in percent.

	Blackberries	Beachwood	Trees	HiMarsh	Eelgrass	Japan Eelgrass	Sed	BOFL	BOMA	SCAM	DeepWater	Macro Algae	# Pixels
Blackberries	95.73			0.53									1765
Beachwood	0.83	86.89		3.25			0.10		1.13	0.16			1359
Trees	1.66	0.55	92.26	3.56			0.63	0.86	0.04				1291
HiMarsh	1.77	11.22	0.32	76.58	0.01	0.15	0.30	17.06	8.94	3.79		0.08	3161
Eelgrass					71.77		0.01				0.19		97532
JapEelgrass					0.00	88.58	40.38			0.20		0.24	181634
Sed				0.31	28.21	11.20	58.32	0.46	7.81	31.03	1.50	41.68	150409
BOFL		1.03	0.32	12.52			0.00	75.13	15.84	1.87			1908
BOMA			0.97	1.63			0.02	6.42	38.54	10.07			1438
SCAM				1.58		0.01	0.20	0.07	27.71	52.22			2401
DeepWater					0.01						98.31		914078
MacroAlgae				0.04		0.06	0.04			0.66		58.00	3004
# Pixels	1803	1266	310	2276	133439	142686	136767	1512	2652	2562	929800	4907	1359980
Overall Accuracy:	90.23												
Kappa Coefficient	0.8079												

Table 24. Confusion matrix of Maximum Likelihood Classification (MLC). High-Marsh species (Grasses, Cattails, Carrex, Juncus, and POPA) and bare sediment classes (Sand and Bare) have been combined into HiMarsh and Sed cover classes respectively. Overall accuracy is elevated because of the large ground truth ROIs for the deepwater class.

	Blackberries	Beachwood	Trees	HiMarsh	Eelgrass	Japan Eelgrass	Sed	BOFL	BOMA	SCAM	Deep Water	Macro Algae	# pixels
Blackberries	95.73	0.32	6.13	0.53									1765
Beachwood	0.83	86.89		2.99			0.10		0.79	0.08			1340
Trees	1.66	0.55	92.26	3.56			0.64	0.86	0.04				1296
HiMarsh	1.77	11.22	0.32	74.65	0.01	0.10	0.31	15.94	8.14	3.63			2993
Eelgrass					98.68		0.03					0.08	147433
JapEelgrass					1.29	89.99	52.96	0.07	2.07	0.04	1.69		200904
Sed				0.22		6.99	45.69	2.05	18.33	42.15		0.26	77838
BOFL		0.95	1.29	10.46		0.07	0.05	51.32	12.78	4.25			1649
BOMA		47.00		6.55		0.47	0.06	21.10	25.87	9.09			3397
SCAM				1.05		2.33	0.14	8.66	31.98	40.09			5545
DeepWater					0.10						98.31		914078
MacroAlgae						0.05	0.03			0.66		58.00	2993
Number of Pixels	1803	1266	310	2276	133439	142686	136767	1512	2652	2562	929800	1251	1361231
Overall Accuracy:	91.592												
Kappa Coefficient	0.835												

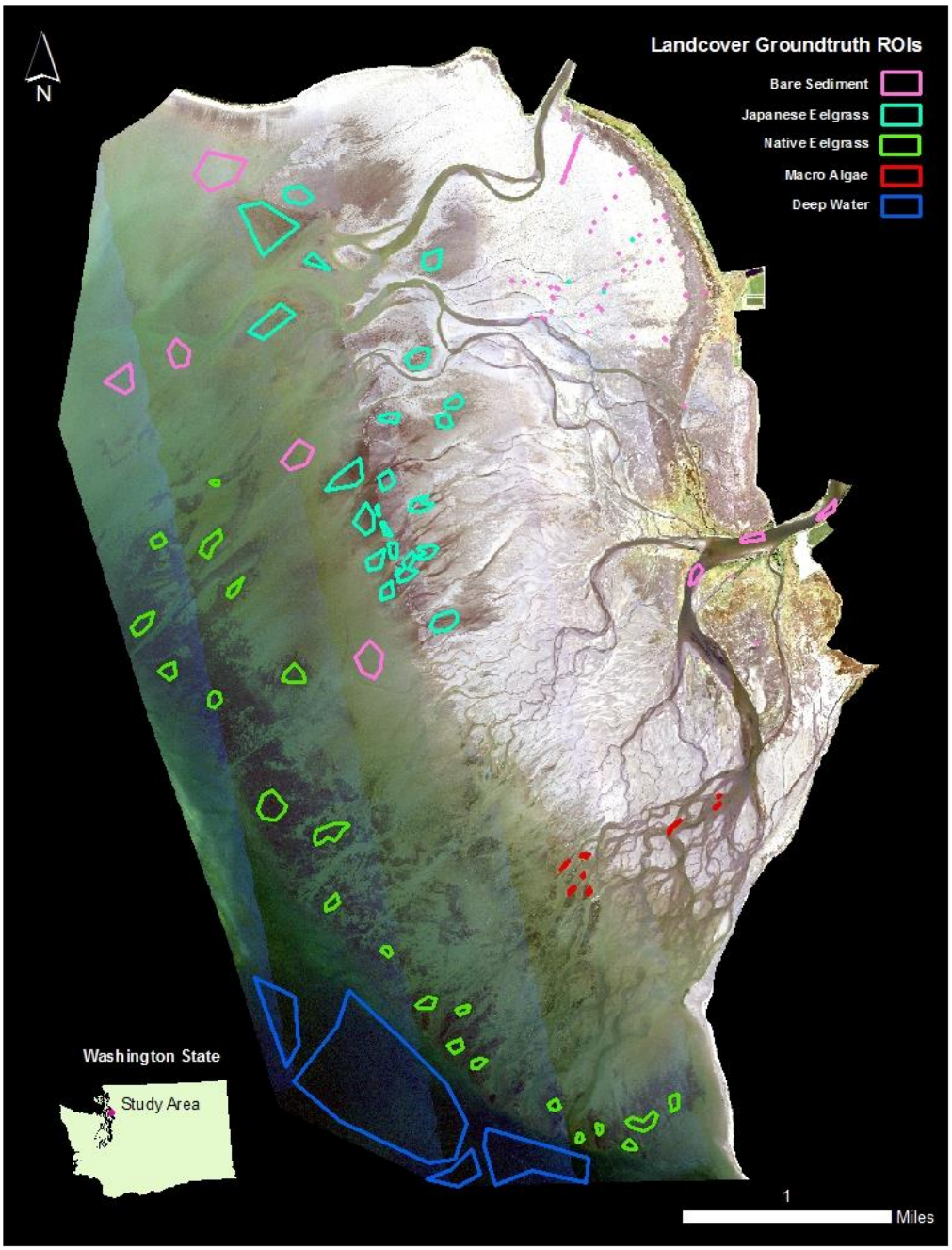

Figure 73. Map detailing the relevant ROI ground truth polygons for the eelgrass assessment. For the native eelgrass ROIs, there is both sparse and dense sub classes. Japanese eelgrass has 6 subclasses: Sparse, Dense combined with submerged, exposed and shoreline. Subclasses are not differentiated here.

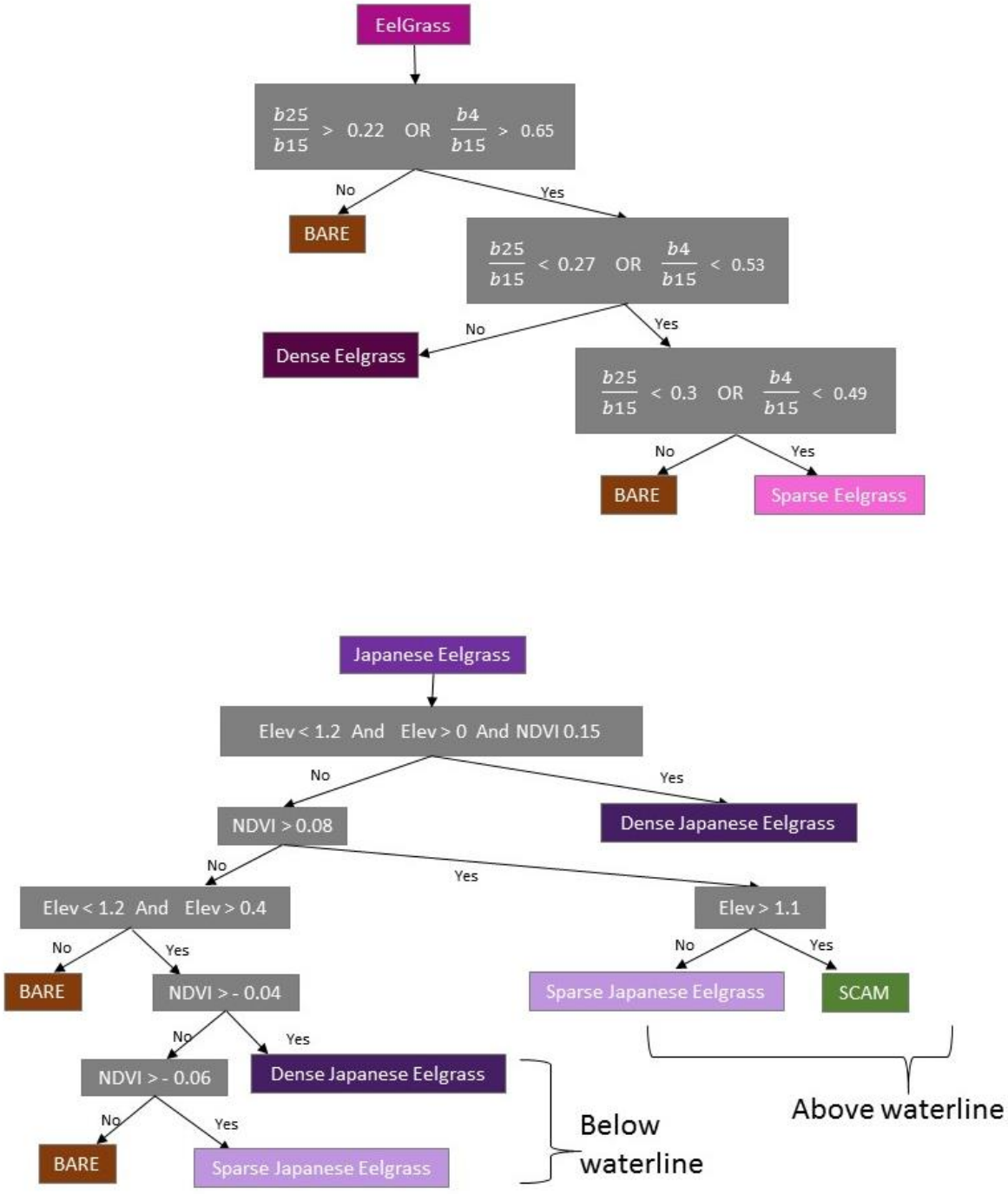

Figure 74. Decision Tree diagrams to isolate eelgrass varieties form water and sediment cover classes. Native eelgrass was determined to have a distinct band ratio of band 25 (b25) over Band 15 (b15) and Band 4 (b4) over b15 based on the spectral signatures from the digitized training ROIs for the CASI data. Where b4, b15, and b25 have the midpoint wavelength of 417, 572 and, 713nm respectively. The areal coverage of Japanese Eelgrass was bisected by the tideline when the CASI imagery was taken and therefore I separated the Japanese eelgrass decision tree to by elevation (tideline was approx. 0.4 m elevation).

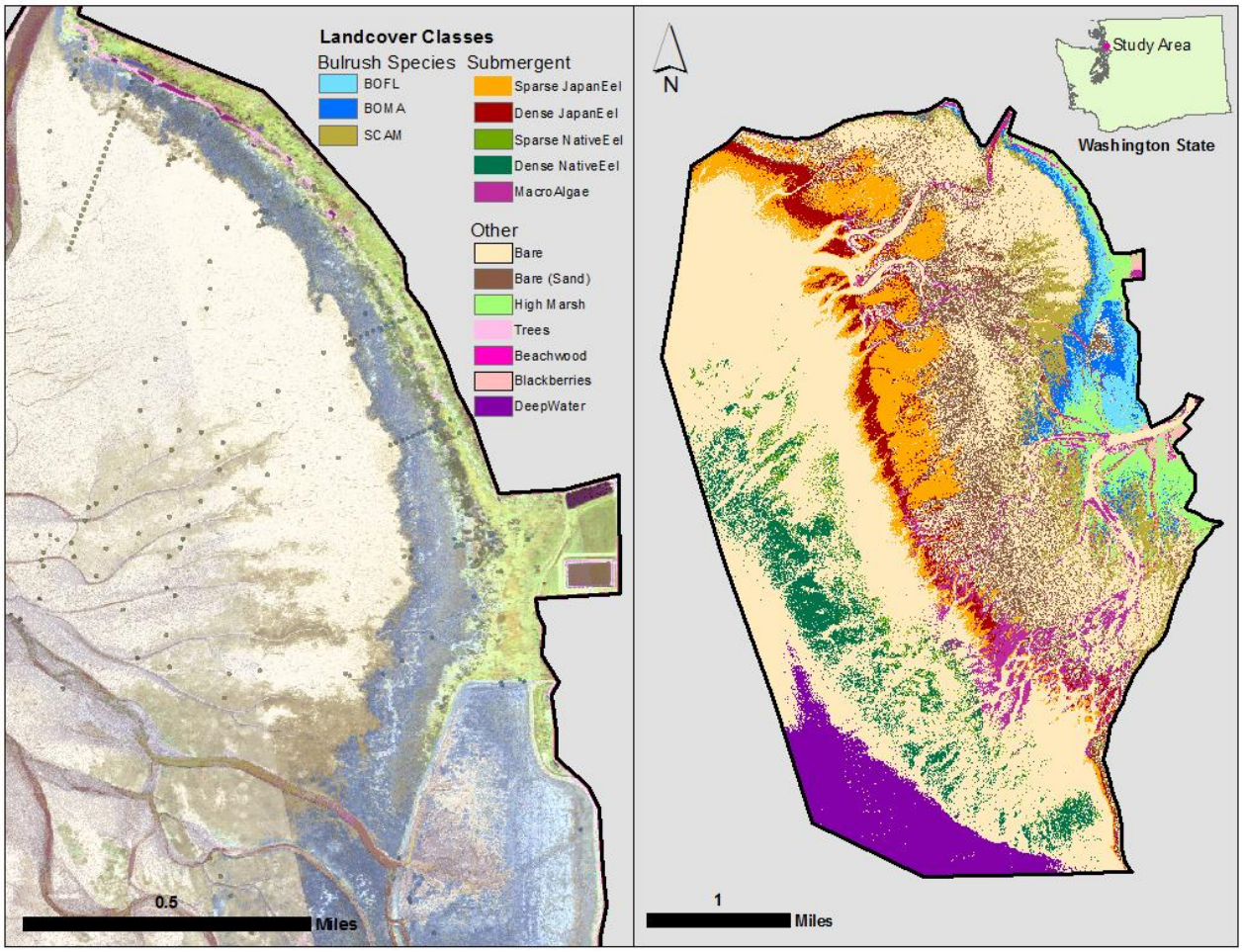

Figure 75. Maps of Decision Tree Classification focused on isolating bulrush species. A) Close up on northern marsh. Green dots represent ground truth points with a 5 m buffer. B) Overall land cover map of deltaic shelf (study area).